

**University of Alberta**

**Mechanistic Simulation Study of Steam-Solvent Coinjection for Bitumen  
and Heavy-Oil Recovery**

by

**Mohsen Keshavarz**

A thesis submitted to the Faculty of Graduate Studies and Research  
in partial fulfillment of the requirements for the degree of

**Master of Science**

in

**Petroleum Engineering**

**Department of Civil and Environmental Engineering**

©Mohsen Keshavarz

Fall 2013

Edmonton, Alberta

Permission is hereby granted to the University of Alberta Libraries to reproduce single copies of this thesis and to lend or sell such copies for private, scholarly or scientific research purposes only. Where the thesis is converted to, or otherwise made available in digital form, the University of Alberta will advise potential users of the thesis of these terms.

The author reserves all other publication and other rights in association with the copyright in the thesis and, except as herein before provided, neither the thesis nor any substantial portion thereof may be printed or otherwise reproduced in any material form whatsoever without the author's prior written permission.

Dedicated to my amazing family whose generous love and support allowed me to be where I am.

## **ABSTRACT**

Solvent-steam coinjection has been proposed as an alternative to SAGD. Detailed oil recovery mechanisms of coinjection are little known due to complex interaction of phase behavior, and fluid and energy flow.

This research conducts a detailed mechanistic study of phase behavior and its contribution to oil displacement efficiency and drainage rate near the chamber edge. Importance of properly considering both phase behavior and flow to design an optimized coinjection process is demonstrated.

We propose a systematic procedure for optimum selection of solvent and its coinjection strategy. Results show that a proper design can significantly improve the oil production rate compared to steam-only injection. We also demonstrate how enhanced displacement efficiency can be achieved during a coinjection process.

## **ACKNOWLEDGMENTS**

I would like to thank all people who have helped and inspired me during my study. I am grateful to my supervisors, Dr. Tayfun Babadagli and Dr. Ryosuke Okuno, for their guidance during my research and study at the University of Alberta. I would like to thank Dr. Babadagli for all his supervision and insightful ideas that improved the practical significance of my research. My special gratitude goes to Dr. Okuno whose continued guidance, patience and support went a long way in making this study and thesis possible. He has always been accessible and willing to help me with my research. I was also delighted to interact with Dr. David Redford and Dr. Peter Toma by attending their lectures. Learning from their wide variety of knowledge gave me a much better insight into the practical applications of my research. I am thankful to Dr. Hassan Dehghanpour and Dr. Sirish L. Shah, my examining committee members.

I gratefully acknowledge the financial support from National Sciences and Engineering Council of Canada (NSERC) for this research through grants held by Dr. Babadagli and Dr. Okuno. Dr. Babadagli holds NSERC Industrial Research Chair in Unconventional Oil Recovery (industrial partners are Schlumberger, CNRL, SUNCOR, Petrobank, Sherritt Oil, APEX Eng., and PEMEX). My thanks are also extended to Computer Modelling Group Ltd. (CMG) for providing the CMG software package for the simulation study.

I thank the staff at the department of Civil and Environmental Engineering for their help. I am also thankful to all the members of EOGRRRC group who helped me through various problems during the study – particularly Khosrow Naderi, Hector Leyva, Alireza Rangrizshokri, Hannes Hoffman and Laura Moreno Arciniegas.

My deepest gratitude goes to my family for their unflagging love and support throughout my life; this dissertation is simply impossible without them. I am indebted to my parents for their care, support and unconditional love that enlightened my path and gave me the strength to pace towards my achievements.

# TABLE OF CONTENTS

CHAPTER 1 : INTRODUCTION .....	1
Background.....	2
Introduction to Steam-Solvent Coinjection.....	4
Statement of the Problem.....	6
Research Objectives.....	8
Structure of the Thesis .....	10
References.....	12
CHAPTER 2 : EFFICIENT OIL DISPLACEMENT NEAR THE CHAMBER EDGE IN ES-SAGD.....	15
Introduction.....	16
Description of Simulation Cases.....	17
Solvent Accumulation near the Chamber Edge .....	20
Increased Oil Production Rate in ES-SAGD .....	22
Displacement Efficiency Enhanced by ES-SAGD .....	25
Conclusions.....	28
Nomenclature.....	30
References.....	53
CHAPTER 3 : OPTIMAL APPLICATION CONDITIONS FOR STEAM-SOLVENT COINJECTION.....	55
Introduction.....	56
Condensation Behavior of Steam and Solvent in Coinjection .....	59
Solvent Selection .....	63
Design of Solvent Concentration .....	66
Simulation Case Studies .....	69
Senlac SAP Pilot .....	69
Long Lake ES-SAGD Pilot .....	72
Conclusions.....	75
Nomenclature.....	77

References.....	108
CHAPTER 4 : A SEMI-ANALYTICAL SOLUTION TO OPTIMIZE SINGLE-COMPONENT SOLVENT COINJECTION WITH STEAM.....	112
Introduction.....	113
Solution for Chamber Edge Conditions .....	116
Oil Drainage Flux Index beyond the Chamber Edge .....	120
Algorithm of Solution.....	125
Sensitivity Analysis .....	126
Effect of solvent accumulation at the chamber edge .....	126
Effect of Operating Pressure and Oil Viscosity.....	129
Validation of the Results Using Numerical Simulations .....	132
Conclusions.....	134
Nomenclature.....	135
References.....	159
CHAPTER 5 : CONTRIBUTIONS AND RECOMMENDATIONS .....	162
Overview, Contributions and Conclusions .....	163
Suggested Future Work .....	168
APPENDIXES .....	170
Appendix A: Generating of K-values for STARS input files .....	171
K-values for water component .....	171
K-values for oil-like components .....	172
Some notes about K-value tables .....	173
References.....	176
Appendix B: A sample STARS data file for simulation of the coinjection process .....	177

## LIST OF TABLES

Table 2-1. Reservoir rock and fluid properties used in simulation cases .....	31
Table 2-2. Properties of the dead-oil component ( $C_D$ ) .....	31
Table 2-3. Properties of n-pentane ( $C_5$ ).....	31
Table 2-4. Overall composition, phase amounts, pressure, and temperature for Figures 2-17 (a)- (e).....	32
Table 2-5. Overall composition, phase amounts, pressure, and temperature for Figures 2-18(a)- (d).....	32
Table 2-6. Overall composition, phase amounts, pressure, and temperature for Figures 2-19 (a)- (c).....	32
Table 3-1. Reservoir and field properties used in numerical simulations .....	78
Table 3-2. Reservoir and fluid properties used in simulation of Senlac SAP pilot .....	78
Table 3-3. Viscosity-temperature for simulation of Senlac SAP pilot .....	79
Table 3-4. Reservoir and fluid data for simulation of Long Lake ES-SAGD pilot .....	79
Table 3-5. Viscosity -temperature behavior for simulation of Long Lake ES-SAGD pilot .....	79
Table 4-1. Properties of components used in chamber edge temperature estimation calculations .....	138
Table 4-2. Properties of oil and solvent components used in calculation of oil component drainage flux index.....	138
Table 4-3. Viscosity-temperature for Lloydminster heavy oil .....	139
Table 4-4. Properties of the reservoir model used in numerical simulations .....	140
Table A-1. STARS default K-value table for water component.....	175
Table A-2. A sample K-value table for STARS input file.....	175

## LIST OF FIGURES

Figure 2-1. Relative permeability curves used in the simulation cases. ....	33
Figure 2-2. Viscosity of bitumen (the $C_D$ component in Table 2-2) at different temperatures.....	34
Figure 2-3. Vapor pressure curves of $C_1$ , $C_5$ , $C_D$ , and water, and the critical locus of the live oil (a mixture of $C_1$ 4% and $C_D$ 96%)......	34
Figure 2-4. Cumulative oil recoveries in the SAGD and ES-SAGD simulations. ....	35
Figure 2-5. Tie triangle for the water, $C_5$ , and $C_D$ mixtures at 224.5°C and 2715 kPa (conditions inside the chamber). ....	36
Figure 2-6. Gravity segregation of condensed water and solvent banks at 27 months in the ES-SAGD simulation. ....	37
Figure 2-7. Distribution of the V phase saturation and temperature the 14 <sup>th</sup> row at 27 months...	39
Figure 2-8. Oil production rates in the SAGD and ES-SAGD simulations.....	40
Figure 2-9. The $C_D$ mole fraction in the L phase at different distances from the chamber edge in the 14 <sup>th</sup> row at 27 months in the ES-SAGD simulation.....	41
Figure 2-10. Distribution of the L phase saturation at different distances from the chamber edge in the 14 <sup>th</sup> row at 27 months in the ES-SAGD and SAGD simulations. ....	41
Figure 2-11. Relative permeability ratio at different distances from the chamber edge in the 14 <sup>th</sup> row at 27 months.....	42
Figure 2-12. Viscosity ratio at different distances from the chamber edge in the 14 <sup>th</sup> row at 27 months.....	42
Figure 2-13. Relative mobility ratio at different distances from the chamber edge in the 14 <sup>th</sup> row at 27 months.....	43
Figure 2-14. Molar density ratio at different distances from the chamber edge in the 14 <sup>th</sup> row at 27 months.....	44
Figure 2-15. Oil-component molar flux ratio at different distances from the chamber edge in the 14 <sup>th</sup> row at 27 months.....	45
Figure 2-16. Distribution of the L phase saturation at 27 months.....	46
Figure 2-17. Overall composition and phase equilibrium at gridblock (47, 7) in the ES-SAGD simulation using the water, $C_5$ , and $C_D$ components. ....	49
Figure 2-18. Overall composition and phase equilibrium at gridblock (9, 12) in the ES-SAGD simulation using the water, $C_5$ , and $C_D$ components. ....	51
Figure 2-19. Overall composition and phase equilibrium at gridblock (25, 5) in the SAGD simulation using the water and $C_D$ components (without the $C_5$ component). ....	52

Figure 3-1. Example for solutions of Equation 3-2 for a few different single-component solvents at an injection pressure $P_{inj}$ .	80
Figure 3-2. Chamber-edge temperatures estimation using Equation 3-2 for single-component solvents from $C_1$ to $C_{12}$ for injection pressures of 2.0 MPa, 3.0 MPa, and 4.0 MPa.	81
Figure 3-3. Water mole fraction in the V phase at the chamber edge edge for coinjection of a single-component solvent and steam.	82
Figure 3-4. Variations of temperature and the V phase saturation simulated along the sixth row from the top of the reservoir model at two years.	84
Figure 3-5. Comparison of numerical simulation results and estimations from Equation 3-2 for the chamber-edge temperature	85
Figure 3-6. Comparison of numerical simulation results and estimations from Equation 3-1 for the water mole fraction in the V phase at the chamber edge.	86
Figure 3-7. Water molar fluxes in steam-only injection and the $C_4$ and $C_8$ coinjection cases.	88
Figure 3-8. Oil recoveries for the steam-only injection and coinjection cases.	89
Figure 3-9. Average bitumen production rates for the first 2.5 years in Figure 3-8.	90
Figure 3-10. Profiles of the L phase viscosities in the 12 <sup>th</sup> row of the reservoir model at 1.5 years.	91
Figure 3-11. Comparison of cumulative oil production	92
Figure 3-12. Profiles of the L phase saturation and solvent ( $C_5$ ) mole fraction in the L phase in solvent/steam coinjection simulations at 1 and 2 years.	94
Figure 3-13. The cumulative oil production with respect to the cumulative volume of $C_5$ coinjected with steam.	94
Figure 3-14. Solvent volumes retained in the reservoir for $C_5$ -steam coinjection simulations with different solvent concentrations.	95
Figure 3-15. Injection and production volumes of $C_5$ in coinjection simulations using two different injection procedures.	96
Figure 3-16. Variation of the solvent concentration in the injectant during the modified coinjection procedure.	97
Figure 3-17. Volumes of $C_5$ left in the reservoir and the L phase saturation distributions after five years of operation for the two injection procedures; one with a constant $C_5$ concentration of 2.0 mol% and the other with a variable $C_5$ concentration.	98
Figure 3-18. Field data and results of simulation history matching for well pair C1 in the Senlac SAP project in 2002.	100
Figure 3-19. The average oil production rates after 8 months of SAP in simulations with different single-component solvents.	101

Figure 3-20. Comparison of EnCana’s original operation (scenario 1) and a modified coinjection process (scenario 2) for the Senlac SAP pilot. ....	102
Figure 3-21. Cumulative solvent injection and production during SAP with scenario 2. ....	103
Figure 3-22. Field data and results of history matching for oil production rate from well pair 3 for the Long Lake SAGD/ES-SAGD project. ....	104
Figure 3-23. Average oil production rates for 1.5 years of the Long Lake ES-SAGD with different single-component solvents. ....	105
Figure 3-24. Comparison between Nexen’s original process (scenario 1) and the modified coinjection (scenario 2) for the Long Lake ES-SAGD pilot. ....	106
Figure 3-25. Injection and production volumes of $C_5$ for scenario 2 for the Long Lake ES-SAGD simulation. ....	107
Figure 4-1. Flowchart of the algorithm used for estimation of $T_{edge}$ for a given pressure and an assumed overall composition. ....	141
Figure 4-2. Tie triangle for a system of water, single component solvent and reservoir oil at a sample pressure and temperature. ....	142
Figure 4-3. Variations of chamber edge temperature vs. solvent mole fraction in the L phase ( $x_{32}=z_3/(z_3+z_2)$ ) ....	144
Figure 4-4. Different forms of solvent distribution profile in the L phase beyond the chamber edge as predicted by Equation 4-16. ....	145
Figure 4-5. Variations of the oil component molar flux integrand in Equation 4-14 vs. the molar concentration of solvent in the L phase right at the chamber interface. ....	146
Figure 4-6. Profiles of the oil component drainage flux index in Equation 4-14 vs. the molar concentration of solvent in the L phase right at the chamber interface. ....	147
Figure 4-7. Profiles of the oil component molar flux integrand in Equation 4-14 vs. the perpendicular distance from the chamber interface for an assumed value of $x_s^{edge} = 0.25$ .....	148
Figure 4-8. Profiles of the oil component molar flux integrand in Equation 4-14 vs. the perpendicular distance from the chamber interface for an assumed value of $x_s^{edge} = 0.7$ .....	149
Figure 4-9. Profiles of the oil component molar flux integrand, temperature and solvent molar concentration in L phase vs. the perpendicular distance from the chamber interface for an assumed value of $x_s^{edge} = 0.95$ .....	151
Figure 4-10. Profiles of the oil component drainage flux index in Equation 4-14 vs. the molar concentration of solvent in the L phase right at the chamber interface. ....	152
Figure 4-11. Profiles of the numerically evaluated oil component drainage flux index in Equation 4-14 vs. the molar concentration of solvent in the L phase right at the chamber interface. ....	153

Figure 4-12. Profiles of the numerically evaluated oil component drainage flux index in Equation 4-14 vs. the molar concentration of solvent in the L phase right at the chamber interface. .... 154

Figure 4-13. Relative permeability curves used in the simulation cases ..... 155

Figure 4-14. Results of numerical simulations of the base case for the average bitumen production rate after the 9th month of coinjection until the 20th month for 3 solvent-steam coinjection processes. .... 156

Figure 4-15. Results of numerical simulations of case 2 for the average bitumen production rate after the 5<sup>th</sup> month of coinjection until the 15<sup>th</sup> month for 3 solvent-steam coinjection processes. .... 157

Figure 4-16. Results of numerical simulations of case 3 for the average bitumen production rate after the 4<sup>th</sup> month of coinjection until the 15<sup>th</sup> month for 3 solvent-steam coinjection processes. .... 158

# **CHAPTER 1 : INTRODUCTION**

## **Background**

Efficient recovery of unconventional oil resources, such as heavy oil and bitumen, is becoming more important considering the ever increasing energy demands as well as continuous depletion of conventional hydrocarbon reservoirs. More than 95% of the bitumen deposits in north America are located in the oil sands of Alberta and are expected to become a major source of fuel in the near future.

The main challenge in in-situ recovery of bitumen is its extremely high viscosity, which makes it essentially immobile at initial reservoir conditions. The most widely used method for bitumen and heavy oil recovery in western Canada is steam-assisted gravity drainage (SAGD) (Butler 1997). SAGD takes advantage of the strong temperature dependency of bitumen viscosity, which is in several orders of magnitude over the temperature range of 10°C to 200°C. In SAGD, two parallel horizontal wells are drilled into the formation with an inter-well spacing of around 5 m. A high quality steam is injected into the reservoir from the upper well (the injector). Steam propagates vertically and laterally into the reservoir in the form of a chamber, called steam chamber. Bitumen is mobilized by the latent heat released by the steam injected. The mobilized bitumen drains under the effect of gravity and is produced along with condensed water from the lower well, which is the producer.

SAGD offers several advantages including high recovery and stable production rates. Nevertheless, there are some drawbacks associated with this process. Among them are high energy consumption and significant environmental concerns including continuous demand for huge fresh water resources and extensive CO<sub>2</sub> emissions due to large amounts of natural gas being combusted for steam generation. Additionally, there is an overarching issue of cumulative effects due to numerous projects concentrated in one region of Alberta. The effects of intense and long-term development in the region will impact multiple environmental fronts, including air quality, water quality and availability, and quality of wildlife habitat, which is threatened with fragmentation (ConocoPhillips Canada 2013).

Lowering steam/oil ratio (SOR), which represents the barrels of water to produce an added barrel of oil, could offer a profitable path to reduce emissions and water demand. The lower the cumulative SOR, the lower the steam use per unit volume of produced oil and thus the more economic and environmental friendly is the process.

## **Introduction to Steam-Solvent Coinjection**

Solvent-steam coinjection has been proposed as an alternative to steam-only injection processes to minimize the energy input per unit of oil recovered. It has been studied or tested under several commercial names such as solvent-aided process (SAP), expanding solvent-SAGD (ES-SAGD), solvent-aided SAGD (SA-SAGD), steam alternating solvent (SAS), and liquid addition to steam enhanced recovery (LASER).

Solvent-steam coinjection is drawing notice from around the world due to its encouraging results in some applications. In almost all of these processes a small amount of hydrocarbon solvent is coinjected with steam; however solvent type and the coinjection scenario can vary from one process to another.

In SAP, a small amount of lighter hydrocarbon solvent (such as propane, butane, pentane, etc.) is added to steam in a SAGD process. SAP was introduced by Gupta et al. (2002) after successful field tests by EnCana. ES-SAGD was initially proposed by Nasr et al. (2002) in which solvents with close saturation temperature to that of steam are coinjected with steam. Hexanes and diluents are included in this category. LASER was first piloted Imperial oil in 2002 and was introduced by Leaute et al. (2002). LASER involves coinjection of a small volume fraction of pentane plus condensate (diluent) with steam at the late cycles of a steam-based recovery process called cyclic steam stimulation (CSS). In steam-alternating solvent (SAS), steam and mainly propane are injected alternately. This process was introduced by Zhao (2004).

Adding a solvent is designed to achieve a range of technical, economic and environmental benefits. Solvent is meant to propagate into the reservoir along with steam in the vapor phase and to condense at the vapor/liquid interface. Dilution of oil by the condensed solvent in conjunction with heat transfer from steam is believed to further reduce the viscosity of bitumen beyond that of steam-only injection. The coinjected solvent is then partially recovered with the production fluids and can be used in the coinjection cycle again.

Successful applications of coinjection in field and lab scale have reported improved oil production rates and ultimate recovery factors as well as reduced

steam oil ratio in comparison with steam-only injection (Nasr et al. 2003; Ivory et al. 2008; Gupta et al. 2005; Gupta and Gittins 2006; Leaute 2002; Leaute and Carey 2005; Redford and McKay 1980; Li and Mamora 2010; Ardali et al. 2012; Mohammadzadeh et al. 2012).

Field applications are mostly limited to pilot scales. EnCana has been developing SAP since 1996 and first piloted the process at its Senlac thermal project in 2002. Shortly after Butane coinjection began, the oil rate jumped by 50% (Gupta and Gittins 2005). Following the encouraging results, SAP was also piloted in Christina Lake in 2004. Production data from this pilot also indicate an uplift of 50% in oil production rate (Gupta and Gittins 2005).

In 2002, Imperial Oil piloted its LASER project in 8 vertical CSS wells by introducing a small concentration of  $C_{5+}$  to the injected steam during cycle 7 of the project. Results indicate that bitumen production rate increased by 100% over that from the neighboring pad wells without LASER implementation (Leaute 2002; Leaute and Carey 2005). Encouraged by the pilot results, Imperial Oil implemented a large scale LASER operation at Cold Lake.

An ES-SAGD test was also conducted by Nexen at Long Lake. A small concentration of Jet B, a mixture of  $C_7$  to  $C_{12}$ , was coinjected with steam for 2.5 months. The results were not as encouraging as the pilot tests by EnCana and Imperial Oil. Oil rate was increased by 6% and SOR was reduced by 7% (Orr 2009).

Suncor tested coinjection of naphtha with steam in a SAGD project at Firebag. However, it did not show any improvements in the well performances (Orr, 2009).

Analytical and numerical studies as well as lab experiments and pilot tests are still ongoing to better understand the key mechanisms of the coinjection and to optimize it. Ardali et al. (2012b) present a detailed review of prior studies. Solvents are very likely to be an inseparable part of steam based recovery processes in the future of oil sands.

## Statement of the Problem

In the previous section, the potential advantages of solvent-steam coinjection over steam-only injection were briefly described. Besides all promising results of coinjection, there are also evidences that coinjection of some solvents with steam has resulted in no improvement or even a worse performance compared to steam-only injection (Jiang et al. 1998; Canbolat et. al 2002; Hosseinienejad-Mohabati et al. 2010; Li and Mamora 2011; Shu and Hartman 1988).

Gates (2007) stated that temperature near the edge of coinjection chamber can be lower than that in SAGD due to gaseous solvents accumulated there. Therefore, higher production rates during coinjection can be achieved only if the dilution effects of the coinjected solvent can offset the temperature reduction effect on the oleic (L) phase viscosity near the chamber edge. This raises the following questions: What are the key factors controlling the temperature distribution and dilution effects near the chamber edge? Is there an optimum balance possible to be achieved between these two? And, if yes, how?

There are also reports of enhancement in the ultimate recovery factor of oil as a result of coinjection compared to steam-only injection (Redford and McKay 1980; Li and Mamora 2010; Ardali et al. 2012a; Mohammadzadeh et al. 2012; Jha et al. 2012); however, detailed mechanisms of these incremental ultimate recovery are not fully understood.

Due to its complexity, most of the studies on coinjection design in the literature focus on selection of solvent and its concentration to achieve this goal. Nevertheless, there is still an ongoing debate on these two design parameters among experts. There are various proposals available in literature which are specific to their experimental conditions or reservoir properties and are not necessarily consistent with each other.

In their proposal for ES-SAGD, Nasr et al. stated that the coinjected solvent should be selected in such a way that it condenses at the same condition with steam. This criterion was to ensure that solvent would condense, with condensed steam, at the boundary of steam chamber resulting in the maximum drainage rate (Nasr et al. 2002). Based on this criterion,  $C_6$  and  $C_7$  (and some

diluents with approximately similar condensation temperatures) were pointed out as the optimum solvent in several studies (e.g., Li and Mamora 2010; Hosseininejad Mohabati et al. 2010; Li and Mamora 2011b; Yazdani et al. 2011; Ardali et al. 2012a).

Solvents resulting in the highest drainage rates in other studies are not always consistent with Nasr et al. (2002). There are evidences of more promising results from heavier solvents than those suggested by Nasr et al. (Redford and McKay 1980; Li and Mamora 2011b). On the other hand, several studies reported the superior performance of lighter solvents under specific experimental/simulation conditions (Govind et al. 2008; Ardali et al. 2010). In addition to this, a variety of proposals also exist for coinjection procedures with different concentrations of coinjected solvents (Gates and Chakrabarty 2008; Gupta and Gittins 2007ab; Edmunds et al. 2010; Jiang et al. 2012).

All these imply that the current level of understanding of the fundamental mechanisms of the coinjection process is not satisfactory. When the high costs of solvents are taken into account, a proper design seems to be even more crucial for the practicality of coinjection processes. This leads to an optimum design of the process for proper solvent type selection as well as a coinjection strategy that can maximize the potential advantages of coinjection, while solvent losses are minimized.

## **Research Objectives**

The key objective of this work is to achieve a better understanding of the key mechanisms of the coinjection by conducting a mechanistic study of the process. This, in turn, requires detailed investigation of multiphase behavior of solvent-water-bitumen mixtures and its interaction with non-isothermal flow. The major goal of this study is achieved through the following subgoals:

1. It is discussed in details why and how coinjection of a small concentration of solvent with steam has potential to significantly improve production rates. Also, the key mechanisms responsible for enhancement of oil displacement efficiency compared to pure steam injection are identified.
2. The improved knowledge of the mechanisms is used to investigate the required circumstances under which the potential advantages of solvent coinjection with steam can be expected. The reasons for less encouraging results from laboratory or field scale applications are discussed.
3. We aim to propose a systematic procedure for selecting an optimum solvent and its concentration in coinjection of a single-component solvent with steam. The optimization considers the oil production rate, ultimate oil recovery, and solvent retention in situ.
4. We propose a semi-analytical method for preliminary screening of the coinjection solvent. Mechanics of coinjection process are understood in much more details with this semi-analytical approach. Effects of operating pressure/temperature as well as viscosity-temperature behavior of the reservoir oil on the performance of coinjection of different solvents with steam are demonstrated.

The first objective is achieved by conducting a detailed investigation on phase behavior and the placement of solvent near the chamber edge. The importance of properly considering both phase behavior and flow to design coinjection is demonstrated.

To achieve the second and the third goals, we conduct numerical simulations for coinjection of several solvents with steam under different operating conditions and with different types of oils. Multiphase behavior of water-hydrocarbon mixtures in the chamber is explained in detail analytically and numerically. We show that an optimum volatility can be expected for the coinjected solvent in terms of oil production rate. Additionally, we demonstrated that it is possible to maximize oil recovery while minimizing solvent retention in situ by controlling the concentration of a given coinjection solvent. Simulation case studies of actual coinjection pilots show the validity of the oil recovery mechanisms described.

The final goal is achieved by developing an algorithm for estimating chamber edge temperature during coinjection. Available correlations are then used to predict temperature and solvent distribution profiles beyond the chamber edge. An improved understanding of the key factors affecting the oil drainage is obtained with the aid of this semi-analytical method. Validation of the predictions by the semi-analytical method against the results of numerical simulation indicates that the proposed method can be used as a preliminary screening method for the coinjection solvent when the contrast of different solvents is meaningful in terms of oil recovery. This can be much faster and more convenient than running full numerical flow simulations of flow and can eliminate the need to run unnecessary simulations.

## Structure of the Thesis

This is a paper-based thesis. After a short introduction section (Chapter 1) that includes a general overview, problem statement and research objectives, three papers which were presented at different conferences and/or under revision for journal publications are presented in Chapters 2 through 4. Each chapter has its own introduction, literature survey, discussions and references.

In Chapter 2, a detailed simulation study is performed to clarify how coinjection (ES-SAGD with  $C_5$  being the coinjected solvent) can achieve higher oil production rate and displacement efficiency than SAGD. Possibility of achieving oil saturations below residual oil saturation ( $S_{or}$ ), without altering interfacial tension (IFT) in simulations, is demonstrated by phase equilibrium in temperature and composition space near the chamber edge.

In Chapter 3, a simplified representation of binary phase behavior of water and a single-component solvent, based on Dong's work (2012) is used to describe the condensation behavior of solvent and steam in the coinjection chamber. An application of Dong's analysis for estimation of the chamber-edge temperature for a wide variety of solvents and operating conditions is presented. The estimations are then compared with results from numerical flow simulations, where some of assumptions made in the estimation are relaxed.

Based on the balance between key controlling factors affecting the oil mobility along the chamber edge, a systematic procedure is proposed for optimum selection of solvent in terms of oil production rates. Then, an injection procedure for the selected solvent is also presented to maximize ultimate oil recovery while minimizing solvent retention in the residual oleic phase.

Eventually, we apply the systematic workflow to two actual field cases, EnCana's SAP pilot in Senlac (Gupta et al. 2005; Gupta and Gittins 2006) and Nexen's ES-SAGD pilot in Long Lake (Nexen 2007; Orr et al. 2010).

In Chapter 4, a simple calculation algorithm is presented for estimation of temperature at the vapor/liquid interface in a system of water, solvent and oil. We demonstrate how the existence of reservoir oil as a third component affects the chamber edge temperature which is not considered by the simplistic

representation of phase behavior using binary mixtures of water and solvent presented in the literature.

Then a step-wised semi-analytical method is proposed to qualitatively evaluate the performance of coinjection process with different solvents, in terms of oil production rates. Effects of operating pressure as well as oil viscosity-temperature behavior on the production rates are interpreted through case studies. Eventually, predictions of the semi-analytical method are validated against the results from numerical simulations.

The final chapter (Chapter 5) gives the main contributions to the literature and industry as well as suggested future work.

## References

- Ardali, M., Barrufet, M.A., Mamora, D.D., Qiu, F., 2012b. A Critical Review of Hybrid Steam/Solvent Processes for the Recovery of Heavy Oil and Bitumen. Paper SPE 159257 presented at SPE Annual Technical Conference and Exhibition, San Antonio, Texas, USA, October 8-10.
- Ardali, M., Barrufet, M., and Mamora, D.D. 2012a. Laboratory Testing of Addition of Solvents to Steam to Improve SAGD Process. Paper SPE 146993 presented at SPE Heavy Oil Conference Canada, Calgary, Alberta, Canada, June 12-14.
- Ardali, M., Mamora, D.D., and Barrufet, M. 2010. A Comparative Simulation Study of Addition of Solvents to Steam in SAGD Process. CSUG/SPE Paper 138170 presented at Canadian Unconventional Resources and International Petroleum Conference, Calgary, Alberta, Canada, October 19-21.
- Butler, R.M. 1997. *Thermal Recovery of Oil and Bitumen*. Prentice Hall.
- Canbolat, S., Akin, S., Kovscek and A.R. 2002. A Study of Steam-Assisted Gravity Drainage Performance in the Presence of Noncondensable Gases. Paper SPE 75130 presented at Improved Oil Recovery Symposium, Tulsa, Oklahoma, USA, April 13-17.
- Computer Modelling Group (CMG) Ltd. STARS User Manual. Version 2011. Calgary, Alberta, Canada, 2011.
- ConocoPhillips Canada. (2013). Retrieved May 1, 2013, from <http://www.conocophillips.ca/EN/about/oil-sands/Pages/EnviroStewardOS.aspx>
- Edmunds, N. and Moini, B. 2010. Advanced Solvent-Additive Processes by Genetic Optimization. *Journal of Canadian Petroleum Technology*, **49** (9): 34-41.
- Gates, I.D. 2007. Oil Phase Viscosity Behavior in Expanding-Solvent Steam-Assisted Gravity Drainage. *Journal of Petroleum Science and Engineering* **59** (1-2): 123-134.
- Gates, I.D. and Chakrabarty, N. 2008. Design of Steam and Solvent Injection Strategy in Expanding Solvent Steam-Assisted Gravity Drainage. *Journal of Canadian Petroleum Technology* **47** (9): 12-19.
- Gupta, S.C. and Gittins, S.D. 2007b. Effect of Solvent Sequencing and Other Enhancements on Solvent Aided Process. *Journal of Canadian Petroleum Technology*, **46** (9): 57-61.
- Gupta, S. and Gittins, S. 2007a. Optimization of Solvent Aided Process. Paper 2007-022 presented at the Petroleum Society's 8th Canadian International Petroleum Conference, Calgary, Alberta, Canada, June 12-14.
- Gupta, S. and Gittins, S.D. 2006. Christina Lake Solvent Aided Process Pilot. *Journal of Canadian Petroleum Technology* **45** (9): 15-18.
- Gupta, S., Gittins, S., and Picherack, P. 2005. Field Implementation of Solvent Aided Process. *Journal of Canadian Petroleum Technology* **44** (11): 8-13.

- Gupta, S., Gittins, S., and Picherak, P. 2002. Field Implementation of Solvent Aided Process "Waxy" Mixtures. Paper 2002-299 presented at the Canadian International Conference, Calgary, Alberta, Canada, June 11-13.
- Govind, P.A., Das, S.K., Srinivasan, S., and Wheeler, T.J. 2008. Expanding Solvent SAGD in Heavy Oil Reservoirs. Paper SPE/PS/CHOA presented at the 2008 SPE International Thermal Operations and Heavy Oil Symposium, Calgary, Alberta, Canada, October 20-23.
- Ivory, J., Zheng, R., Nasr, T., Deng, X., Beaulieu, G., and Heck, G. 2008. Investigation of Low Pressure ES-SAGD. Paper SPE 117759 presented at 2008 SPE International Thermal Operations and Heavy Oil Symposium, Calgary, Alberta, Canada, October 20-23.
- Jha, R.K., Kumar, M., Benson, I., and Hanzlik, E. 2012. New Insights into Steam-Solvent Co-Injection Process Mechanism. Paper SPE 159277 presented at 2012 SPE Annual Technical Conference and Exhibition, San Antonio, Texas, October 8-10.
- Jiang, Q., Butler, R., and Yee, C.T. 1998. The Steam and Gas Push (SAGP)-2: Mechanism Analysis And Physical Model Testing. Petroleum Society's 49th Annual Technical Meeting, Calgary, Alberta, Canada, June 8-10.
- Nasr, T.N., Beaulieu, G., Golbeck, H., and Heck, G. 2003. Novel Expanding Solvent-SAGD Process "ES-SAGD". *Journal of Canadian Petroleum Technology* **42** (1): 13-16.
- Nasr, T.N., Beaulieu, G., Golbeck, H., and Heck, G. 2002. Novel Expanding Solvent-SAGD Process "ES-SAGD". Paper 2002-079 presented at the Canadian International Conference, Calgary, Alberta, Canada, June 11-13.
- Leaute, R.P. 2002. Liquid Addition to Steam for Enhancing Recovery of Bitumen with CSS: Evolution of Technology from Research Concept to a Field Pilot at Cold Lake. SPE/Petroleum Society of CIM/CHOA Paper 79011, Calgary, Alberta, Canada, November 4-7.
- Leaute, R.P. and Carey, B.S. 2005. Liquid Addition to Steam for Enhancing Recovery (LASER) of Bitumen with CSS: Results from the First Pilot Cycle. Paper 2005-161 presented at the 56<sup>th</sup> Canadian International Petroleum Conference, Calgary, Alberta, Canada, June 7-9.
- Li, W. and Mamora, D.D. 2010. Phase Behavior of Steam with Solvent Coinjection under Steam Assisted Gravity Drainage (SAGD) Process. Paper SPE 130807 presented at the SPE EUROPEC/EAGE Annual Conference and Exhibition, Barcelona, Spain, June 14-17.
- Li, W., Mamora, D.D., and Li, Y. 2011b. Solvent-Type and -Ratio Impacts on Solvent-Aided SAGD Process. *SPE Reservoir Evaluation and Engineering* **14** (3): 320-331.
- Mohammadzadeh, O., Rezaei, N., and Chatzis, I. 2012. More Insight into the Pore-Level Physics of the Solvent-Aided SAGD (SA-SAGD) Process for Heavy Oil and Bitumen Recovery. Paper SPE 157776 presented at SPE Heavy Oil Conference Canada, Calgary, Alberta, Canada, June 12-14.

- Orr, B. 2009. ES-SAGD; Past, Present and Future. Paper SPE-129518-STU presented at the 2009 SPE International Student Paper Contest at the SPE Annual Technical Conference and Exhibition, New Orleans, Louisiana, USA, October 4-7.
- Redford, D.A. and McKay, A.S. 1980. Hydrocarbon-Steam Processes for Recovery of Bitumen from Oil Sands. Paper SPE 8823 presented at SPE/DOE Enhanced Oil Recovery Symposium, Tulsa, Oklahoma, USA, April 20-23.
- Shu, W.R. and Hartman, K.J. 1988. Effect of Solvent on Steam Recovery of Heavy Oil. *SPE Reservoir Engineering* **3** (2): 457-465.
- Yazdani, A., Alvestad, J., Kjonsvik, D., Gilje, E., and Kowalewski, E. 2011. A Parametric Simulation Study for Solvent Co-injection Process in Bitumen Deposits. Paper SPE 148804 presented at the Canadian Unconventional Resources Conference, Calgary, Alberta, Canada, November 15-17.
- Zhao, L. 2004. Steam Alternating Solvent Process. Paper 86975 presented at SPE International Thermal Operations and Heavy Oil Symposium and Western Regional Meeting, Bakersfield, California, USA, March 16-18.

## **CHAPTER 2 : EFFICIENT OIL DISPLACEMENT NEAR THE CHAMBER EDGE IN ES-SAGD**

A version of this chapter has been submitted to Journal of Petroleum Science and Engineering for publication.

## **Introduction**

Efficient recovery of unconventional oil resources, such as heavy oil and bitumen, is becoming more important considering the ever increasing energy demands. The main challenge in in-situ recovery of bitumen is its extremely high viscosity, which makes it essentially immobile at initial reservoir conditions. The most widely used method for bitumen recovery is steam-assisted gravity drainage (SAGD) (Butler 1997). SAGD takes advantage of the strong temperature dependency of bitumen viscosity. Viscosity of typical bitumen falls several orders of magnitude over the temperature range of 10 °C to 200 °C. In SAGD, steam of a high quality is injected using a horizontal injection well, which is located a few meters above a horizontal production well. Bitumen is mobilized by the latent heat released by the steam injected. Gravity is the main driving force for the mobilized oil to drain towards the production well. The disadvantages of SAGD are the costs and CO<sub>2</sub> emissions associated with generation of a significant amount of steam.

Expanding-solvent-steam assisted gravity drainage (ES-SAGD) has been proposed as an alternative to improve the efficiency of SAGD. In ES-SAGD, a small amount of hydrocarbon solvent is coinjected with steam to further reduce the viscosity of bitumen near the chamber edge (Nasr and Isaacs 2001; and Nasr et al. 2003). In ES-SAGD, the coinjected solvent is selected such that it will condense and evaporate at the same pressure and temperature as water. Gates (2007) reported that ES-SAGD requires a smaller amount of steam to recover the same amount of bitumen, compared to SAGD.

ES-SAGD, if designed properly, also can exhibit higher oil production rate than SAGD (Nasr et al. 2003; Gates 2007; Ivory et al. 2008; Li et al. 2011ab; Yazdani et al. 2011). However, there is still an ongoing debate on the selection of solvent compounds, solvent concentrations, and operating conditions for an optimized ES-SAGD. Gates (2007) stated that temperature near the chamber edge in ES-SAGD can be lower than that in SAGD due to gaseous solvents accumulated there. Higher production rates during ES-SAGD can be achieved only if the dilution effects of the coinjected solvent can offset the temperature

reduction effect on the oleic (L) phase viscosity near the chamber edge. This indicates that understanding of the mechanisms in ES-SAGD requires detailed investigation of the non-isothermal multiphase flow near the chamber edge.

A few papers on steam-solvent coinjection indicated that it can reduce oil saturation below a residual oil saturation obtained from SAGD. Deng et al. (2010) presented figures indicating such reduced oil saturation inside the chamber, but their details were not discussed. Li et al. (2011a) stated that liquid solvent can flush out all residual oil. However, they did not explain how such miscibility can be developed in steam-solvent coinjection for bitumen. Yazdani et al. (2011) stated that lowered oil saturation can be obtained by interfacial tension (IFT) reduction between phases during steam-solvent coinjection. They recommended modifying the end points of relative permeability curves according to laboratory tests to capture IFT reduction in coinjection simulation.

In this chapter, a detailed simulation study is performed to clarify how ES-SAGD can achieve higher oil production rate and displacement efficiency than SAGD. We first describe simulation cases performed in this research. Results are then explained in terms of oil production rate and displacement efficiency in ES-SAGD and SAGD. We show that ES-SAGD can achieve high displacement efficiency without considering IFT reduction in simulation. Phase equilibrium in temperature and composition space near the chamber edge play important roles in the oil displacement mechanism. Although this chapter deals with ES-SAGD as a specific type of solvent-steam coinjection processes, but the discussion can be extended to any other coinjection process of a similar nature.

### **Description of Simulation Cases**

Simulations are conducted using the STARS simulator of Computer Modelling Group (2011). The 2-D reservoir model used in this research consists of 70, 1, and 20 gridblocks in the x, y, and z directions, respectively. A uniform gridblock size of  $1.0 \times 37.5 \times 1.0 \text{ m}^3$  is used resulting in model dimensions of 70.0 m, 37.5 m, and 20.0 m in the x, y, and z directions, respectively. The injection well is located 4.0 m above the production well, which is located 3.0 m above the bottom of the reservoir model. The simulations are performed only for

a half of the ES-SAGD chamber. Thus, the wells are placed in the left-most grids of the 2-D reservoir model.

The initial reservoir pressure and temperature are 1500 kPa and 13 °C, respectively. The initial oil saturation is 0.75. The aqueous (W) phase initially exists at its irreducible saturation of 0.25. Key properties of the homogeneous reservoir are given in **Table 2-1**. The relative permeabilities used are shown in **Figure 2-1**. Capillarity is not considered in this research.

Typical dead-oil properties for Athabasca bitumen are considered as shown in **Table 2-2**, which were taken from Mehrotra and Syrczek (1987). The oil viscosity is approximately  $10^6$  cp at the initial conditions, and changes with temperature as shown in **Figure 2-2** (Mehrotra and Syrczek 1986). A typical gas-oil ratio (GOR) for Athabasca oil sand is about  $2.0 \text{ m}^3/\text{m}^3$  (Ivory et al. 2008). We make a live oil using a GOR of  $1.8 \text{ m}^3/\text{m}^3$ , methane ( $C_1$ ) for the gas, and the dead-oil component ( $C_D$ ) given in Table 2-2. The resulting mole fraction of  $C_1$  in the live oil is 0.04. **Figure 2-3** shows the vapor pressure curves of  $C_1$  and  $C_D$ , and the critical locus of the live oil. The critical locus of the live oil at high  $C_1$  concentrations cannot be found using the PR EOS within the pressure range shown.

The injection and production wells are operated at constant bottom-hole pressures of 2730 kPa and 1500 kPa, respectively. The steam table indicates that the saturated steam temperature at 2730 kPa is 228.7°C. A maximum flow rate of  $1.0 \text{ m}^3/\text{day}$  is assigned to steam at the production well to control steam production during the simulation. Preheating of the reservoir is performed for six months.

A steam quality of 0.9 is used in all simulations. As a solvent, n-pentane ( $C_5$ ) is coinjected with steam at 2.0 mol%. The key properties of  $C_5$  are listed in **Table 2-3**. Binary interaction parameters are 0.0206 for  $C_1$ - $C_5$ , 0.1174 for  $C_1$ - $C_D$ , and 0.04453 for  $C_5$ - $C_D$ . Figure 2-3 shows the vapor pressures of water and  $C_5$ . The condensation temperature of  $C_5$  at the injection pressure, 2730 kPa, is lower than that of water.

There are four components in the simulations; water, C<sub>1</sub>, C<sub>5</sub>, and C<sub>D</sub>. The STARS simulator represents the fluid phase behavior using K-value tables. Constant-K flash with the Rachford-Rice equations (1952) is used to calculate up to three equilibrium phases (L, gaseous (V), and W). The K-values for the hydrocarbon components, C<sub>1</sub>, C<sub>5</sub>, and C<sub>D</sub>, are generated by performing a series of flash calculations using the Peng-Robinson (PR) equation of state (1976) with the van der Waals mixing rules. Composition dependency of K-values is not considered within an individual simulation in this research. We use a mixture of 20% C<sub>5</sub> and 80% live oil, which consists of 96% C<sub>D</sub> and 4% C<sub>1</sub>, for generating K-values for the hydrocarbon components. Detailed instructions on K-value tables generation is provided in Appendix A.

Hydrocarbon K-values can be also generated internally in the STARS simulator using a correlation. However, such a correlation should be carefully used for ES-SAGD simulation because K-values can significantly affect solvent propagation in the simulation. More reliable K-values can be generated using an EOS as in this research. Also, more detailed compositional phase behavior can be modeled in simulation if a plus fraction is modeled using a reliable heavy-oil characterization method (e.g., Kumar and Okuno 2012) and PVT data available.

The K-values for the water component at a given temperature are assumed to be the saturation pressure of water at that temperature divided by the total pressure. It is also assumed that the W phase consists of only the water component, and the L phase consists of only hydrocarbon components. The water and hydrocarbon components can coexist in the V phase.

The mixing rule used for viscosity of phase  $j$ ,  $\mu_j$ , is

$$\ln(\mu_j) = \sum_{i=1}^{N_C} x_{ij} \ln(\mu_{ij}), \quad (2-1)$$

where  $N_C$  is the number of components,  $x_{ij}$  is the mole fraction of component  $i$  in phase  $j$ , and  $\mu_{ij}$  is the component viscosity of component  $i$  in phase  $j$ . The mixing rule used for molar density of phase  $j$ ,  $\rho_j$ , is

$$\frac{1}{\rho_j} = \sum_{i=1}^{N_C} \frac{x_{ij}}{\rho_{ij}}, \quad (2-2)$$

where  $\rho_{ij}$  is the component molar density of component  $i$  in phase  $j$ .

**Figure 2-4** shows the oil recovery histories for the ES-SAGD and SAGD simulations, where the amount of solvent recovered is not considered for the ES-SAGD plots. There are two main differences between the two recoveries. One is the higher oil production rate observed for ES-SAGD, and the other is the ultimate oil recovery enhanced by ES-SAGD. These two points will be discussed in sections 4 and 5. We show that efficient ES-SAGD involves accumulation of solvent near the chamber edge, which will be discussed in the subsequent section.

As mentioned earlier, we set a mixing ratio of  $C_5$  with the live oil to 0.2 when generating K-values for the simulation. We tested another mixing ratio of 0.6 to observe the potential effects on ES-SAGD simulation results. Figure 2-4 compares oil recoveries for the two mixing ratios. The effect of the mixing ratio used on oil recovery prediction is not significant. The slight difference observed is due to different phase compositions predicted during the simulations.

### **Solvent Accumulation near the Chamber Edge**

In ES-SAGD, solvent components are transported efficiently to the chamber edge in the V phase. **Figure 2-5** presents the tie triangle in composition space for water,  $C_5$ , and  $C_D$  at 224.5°C at 2715 kPa based on the K-values generated in the previous section. Here, only three components are used for simplicity for the illustration. The V phase contains  $C_5$  at a higher concentration than the L phase; i.e., the K value of  $C_5$  is greater than 1.0 at these conditions. More importantly, the mobility of the V phase is much higher than that of the L phase. Propagation of solvent components in ES-SAGD should be carefully designed based on the interaction of flow and phase behavior. If solvent components are present at substantially low concentrations in the V phase near the chamber edge, such ES-SAGD will show oil recovery similar to that of the conventional SAGD at the costs associated with solvent coinjection.

**Figure 2-6** shows the distributions of the W phase and the  $C_5$  mole fraction in the L phase at 27 months. The V phase releases its latent heat near the chamber edge resulting in accumulation of the W phase there. The  $C_5$  component transported mainly in the V phase condenses near the chamber edge,

where the concentration of  $C_5$  becomes significantly high in the L phase. A  $C_5$  concentration of 0.95 in the L phase is observed in the simulation. Gravity segregation is observed for the condensed water and  $C_5$  along the chamber edge. That is, the hot W phase flows below the  $C_5$ -rich L phase in the simulation studied.

The condensation temperature of  $C_5$  is lower than that of water at a given pressure as seen in Figure 2-3. For this reason, the ES-SAGD exhibits temperature distributions that are different from those in the conventional SAGD. **Figures 2-7** (a) and (b) show the temperature and V phase saturation profiles of the SAGD and ES-SAGD simulations for the 14<sup>th</sup> row from the top of the reservoir model (i.e., six meters from the reservoir bottom) at 27 months. In this research, the chamber edge is defined where the gas saturation changes to zero. In the SAGD simulation, the temperature is nearly constant when the V phase exists in Figure 2-7 (a). The V phase releases its latent heat on the steam chamber edge, and temperature decreases in the hot water bank.

The chamber temperature in the ES-SAGD simulation starts decreasing while the V phase is present. The concentration of  $C_5$  in the V phase becomes high in this temperature transition zone inside the chamber. That is, the ES-SAGD simulation shows accumulation of  $C_5$  in the V phase inside the chamber, and that in the L phase outside the chamber.

The accumulation of  $C_5$  in the V phase in the ES-SAGD simulation causes the chamber-edge temperature to be significantly lower than that in the SAGD simulation (Figures 2-7 (a) and (b)). The difference observed is as much as 87°C. This means that the mobile liquid phases' temperature in the ES-SAGD simulation is significantly lower than that in the SAGD simulation. The most effective solvent dilution will not occur for the oil at the chamber temperature (227°C in this study), but for the oil at a much lower temperature (140°C in this study). A question then arises as to how the ES-SAGD simulation results in a higher oil production rate than the SAGD simulation as given in Figure 2-4. This point will be addressed in the subsequent section.

### Increased Oil Production Rate in ES-SAGD

The histories of bitumen production rates in the SAGD and ES-SAGD simulations are compared in **Figure 2-8**. The production of C<sub>5</sub> as part of oil is excluded for the ES-SAGD case. Improved oil production rates are observed during the early and intermediate stages in the ES-SAGD simulation, where the oil production rate of ES-SAGD is two to three times higher than that of SAGD. Interpretation of the increased oil rate in ES-SAGD should consider the solvent accumulation and temperature distribution near the chamber edge described in the previous section. A simple analysis is given below as to how the improved oil production rate is achieved in ES-SAGD.

Darcy's law for the L phase in the direction parallel to the chamber edge during SAGD is

$$u_o = - \frac{kk_{ro}}{\mu_o} \frac{\partial \Phi_o}{\partial \eta}, \quad (2-3)$$

where  $\eta$  is the distance in the direction parallel to the chamber edge. The oil-component molar flux in the L phase  $j_o$  [mole/m<sup>2</sup>-sec] for SAGD is

$$j_o = - \frac{kk_{ro}}{\mu_o} \frac{\partial \Phi_o}{\partial \eta} \rho_o, \quad (2-4)$$

where  $\rho_o$  is the molar density of the L phase. Similarly for the oil-component molar flux in the L phase  $j'_o$  for ES-SAGD,

$$j'_o = - \frac{kk'_{ro}}{\mu'_o} \frac{\partial \Phi'_o}{\partial \eta} \rho'_o x'_o. \quad (2-5)$$

The L phase in ES-SAGD consists of solvent and reservoir oil components. Equation 2-5 represents the mole fraction of reservoir oil components in the L phase for ES-SAGD as  $x'_o$ . It is 1.0 for the conventional SAGD. The terms  $\mu'_o$  and  $\rho'_o$  are the viscosity and molar density of the L phase as an oil-solvent mixture, respectively. Assuming the same potential gradient for Equations 2-4 and 2-5, the ratio of the oil component molar flux in ES-SAGD to that in SAGD is

$$\frac{j'_o}{j_o} = \frac{k'_{ro}}{k_o} \frac{\mu_o}{\mu'_o} \frac{\rho'_o}{\rho_o} x'_o. \quad (2-6)$$

Equation 2-6 has four terms that affect the oil-component molar flux ratio; the relative permeability ratio, the viscosity ratio, the molar density ratio, and the oil-component mole fraction in the L phase. Using Equation 2-6, one can identify the individual contributions of the four terms at different distances from the chamber edge. Equation 2-6 also indicates that improved oil production rate simulated for ES-SAGD depends on how physical properties, like relative permeabilities and phase viscosities, are modeled in the simulation.

**Figure 2-9** shows the oil-component (i.e.,  $C_D$ ) mole fraction in the L phase outside the chamber edge in the 14<sup>th</sup> row from the top of the reservoir model. Due to solvent accumulation near the chamber edge, the oil-component mole fraction just outside the chamber edge can be as small as 0.05. This shows that the amount of the oil component can be substantially small in the mobile oil zone.

The relative permeability ratio  $k'_{ro}/k_o$  depends on the L phase saturations for the SAGD and ES-SAGD cases, which vary with the distance from the chamber edge. **Figure 2-10** shows that the L phase saturation distribution of the ES-SAGD simulation is significantly different from that of the SAGD simulation. In the ES-SAGD simulation, the L phase saturation is significantly increased in the condensed  $C_5$  bank near the chamber edge, but it is reduced in the hot water bank. At 15 m from the chamber edge, the relative permeability ratio shows a minimum due to the limited L phase saturation in the ES-SAGD hot water bank. In the SAGD simulation, the hot water bank exists just outside the chamber edge.

**Figure 2-11** shows the relative permeability ratio at different distances from the chamber edge. In ES-SAGD, the gravity segregated flow of hot water and condensed solvent banks raises the L phase saturation just outside the chamber edge. Therefore, the L phase relative permeability in this region is much higher in ES-SAGD than in SAGD (0 – 9 m in Figure 2-11). The relative permeability ratio is decreased in the water bank (9 – 23 m in Figure 2-11).

The viscosity ratio  $\mu_o/\mu'_o$  given in **Figure 2-12** is controlled mainly by the temperature distribution and solvent dilution. As explained in section 3, the

chamber edge temperature in ES-SAGD can be much lower than in SAGD due to accumulation of gaseous solvent along the chamber edge. In the region further than 22 m, the L phase viscosity is higher in ES-SAGD as a result of the lower chamber edge temperature. However, accumulation of condensed solvent just outside the chamber edge can reduce the viscosity of the L phase to two orders of magnitude smaller values. The relative mobility ratio  $(k'_{ro}/k_o)(\mu_o/\mu'_o)$  is shown in **Figure 2-13**, which exhibits combined effects of the relative permeability and viscosity ratios.

**Figure 2-14** shows the L phase molar density ratio  $\rho'_o/\rho_o$ . Mixing of the condensed solvent with the reservoir oil reduces the mass density of the oleic phase, but it increases the molar density according to Equation 2-2. The reason is that the coinjected solvent has a lower mass density and a higher molar density compared to the original reservoir oil.

Finally, the ratio of the oil component molar flux in ES-SAGD to that in SAGD is given in **Figure 2-15** based on Equation 2-6. The denominator of Equation 2-6 becomes less significant with the distance from the chamber edge. That is, the molar flux ratio has more significant impact on the ES-SAGD oil production rate in the region closer to the chamber edge. There are two distinct regions in Figure 2-15 as follows:

- Region 1 (0 – 23 m): At distances up to 10 m, ES-SAGD shows the oil-component molar flux that is significantly increased, compared to SAGD. Accumulation of condensed solvent in this region in ES-SAGD not only reduces the viscosity of the L phase (Figure 2-12), but also results in higher relative permeability to the L phase (Figure 2-11). The descending trend of the curve follows the same trend of the relative permeability ratio.
- Region 2 (23 – 40 m): In this region, the difference in the temperature profiles (Figure 2-7) becomes the controlling parameter. The relative mobility ratio is higher for SAGD due to its lower oil viscosity in this region. The ascending trend of the curve towards unity near 40 m indicates that heat effects are diminishing.

The analysis in this section shows that increased oil production rate in ES-SAGD may result from the combined effects of bitumen dilution with solvent, solvent accumulation, and temperature distribution near the chamber edge. In this research, the ES-SAGD simulation achieves two to three times higher oil production rate than the SAGD simulation in the early to intermediate stages of the process (Figure 2-8). The faster oil recovery results in faster propagation of the ES-SAGD chamber. The lower oil production rates of ES-SAGD compared to SAGD that can occur in the late stages of the process is due to the fact that the ES-SAGD chamber has reached the side boundary of the reservoir.

### **Displacement Efficiency Enhanced by ES-SAGD**

In this section, we investigate how ES-SAGD can achieve oil saturation lower than the residual saturation on the basis of phase equilibrium in composition and temperature space in numerical simulation. Figure 2-4 shows that the ES-SAGD simulation results in 27% more oil recovery at six years, and 17% more oil recovery at 10 years, compared to the SAGD simulation. The enhanced oil recovery is a direct result of faster propagation of the ES-SAGD chamber and enhanced displacement efficiency in the chamber as shown in **Figure 2-16**. Oil saturation in the SAGD simulation studied cannot be lower than the residual saturation of 0.13. In the ES-SAGD simulation, oil saturation in the chamber can be much lower than the residual saturation. An oil saturation as low as 0.001 is observed in the region away from the well pair. In the near-well region of the ES-SAGD simulation, oil saturation is similar to that in the SAGD simulation.

Note that ES-SAGD simulation does not consider the IFT dependency of relative permeabilities. Hence, the reduced oil saturation in the chamber is not because of the IFT reduction in this simulation. This oil saturation reduction can be explained by considering interaction of solvent accumulation, temperature variation, and phase equilibrium in the ES-SAGD simulation.

We use three components in the ES-SAGD simulation in this section. They are water,  $C_5$ , and  $C_D$ ; i.e., the reservoir oil in this simulation is dead oil. The solvent compound coinjected is  $C_5$ . The properties of  $C_D$  and  $C_5$  are given in Tables 2-2 and 2-3. Three is the minimum number of components required to

explain enhanced displacement efficiency in ES-SAGD. The ternary system also allows for visual illustration of the mechanisms using simple ternary diagrams.

In an ES-SAGD chamber (Figure 2-16), there are three equilibrium phases, the L, V, and W phases. The V phase disappears at the chamber edge as illustrated in Figure 2-7. Beyond the chamber edge, there are two liquid phases, the L and W phases. Temperature decreases with the distance from the well pair. A significant change in temperature occurs near the chamber edge as given in Figure 2-7. ES-SAGD also involves significant composition variation resulting from accumulation of condensed water and solvent near the chamber edge as explained in section 2-3.

**Figures 2-17(a)-(e)** and **Table 2-4** present overall compositions, phase compositions, phase amounts, pressure, and temperature at gridblock (47, 7) at different times in the ES-SAGD simulation using water,  $C_5$ , and  $C_D$ . Gridblock (1, 1) is defined at the left-top gridblock. The bold point in each diagram represents the overall composition in that gridblock. Figure 2-17(a) shows that the initial reservoir fluid composition lies on a tie line between the L and W phases, which corresponds to the water- $C_D$  edge of the diagram. The  $C_5$  component does not exist in the gridblock yet.

Significant accumulation of condensed  $C_5$  near the chamber edge results in a gravity segregation of the condensed W phase and the solvent-rich L phase. The gridblock is affected initially by the condensed W phase (Figure 2-17(b)), and then by the solvent-rich L phase (Figure 2-17(c)). The overall mole fraction of water is as high as 0.95 in Figure 2-17(b) as also given in Table 2-4. The mole fraction of  $C_5$  also increases to 0.04, which shifts the equilibrium L phase composition towards the  $C_5$  vertex along the  $C_5$ - $C_D$  edge. In Figure 2-17(c), the L phase becomes significantly rich in  $C_5$ . The  $C_5$  mole fraction is as high as 0.97 in the L phase. This occurs because the  $C_5$  overall composition increases from 0.04 to 0.2 near the water- $C_5$  edge while moving from Figures 2-17(b) to (c). Since the overall composition in ES-SAGD varies at high concentrations of the water component, the equilibrium L phase composition is sensitive to variation of the overall composition.

After this stage, the ES-SAGD chamber contains the gridblock, where the three phases, L, V, and W, are present. During this phase transition, the L phase saturation becomes lower than the residual oil saturation. The L phase saturation is 0.6227 for Figure 2-17(c) and 0.0534 for Figure 2-17(d), and the residual saturation is 0.13 in this simulation. The reduction in the L phase saturation occurs because the L phase in Figure 2-17(c) splits into the V and L phases in Figure 2-17(d) in the presence of the invariant W phase. The small L phase saturation in Figure 2-17(d) directly comes from the geometric relationship between the overall composition and the L phase composition. This implies that the L phase has moved away from the  $C_5$  vertex, while the overall composition is located near the water- $C_5$  edge. This geometric relationship results in a small L phase mole fraction, and therefore a small L phase saturation, which is a function of molar densities and mole fractions of the equilibrium phases. From this point on, the V and L phases become less rich in  $C_5$  as illustrated in Figures 2-17(d) and (e).

The mechanism described above for reduction of the L phase saturation requires significant accumulation of solvent and phase transition near the chamber edge. Depending on how fast the condensed  $C_5$  is removed from the chamber edge as part of the draining L phase, it starts accumulating in this region. At the early stage of the process, significant reduction in the L phase saturation cannot be expected because solvent accumulation is not considerable. This explains why the region with reduced L phase saturations exists closer to the chamber edge in Figure 2-16. The gridblocks in this region are affected by the condensed  $C_5$ -rich bank when solvent accumulation has become considerable at the chamber edge.

**Figures 2-18(a)-(d)** along with **Table 2-5** illustrate the phase behavior in gridblock (9, 12), which is closer to the well pair than gridblock (47, 7) discussed above. This gridblock does not show L phase saturations lower than the residual saturation throughout the simulation. The difference between Figures 2-17 and 2-18 is that the overall mole fraction of  $C_5$  in Figure 2-18 does not go beyond 0.04, even when the gridblock is located in the condensed  $C_5$ -rich

bank. More time is required to accumulate a sufficient amount of  $C_5$  (e.g., a concentration of 0.2) depending on phase behavior of the water/bitumen/solvent mixtures. Therefore, the overall composition in Figure 2-18 does not get sufficiently close to the water- $C_5$  edge. In this case, the phase transition between two to three phases at the chamber edge cannot reduce the L phase saturation below the residual saturation.

**Table 2-6** shows the variations in the overall composition, phase amounts, pressure, and temperature at gridblock (25, 5) for the SAGD simulation with water and  $C_D$ . There is no  $C_5$  injected in this simulation. The composition variation occurs only along the water- $C_D$  edge of the ternary diagrams in **Figure 2-19**, which corresponds to the tie line representing either the L-W or L-V equilibrium. The series of ternary diagrams present that the overall mole fraction of the water component increases as soon as the cell is affected by the condensed water bank at the chamber edge. The overall composition remains more or less unchanged after this time.

The analysis in this section is based on a dead oil reservoir with three components. We confirmed that the mechanism identified is valid for the live-oil case with four components given in previous sections of this chapter.

## Conclusions

We conducted a detailed simulation study on ES-SAGD mechanisms. Explanations were given as to how ES-SAGD can achieve higher oil production rate and displacement efficiency than SAGD. The conclusions are as follows:

1. ES-SAGD can efficiently transport its solvent compounds to the chamber edge using the gaseous phase. Accumulation of the solvent component occurs in the gaseous phase inside the chamber edge, while it occurs in the oleic phase outside the chamber edge. The solvent accumulation in the early stage of ES-SAGD is not sufficient to exhibit the advantage of ES-SAGD over SAGD in term of local displacement efficiency. The solvent accumulation in the gaseous phase can result in a chamber-edge temperature that is significantly lower than that in SAGD.

2. ES-SAGD can achieve oil saturation lower than the residual saturation in the chamber. The oil saturation reduction results mainly from two processes; (1) solvent accumulation in the oleic phase outside the chamber edge, and (2) phase transition near the chamber edge (i.e., V-L-W inside and L-W outside the chamber edge). The solvent accumulation lowers the oil-component concentrations. The diluted oil is then redistributed in the gaseous and oleic phases in the presence of the water phase during the phase transition. The concentration of the oil component is high in the equilibrium oleic phase. However, the amount of the oleic phase can be significantly small, resulting in low oil saturations in the ES-SAGD chamber. We observed that the ultimate oil recovery of ES-SAGD is approximately 20% greater than that of SAGD in this research.
3. The difference between the oil production rate in ES-SAGD and that in SAGD depends mainly on three factors; i.e., solvent accumulation, temperature distribution, and bitumen dilution with solvent near the chamber edge. In the simulation cases studied, ES-SAGD exhibited two to three times faster oil production than SAGD during the early to intermediate stages of the process.

## Nomenclature

$C_1$	Methane
$C_5$	n-Pentane
$C_D$	Dead-oil component given in Table 2-2
I	Component index
J	Phase index
$j_o$	Oil-component molar flux in the oleic phase
K	Permeability
$k_r$	Relative permeability
L	Oleic phase
u	Velocity
V	Gaseous phase
W	Aqueous phase
x	Mole fraction
$\mu$	Viscosity
$\rho$	Molar density

## Abbreviations

SAGD	Steam-assisted gravity drainage
ES-SAGD	Expanding-solvent-steam assisted gravity drainage
IFT	Interfacial tension

<b>Properties</b>	<b>Values</b>
Porosity	33%
Horizontal permeability	4000 md
Vertical permeability	3000 md
Initial reservoir pressure at depth of 500 m	1500 kPa
Initial reservoir temperature	13°C
Initial oil saturation	0.75
Initial water saturation	0.25
Three-phase relative permeability model (CMG 2011)	Stone's model II
Formation compressibility	1.8E-5 1/kPa
Rock heat capacity (Butler, 1997)	2600 kJ/m <sup>3</sup> °C
Rock thermal conductivity (Butler, 1997)	660 kJ/m day °C
Over/underburden heat capacity (Butler, 1997)	2600 kJ/m <sup>3</sup> °C
Over/underburden thermal conductivity (Butler, 1997)	660 kJ/m day °C
Bitumen thermal conductivity (Butler, 1997)	11.5 kJ/m day °C
Gas thermal conductivity (Yazdani <i>et al.</i> , 2011)	2.89 kJ/m day °C
Water thermal conductivity	1500 kJ/m day °C

<b>Properties</b>	<b>Values</b>
Molecular weight	594.6 kg/kgmole
Critical pressure	785.98 kPa
Critical temperature	817.75°C
Acentric factor	1.361
Normal boiling point	663.95°C
Specific Gravity	1.077

<b>Properties</b>	<b>Values</b>
Molecular weight	72.1 kg/kgmole
Critical pressure	3374.12 kPa
Critical temperature	196.45°C
Acentric factor	0.251
Normal boiling point	36.05°C

**Table 2-4. Overall composition, phase amounts, pressure, and temperature for Figures 2-17 (a)-(e)**

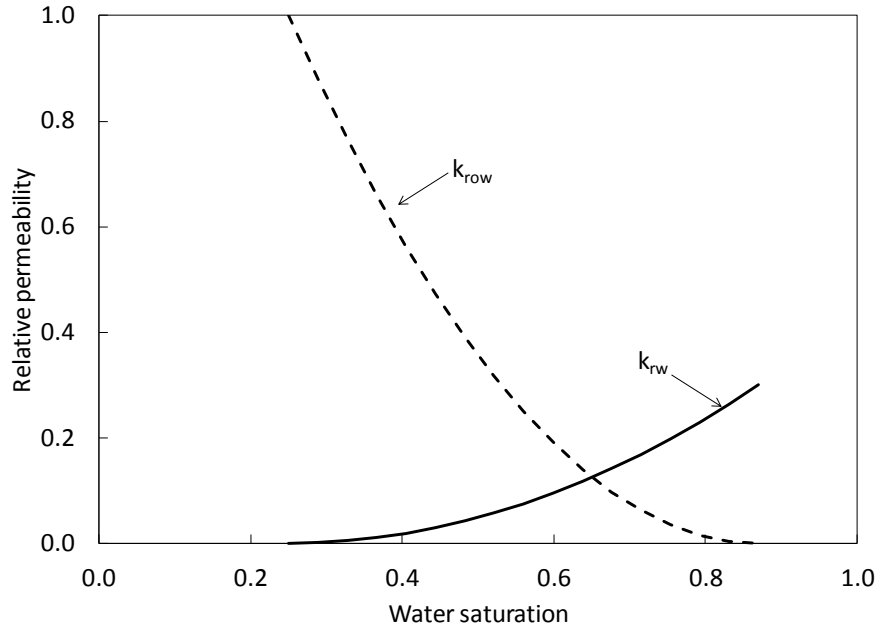
<b>Properties</b>	<b>(a)</b>	<b>(b)</b>	<b>(c)</b>	<b>(d)</b>	<b>(e)</b>
Overall mole fraction of water	0.9145	0.9523	0.7873	0.9688	0.9824
Overall mole fraction of C <sub>D</sub>	0.0855	0.0055	0.0071	0.0053	0.0060
Overall mole fraction of C <sub>5</sub>	0.0000	0.0422	0.2057	0.0259	0.0116
Mole fraction of the W phase	0.9145	0.9523	0.7873	0.9514	0.9525
Mole fraction of the L phase	0.0855	0.0477	0.2127	0.0089	0.0070
Mole fraction of the V phase	0.0000	0.0000	0.0000	0.0397	0.0405
Saturation of the W phase	0.2580	0.6794	0.3273	0.2913	0.2645
Saturation of the L phase	0.7420	0.3206	0.6727	0.0534	0.0479
Saturation of the V phase	0.0000	0.0000	0.0000	0.6553	0.6876
Temperature (°C)	13.1	121.8	160.4	185.4	211.0
Pressure (kPa)	2153	2666	2667	2669	2689

**Table 2-5. Overall composition, phase amounts, pressure, and temperature for Figures 2-18(a)-(d).**

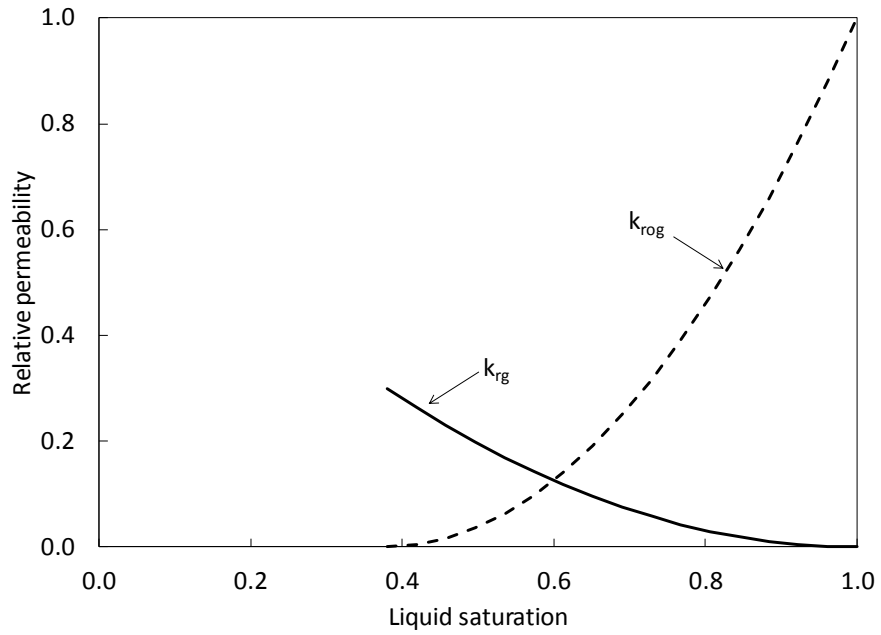
<b>Properties</b>	<b>(a)</b>	<b>(b)</b>	<b>(c)</b>	<b>(d)</b>
Overall mole fraction of water	0.9111	0.9512	0.9671	0.9808
Overall mole fraction of C <sub>D</sub>	0.0889	0.0098	0.0268	0.0173
Overall mole fraction of C <sub>5</sub>	0.0000	0.0390	0.0061	0.0019
Mole fraction of the W phase	0.9111	0.9512	0.9490	0.9477
Mole fraction of the L phase	0.0889	0.0488	0.0294	0.0177
Mole fraction of the V phase	0.0000	0.0000	0.0216	0.0346
Saturation of the W phase	0.2501	0.6326	0.3115	0.2612
Saturation of the L phase	0.7499	0.3674	0.2469	0.1299
Saturation of the V phase	0.0000	0.0000	0.4416	0.6089
Temperature (°C)	30.4	163.8	217.6	225.0
Pressure (kPa)	2698	2696	2696	2707

**Table 2-6. Overall composition, phase amounts, pressure, and temperature for Figures 2-19 (a)-(c)**

<b>Properties</b>	<b>(a)</b>	<b>(b)</b>	<b>(c)</b>
Overall mole fraction of water	0.9147	0.9779	0.9823
Overall mole fraction of C <sub>D</sub>	0.0853	0.0221	0.0177
Mole fraction of the L phase	0.0853	0.0221	0.0177
Mole fraction of the V and W phase	0.9147	0.9779	0.9823
Saturation of the W phase	0.2586	0.6222	0.2567
Saturation of the L phase	0.7414	0.3778	0.1300
Saturation of the V phase	0.0000	0.0000	0.6133
Temperature (°C)	13.2	226.9	227.3
Pressure (kPa)	2142	2681	2701



(a)



(b)

**Figure 2-1. Relative permeability curves used in the simulation cases.**

(a) the water-oil system and (b) the oil-gas system.

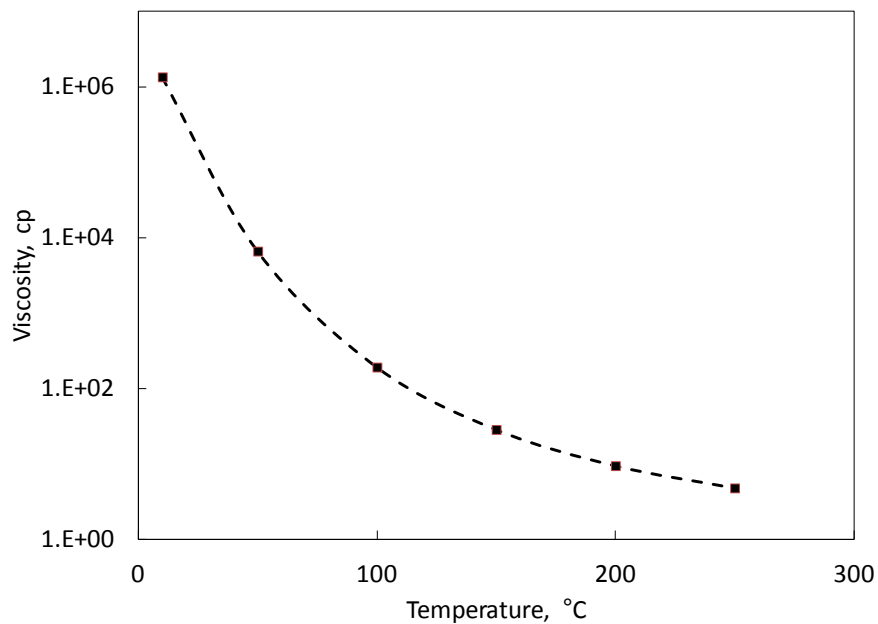


Figure 2-2. Viscosity of bitumen (the  $C_D$  component in Table 2-2) at different temperatures.

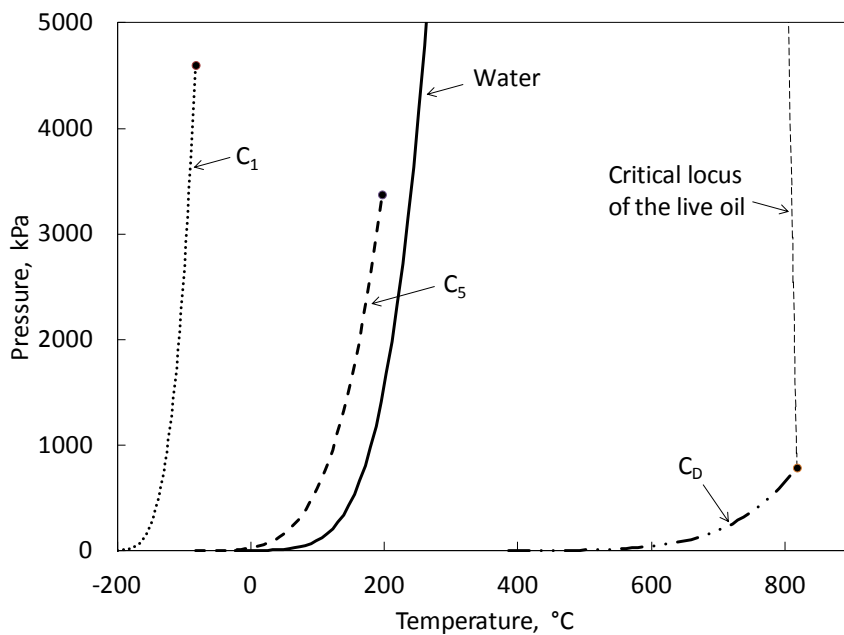
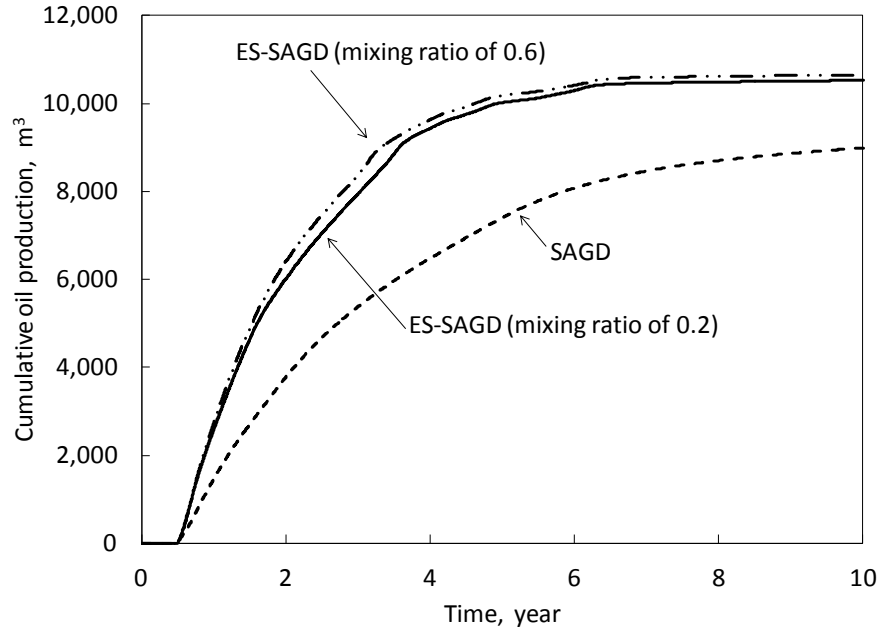


Figure 2-3. Vapor pressure curves of  $C_1$ ,  $C_5$ ,  $C_D$ , and water, and the critical locus of the live oil (a mixture of  $C_1$  4% and  $C_D$  96%).

The critical locus of the live oil at high  $C_1$  concentrations cannot be found using the PR EOS within the pressure range shown. The black circles indicate the critical points of the hydrocarbon components.



**Figure 2-4. Cumulative oil recoveries in the SAGD and ES-SAGD simulations.**

The amount of solvent recovered is not considered for the ES-SAGD plots. The ES-SAGD simulation shows higher oil production rate and more oil recovery than the SAGD simulation. The two ES-SAGD cases use different mixing ratios of oil and solvent to generate K-value tables. The effect of the mixing ratio used is insignificant on oil recovery prediction in this research.

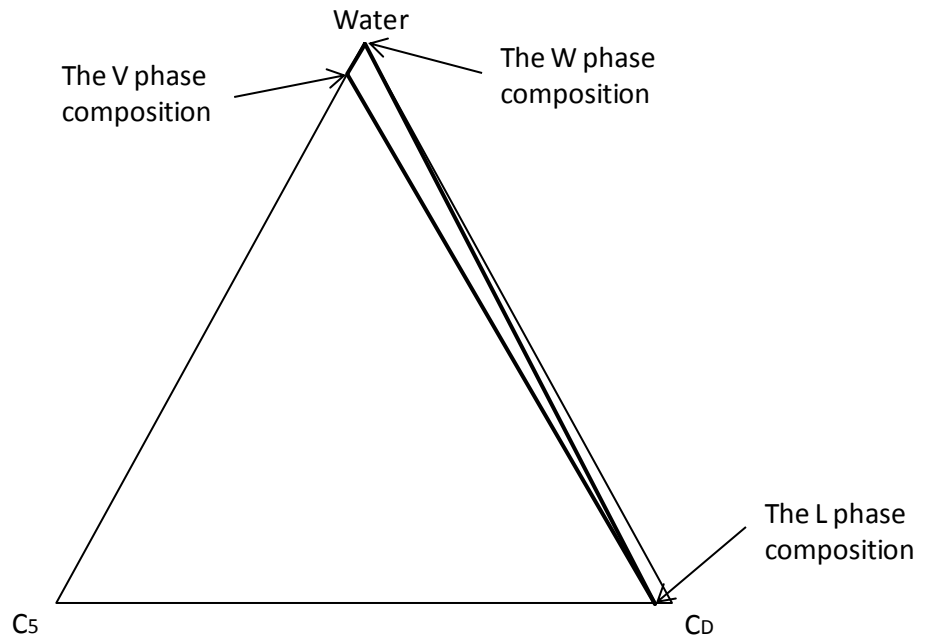


**Figure 2-5. Tie triangle for the water, C<sub>5</sub>, and C<sub>D</sub> mixtures at 224.5°C and 2715 kPa (conditions inside the chamber).**

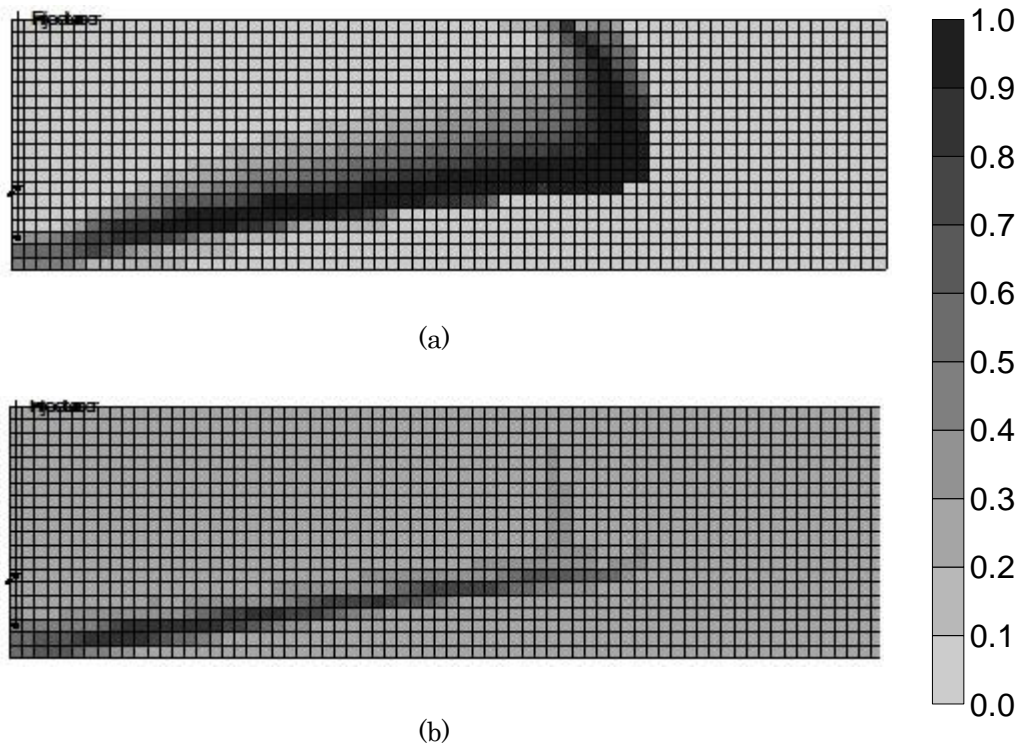
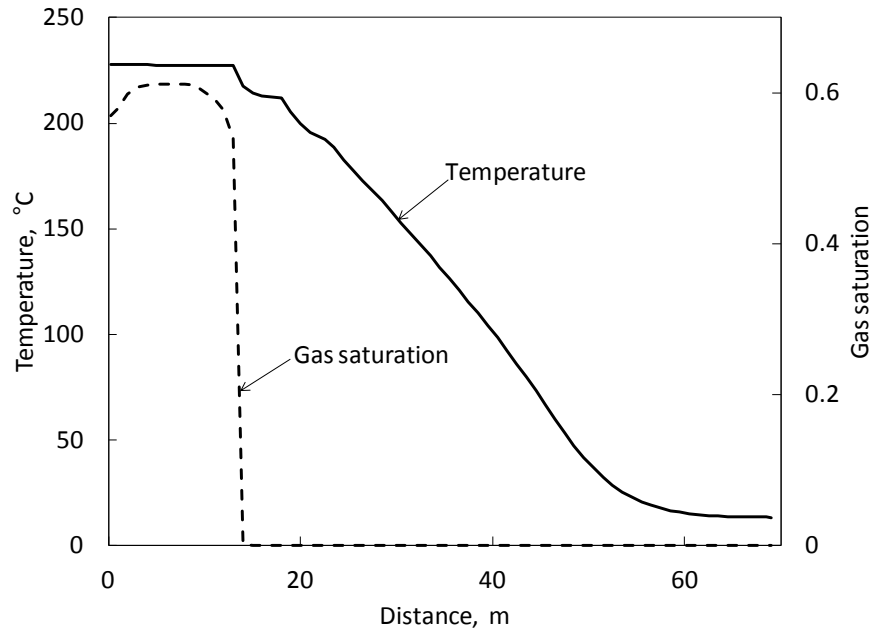
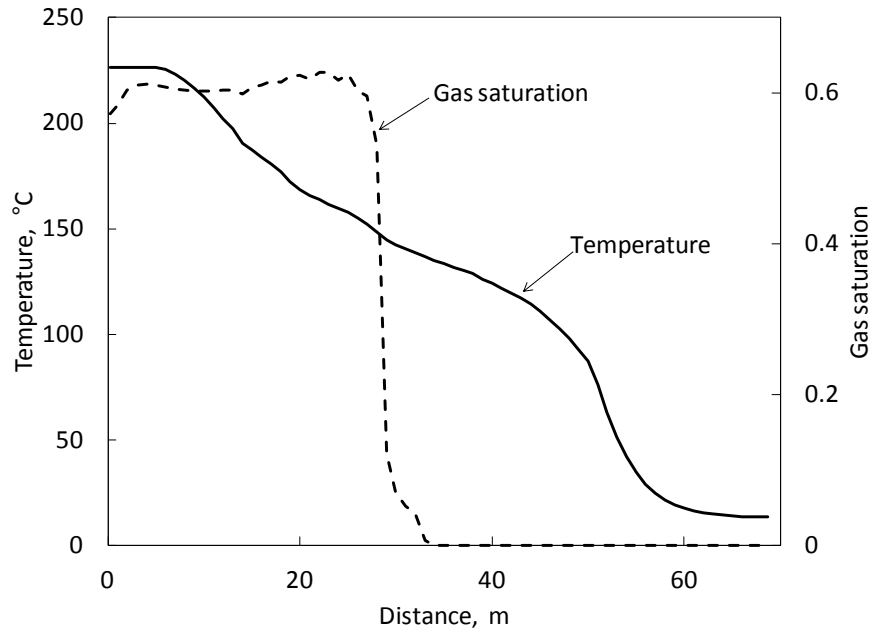


**Figure 2-6. Gravity segregation of condensed water and solvent banks at 27 months in the ES-SAGD simulation.**

(a) Distribution of the C<sub>5</sub> mole fraction in the L phase, (b) Distribution of the W phase saturation.



(a)



(b)

**Figure 2-7. Distribution of the V phase saturation and temperature the 14<sup>th</sup> row at 27 months**

(a) the SAGD simulation, and (b) the ES-SAGD simulation. The chamber edge is defined where the V phase saturation becomes zero. The chamber-edge temperature for the ES-SAGD simulation is 87°C lower than that for the SAGD simulation.

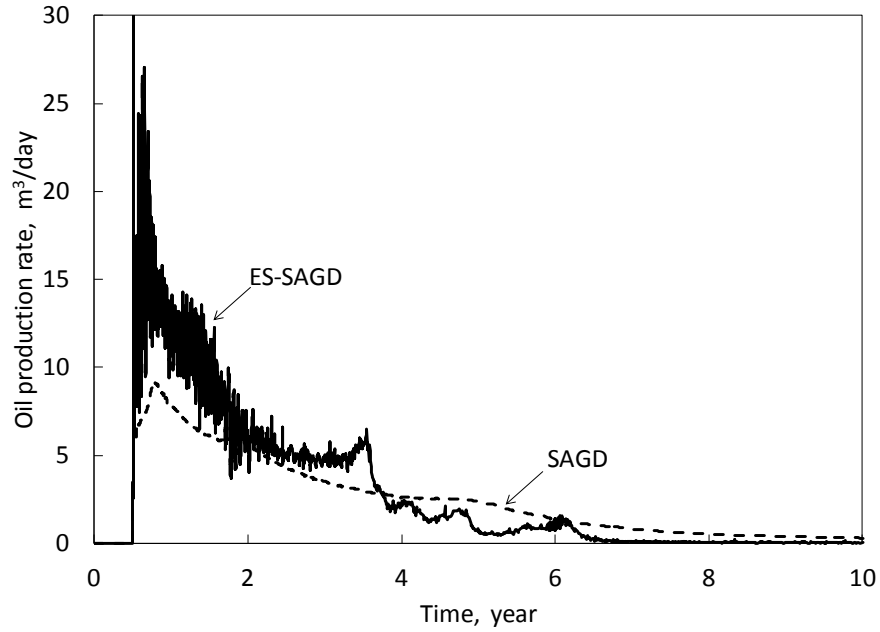


**Figure 2-8. Oil production rates in the SAGD and ES-SAGD simulations**

The production of  $C_5$  as part of oil is excluded for the ES-SAGD simulation. The ES-SAGD simulation exhibits two to three times higher oil rate than the SAGD simulation in the early times. The ES-SAGD oil rate becomes lower than the SAGD oil rate after the ES-SAGD chamber reaches the side boundary of the reservoir. SAGD chamber is slower and has not reached to the side boundary of the reservoir at this moment; thus, it still has some oil ahead of it to recover.

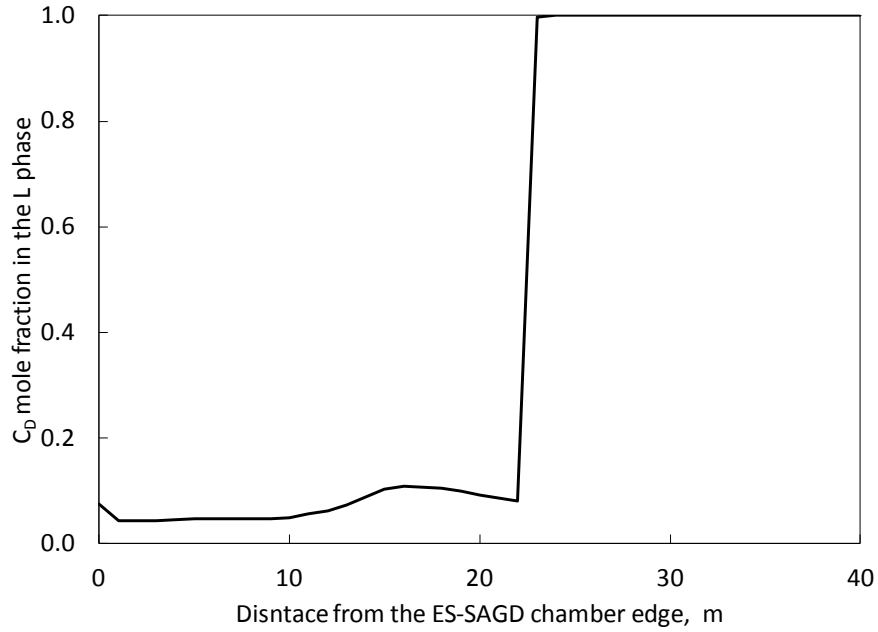


**Figure 2-9. The  $C_D$  mole fraction in the L phase at different distances from the chamber edge in the 14<sup>th</sup> row at 27 months in the ES-SAGD simulation.**

It can be as small as 0.05 in the condensed-C5 bank located 0 - 15 m outside the chamber edge.

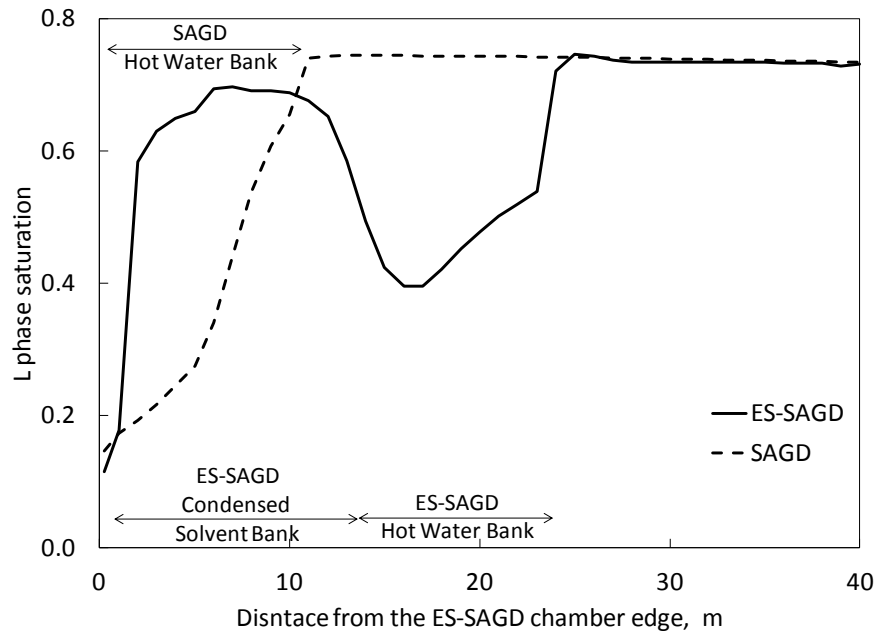


**Figure 2-10. Distribution of the L phase saturation at different distances from the chamber edge in the 14<sup>th</sup> row at 27 months in the ES-SAGD and SAGD simulations.**

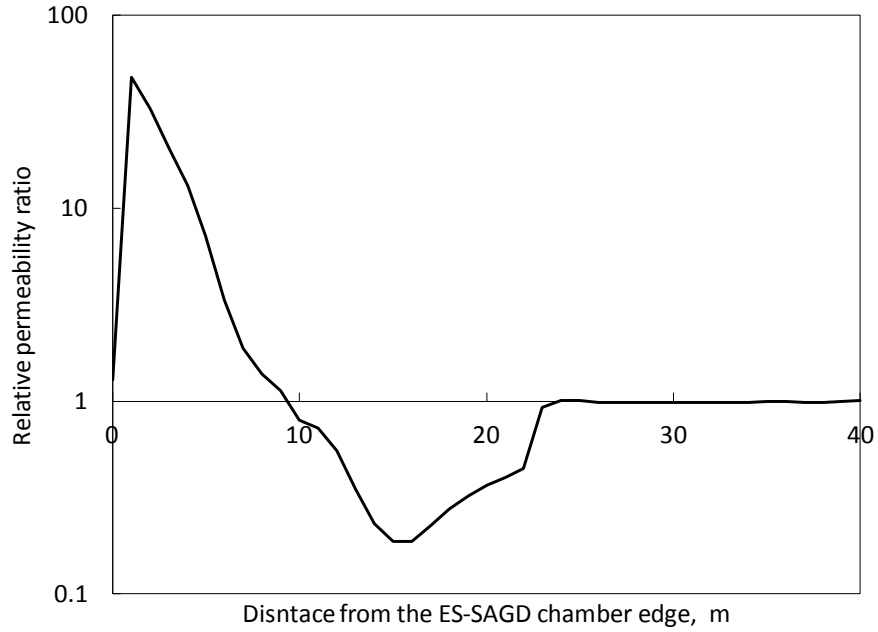


**Figure 2-11. Relative permeability ratio at different distances from the chamber edge in the 14<sup>th</sup> row at 27 months.**

The relative permeability ratio is defined by Equation 2-6.

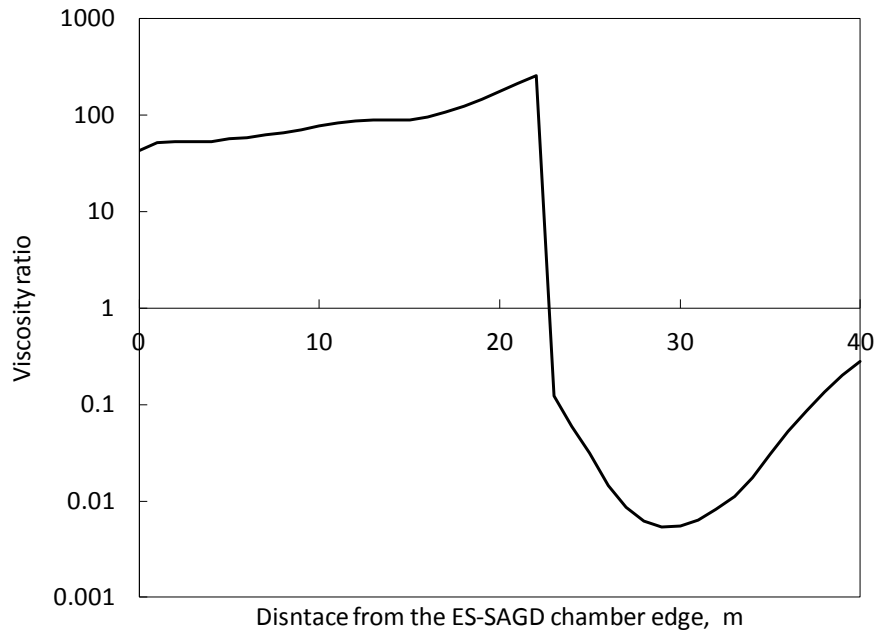


**Figure 2-12. Viscosity ratio at different distances from the chamber edge in the 14<sup>th</sup> row at 27 months.**

The viscosity ratio is defined by Equation 2-6.

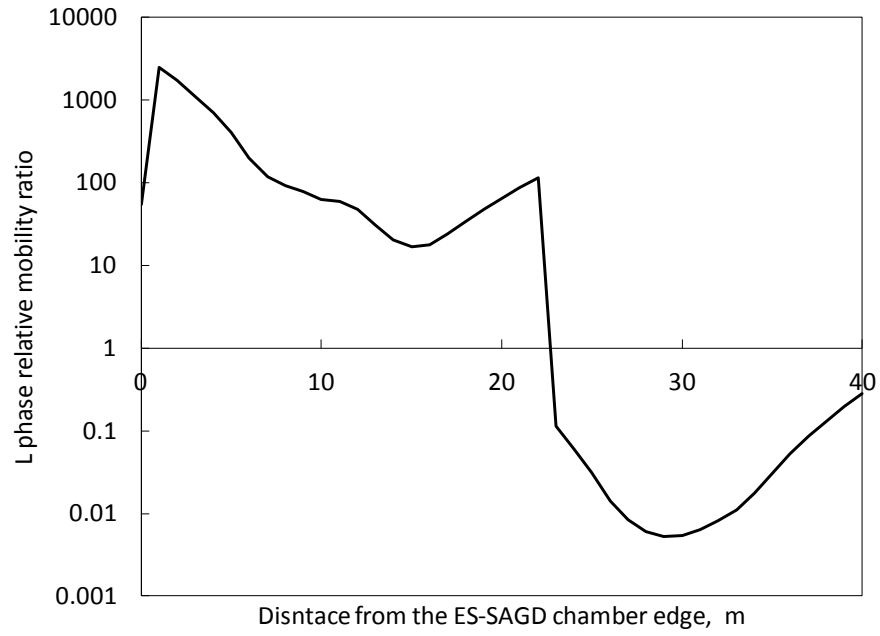


**Figure 2-13. Relative mobility ratio at different distances from the chamber edge in the 14<sup>th</sup> row at 27 months.**

The relative mobility ratio is defined by Equation 2-6.

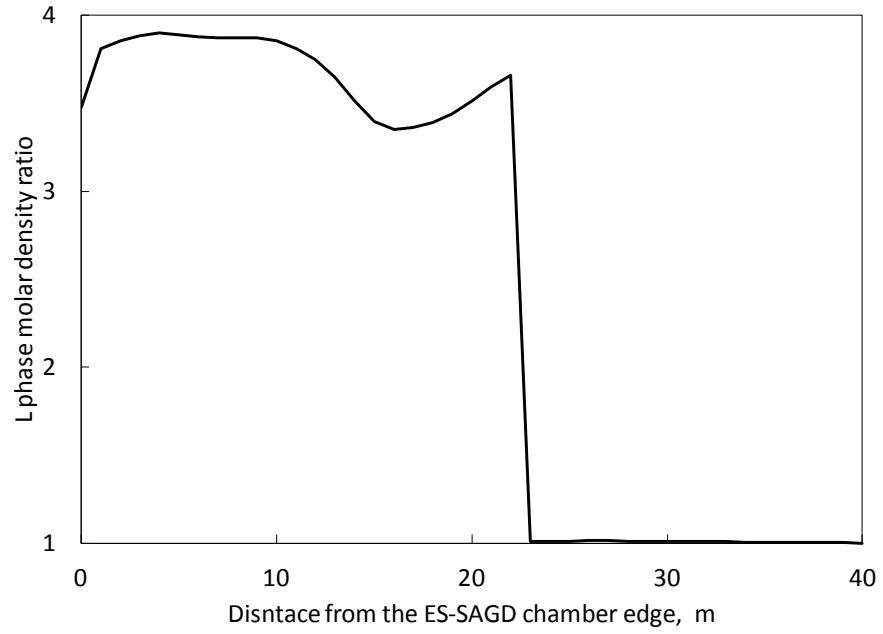


**Figure 2-14. Molar density ratio at different distances from the chamber edge in the 14<sup>th</sup> row at 27 months.**

The molar density ratio is defined by Equation 2-6.

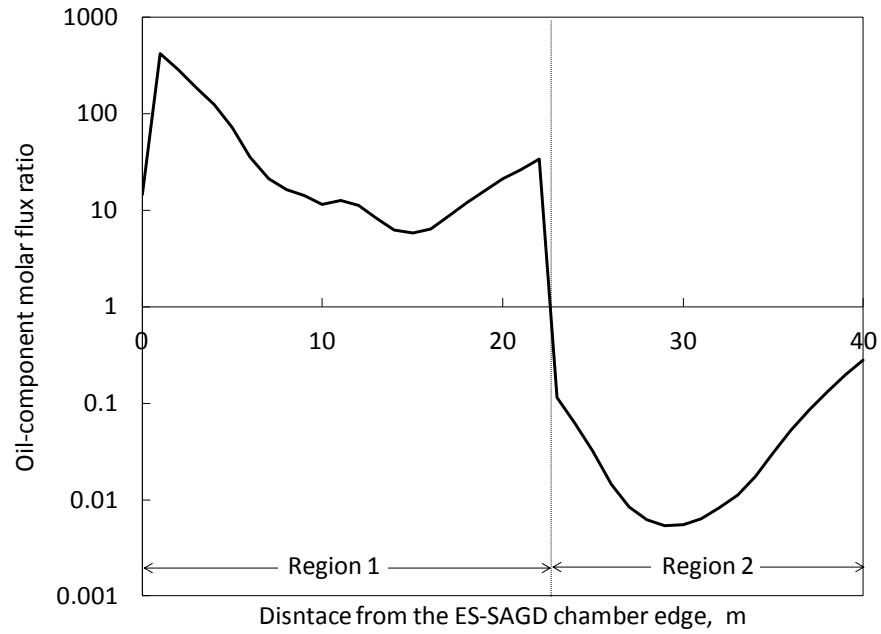


**Figure 2-15. Oil-component molar flux ratio at different distances from the chamber edge in the 14<sup>th</sup> row at 27 months.**

The oil-component molar flux ratio is defined in Equation 2-6.

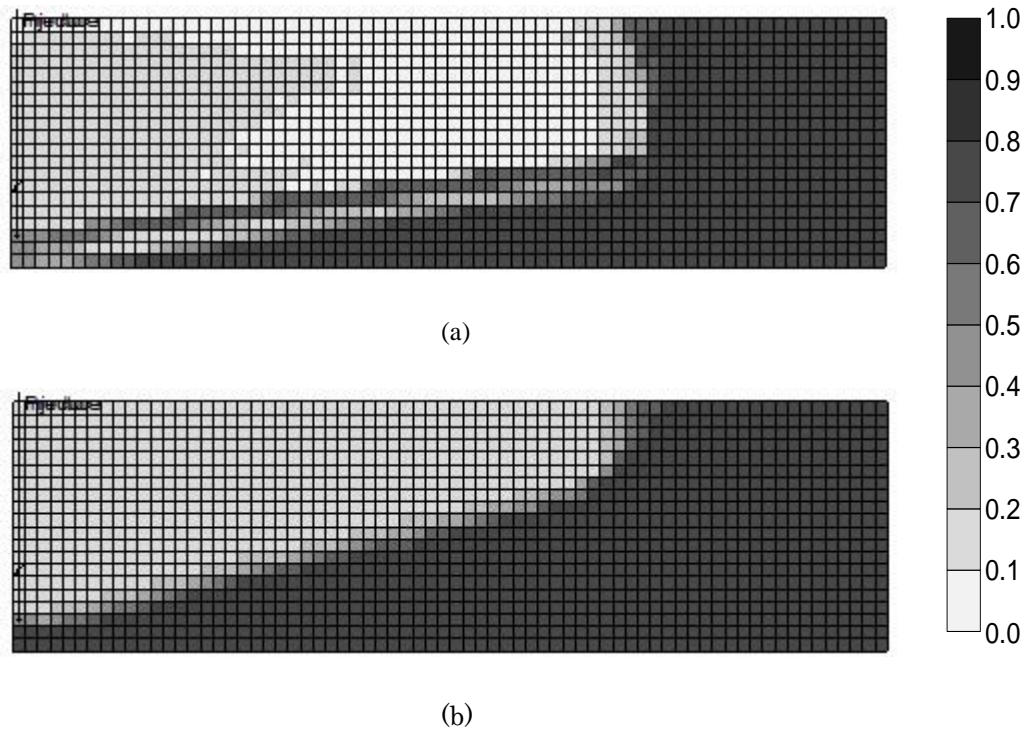
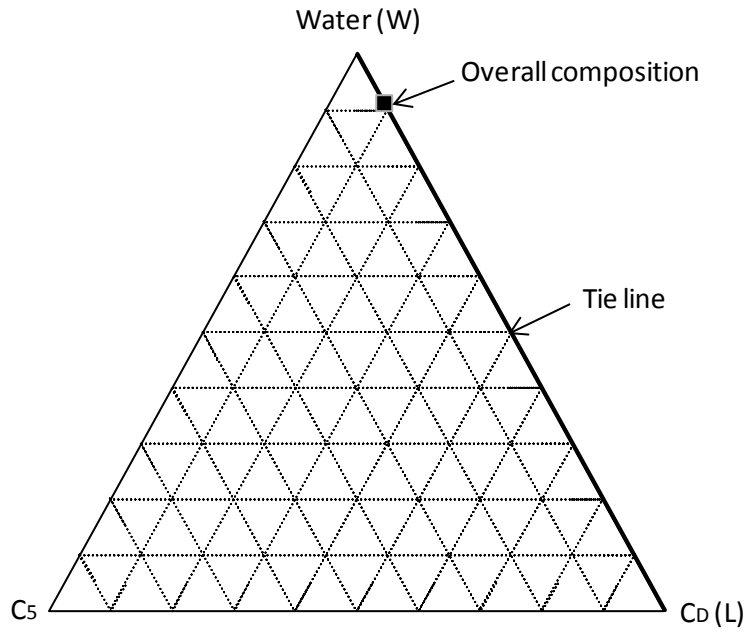
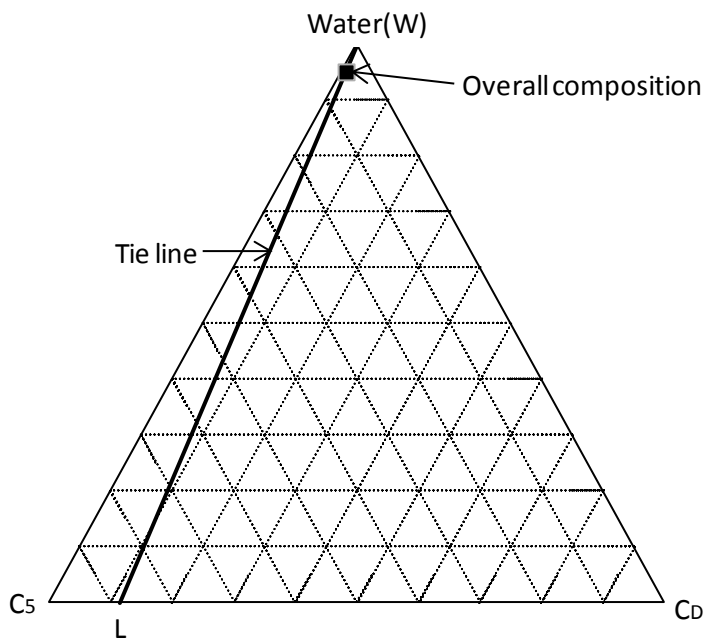


**Figure 2-16. Distribution of the L phase saturation at 27 months.**

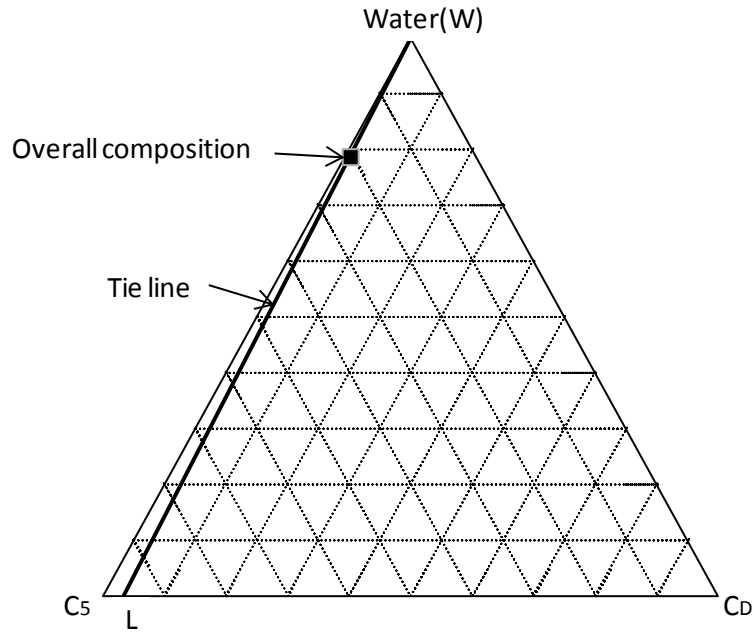
(a) SAGD simulation, and (b) the ES-SAGD simulation. The L phase saturation near the ES-SAGD chamber edge is substantially lower than the residual oil saturation 0.13. The L phase saturation in the SAGD chamber and in the near-well region of the ES-SAGD chamber is about 0.13.



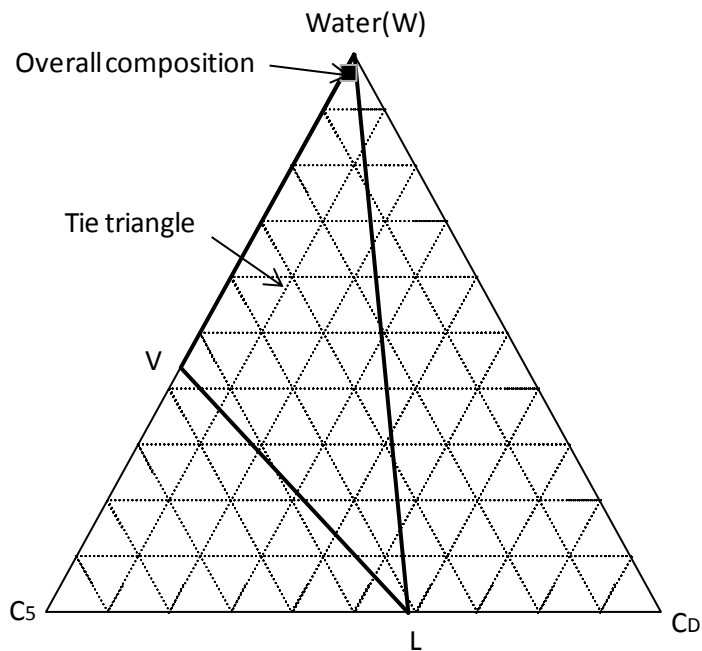
(a) 6 months from the start of the three-component ES-SAGD simulation. Gridblock (47, 7) is not affected by  $C_5$ .



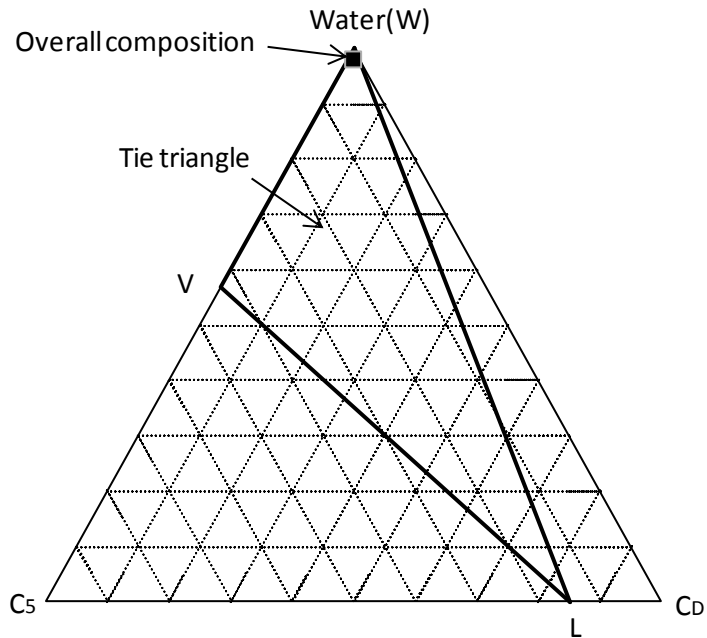
(b) 12.5 months from the start of the three-component ES-SAGD simulation. Gridblock (47, 7) is in the condensed water bank.



(c) 15 months from the start of the three-component ES-SAGD simulation. Gridblock (47, 7) is in the condensed  $C_5$  bank.

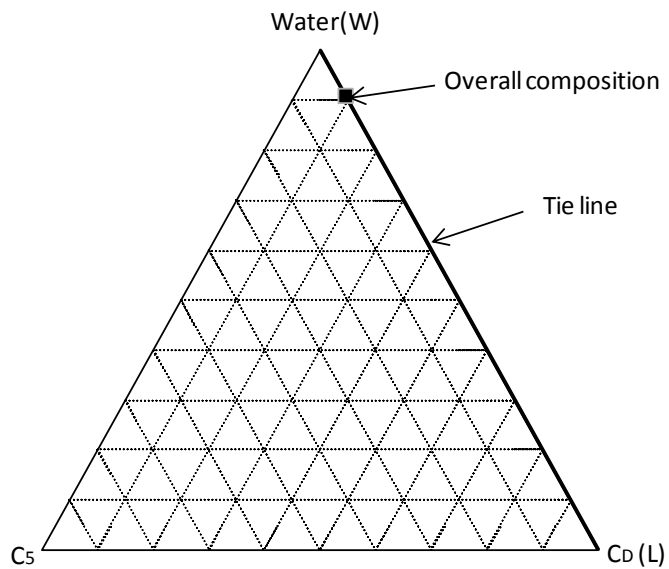


(d) 18 months from the start of the three-component ES-SAGD simulation. Gridblock (47, 7) is just inside the ES-SAGD chamber. The L phase in the previous figure is split into the V and L phases in the presence of the invariant W phase.

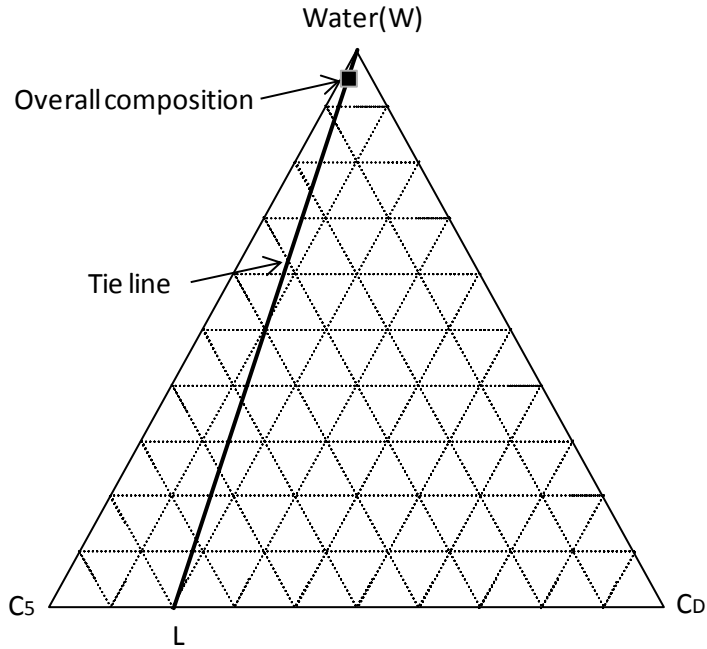


(e) 2 years from the start of the three-component ES-SAGD simulation. Gridblock (47, 7) is inside the ES-SAGD chamber. The V and L phases become less rich in  $C_5$ .

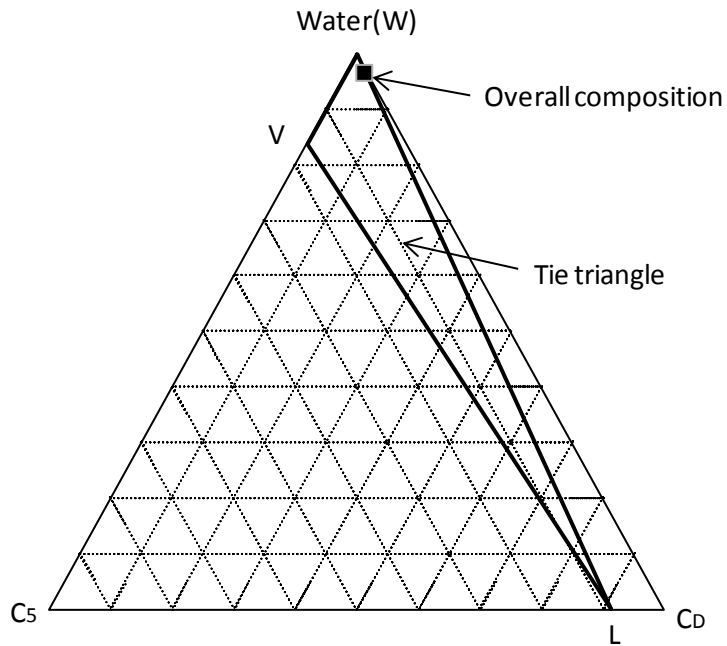
**Figure 2-17. Overall composition and phase equilibrium at gridblock (47, 7) in the ES-SAGD simulation using the water,  $C_5$ , and  $C_D$  components.**



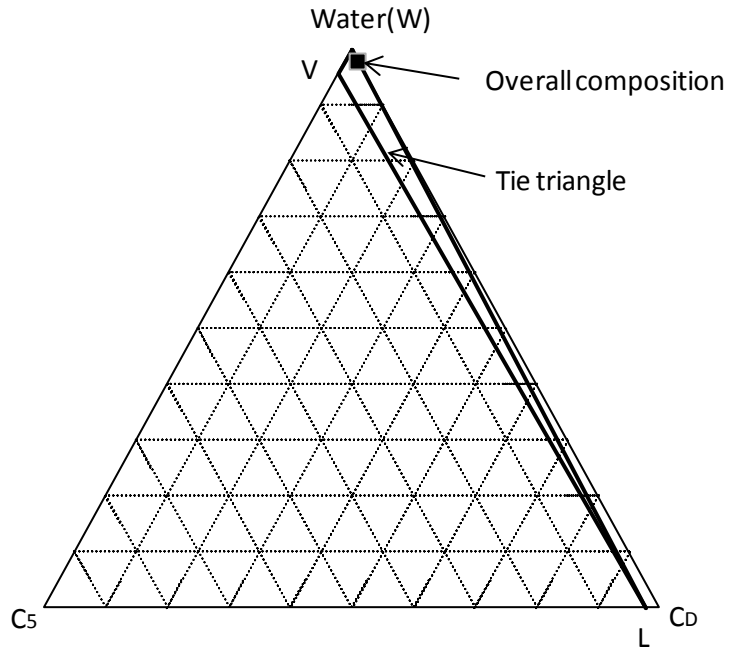
(a) 2 months from the start of the three-component ES-SAGD simulation. Gridblock (9, 12) is not affected by  $C_5$ .



(b) 3.5 months from the start of the three-component ES-SAGD simulation. The C<sub>5</sub> concentration in gridblock (9, 12) cannot be as high as in gridblock (47, 7) given in Figure 2-17.

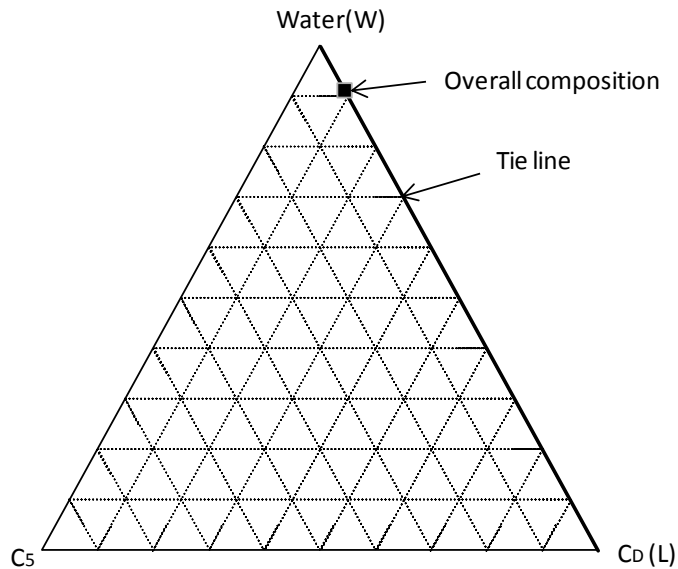


(c) 4 months from the start of the three-component ES-SAGD simulation. The C<sub>D</sub> concentration in the tie triangle is not as small as in gridblock (47, 7) given in Figure 2-17, resulting in a higher L phase mole fraction.

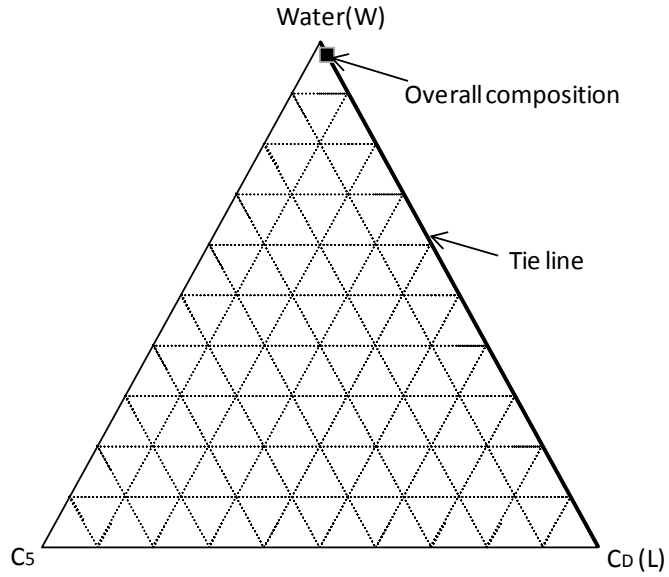


(d) 18 months from the start of the three-component ES-SAGD simulation. The  $C_D$  concentration in the tie triangle is not as small as in gridblock (47, 7) given in Figure 2-17, resulting in a higher L phase mole fraction.

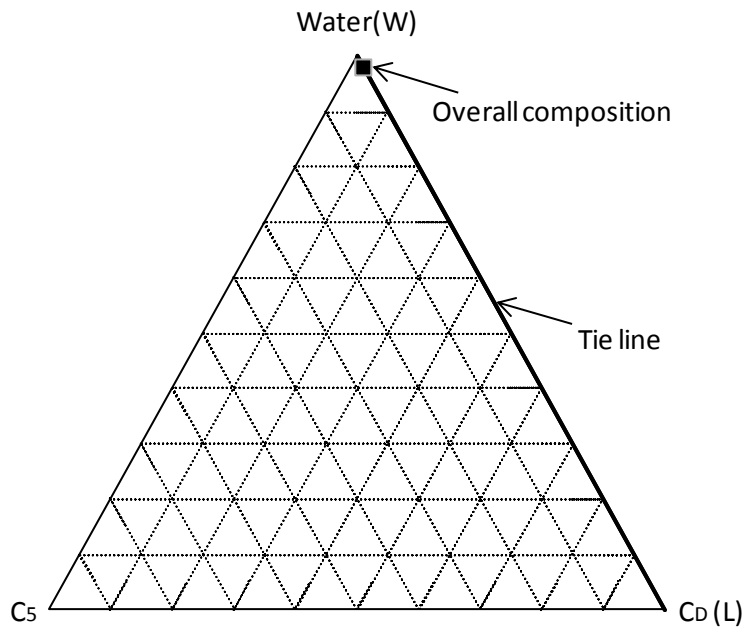
**Figure 2-18. Overall composition and phase equilibrium at gridblock (9, 12) in the ES-SAGD simulation using the water,  $C_5$ , and  $C_D$  components.**



(a) 4 months from the start of the two-component SAGD simulation.



(b) 11 months from the start of the two-component SAGD simulation.



(c) 2 years from the start of the two-component SAGD simulation.

**Figure 2-19. Overall composition and phase equilibrium at gridblock (25, 5) in the SAGD simulation using the water and C<sub>D</sub> components (without the C<sub>5</sub> component).**

## References

- Butler, R.M., 1997. Thermal Recovery of Oil and Bitumen. Prentice Hall.
- Computer Modelling Group (CMG) Ltd. STARS User Manual. Version 2011. Calgary, Alberta, Canada, 2011.
- Deng, X., Huang, H., Zhao, L., Law, D.H.-S., Nasr, T.N., 2010. Simulating the ES-SAGD Process With Solvent Mixture in Athabasca Reservoirs. *Journal of Canadian Petroleum Technology* **49** (1): 38-46.
- Gates, I.D., 2007. Oil phase viscosity behavior in Expanding-Solvent Steam-Assisted Gravity Drainage. *Journal of Petroleum Science and Engineering* **59** (1-2): 123-134.
- Ivory, J., Zheng, R., Nasr, T., Deng, X., Beaulieu, G., Heck, G., 2008. Investigation of Low Pressure ES-SAGD. Paper SPE 117759 presented at 2008 SPE International Thermal Operations and Heavy Oil Symposium, Calgary, Alberta, Canada, October 20-23.
- Kumar, A., Okuno, R., 2012. Fluid Characterization using an EOS for Compositional Simulation of Enhanced Heavy-Oil Recovery. Submitted for *SPE J.* on June 18.
- Li, W., Mamora, D.D., 2010. Phase Behavior of Steam with Solvent Coinjection under Steam Assisted Gravity Drainage (SAGD) Process. Paper SPE 130807 presented at the SPE EUROPEC/EAGE Annual Conference and Exhibition, Barcelona, Spain, June 14-17.
- Li, W., Mamora, D.D., Li, Y., 2011a. Light-and Heavy-Solvent Impacts on Solvent-Aided-SAGD Process: A Low-Pressure Experimental Study. *Journal of Canadian Petroleum Technology* **50**(4): 19-30.
- Li, W., Mamora, D.D., Li, Y., 2011b. Solvent-Type and -Ratio Impacts on Solvent-Aided SAGD Process. *SPE Reservoir Engineering and Evaluation* **14** (3): 320-331.
- Mehrotra, A.K., Svrcek, W.Y., 1986. Viscosity of Compressed Athabasca Bitumen. *Canadian Journal of Chemical Engineering* **64** (5): 844-847.
- Mehrotra, A.K., Svrcek, W.Y., 1987. Corresponding States Method for Calculating Bitumen Viscosity. *Journal of Canadian Petroleum Technology* **26** (5): 60-66
- Nasr, T.N., Beaulieu, G., Golbeck, H., and Heck, G., 2003. Novel Expanding Solvent-SAGD Process “ES-SAGD”. *Journal of Canadian Petroleum Technology* **42** (1): 13-16.
- Nasr, T., Isaacs, E., 2001. Process for Enhancing Hydrocarbon Mobility Using a Steam Additive. U.S. Patent 6230814.
- Peng, D.-Y., Robinson, D.B., 1976. A New Two-Constant Equation of State. *Industrial and Engineering Chemistry Fundamentals* **15** (1): 59-64.
- Rachford, Jr., H.H., Rice, J.D., 1952. Procedure for Use of Electronic Digital Computers in Calculating Flash Vaporization Hydrocarbon Equilibrium. *Petroleum Transactions, AIME* **195**: 327-328.
- Yazdani, A., Alvestad, J., Kjonsvik, D., Gilje, E., Kowalewski, E., 2011. A Parametric Simulation Study for Solvent Co-injection Process in Bitumen Deposits. Paper SPE

148804 presented at the Canadian Unconventional Resources Conference, Calgary, Alberta, Canada, November 15-17.

## **CHAPTER 3 : OPTIMAL APPLICATION CONDITIONS FOR STEAM-SOLVENT COINJECTION**

A version of this chapter was presented at the SPE Heavy Oil Conference Canada held in Calgary, Alberta, Canada, 11–13 June 2013 and is under review for publication in SPE Reservoir Evaluation & Engineering.

## **Introduction**

The main challenge in bitumen and heavy-oil recovery is their low mobility at initial reservoir conditions. Steam-assisted gravity drainage (SAGD) is the most widely used method for bitumen and heavy-oil recovery in western Canada. SAGD uses pairs of horizontal wells and an injector drilled approximately 5 m above a producer for each pair. High quality steam is injected into the reservoir and forms a steam chamber. Injected steam releases latent heat on contact with low-temperature fluids and rock near the chamber edge. Heated bitumen then drains towards the producer using gravity (Butler 1997). Disadvantages of SAGD include high energy demands and associated environmental costs.

Coinjection of solvent and steam was proposed by Nasr and Isaacs (2001) under the commercial name of expanding-solvent SAGD (ES-SAGD). Their objective was to improve the efficiency of SAGD by taking advantage of both heat and solvent dilution effects on oil viscosity. Coinjection has been studied under various commercial names since then, such as solvent-aided process (SAP), solvent-aided SAGD (SA-SAGD), steam alternating solvent (SAS), and liquid addition to steam enhanced recovery (LASER). Improved oil production rates and lower steam-oil ratios (SOR) in coinjection have been reported in the literature (Nasr et al. 2003; Gates 2007; Ivory et al. 2008, Li et al. 2011ab; Yazdani et al. 2011); they include EnCana's SAP pilot in Senlac (Gupta et al. 2005; Gupta and Gittins 2006) and in Cristina Lake (Gupta and Gittins 2006), and Imperial Oil's LASER pilot in Cold Lake (Leaute 2002; Leaute and Carey 2005).

There also exist reports of incremental oil recovery by coinjection compared to steam-only injection (Redford and McKay 1980; Li and Mamora 2010; Ardali et al. 2012a; Mohammadzadeh et al. 2012; Jha et al. 2012). Keshavarz et al. (2012) explained detailed mechanisms responsible for the enhanced oil production rate and local displacement efficiency in steam-solvent coinjection.

In addition to successful tests of coinjection, there have also been less successful results found; for example, Nexen's ES-SAGD test in Long Lake in

2006 were less encouraging than the pilot tests by EnCana and Imperial Oil (Orr 2009; Orr et al. 2010), where a diluent containing hydrocarbons from  $C_7$  to  $C_{12}$  was coinjected with steam. Suncor's ES-SAGD project in the Firebag area exhibited little improvement in the oil production rate, and naphtha was coinjected with steam (Orr 2009). Low volatility of the coinjected solvent/diluent has been considered to be responsible for these less encouraging results.

Coinjection of steam and solvent involves multiphase behavior of solvent-water-bitumen mixtures and its interaction with non-isothermal flow under heterogeneities. Due to its complexity, most of the studies on coinjection design in the literature focus on selection of solvent and its concentration to improve the oil production rate under simplified reservoir conditions. Nevertheless, there are various different proposals on these two design parameters in the literature and many of them are specific to their reservoir or experimental conditions. Different reservoirs, however, should have different optimum sets of operation parameters for successful coinjection. Thus, the main objective of this chapter is to demonstrate a systematic workflow to optimize single-component solvent and its concentration in terms of oil production rate, ultimate oil recovery, and solvent retention (or solvent losses) for given reservoir conditions. To emphasize the diversity of prior proposals and the importance of our research, a brief review of prior studies on coinjection design is provided below.

Nasr et al. (2003) considered that the condensation temperatures of solvent and water should be similar to each other at the operational pressure. The idea was to have solvent and steam condense simultaneously near the chamber edge. This criterion has been used in many studies, and  $C_6$  or  $C_7$  were pointed out as the optimum solvent in most of these studies (e.g., Li and Mamora 2010; Hosseinijad Mohabati et al. 2010; Li and Mamora 2011b; Yazdani et al. 2011; Ardali et al. 2012a). A closer investigation of steam-solvent phase behavior by Dong (2012) showed that the criterion of Nasr et al. (2003) does not result in simultaneous condensation of water and solvent at the chamber edge. He stated

that gradual condensation of steam along the temperature gradient occurs inside the chamber.

In addition, solvents resulting in the highest drainage rates in other studies are not always consistent with Nasr et al. (2003). Redford and McKay (1980) investigated normal hydrocarbons from methane to pentane and a number of commercial hydrocarbon blends as additives to low-pressure steam. They reported that coinjection of heavier hydrocarbon blends resulted in improved bitumen production from Athabasca oil sand, provided enough light blends were also present. They properly made mention of the dependency of solvent selection on PVT properties of the fluid system. Promising results from addition of heavy solvents to steam were also reported by Li and Mamora (2011b) in their simulation study of C<sub>3</sub>, C<sub>5</sub>, C<sub>7</sub>, and C<sub>12</sub> coinjection with steam. Shu and Hartman (1988) investigated the effects of the solvent type and its concentration on oil recovery by categorizing solvents into three groups: light, medium and heavy solvents. Their results showed that medium solvents (i.e., naphtha) gave the best results in the total oil production at a somewhat greater solvent loss. They observed little improvement in oil recovery with heavy solvents (C<sub>16</sub> to C<sub>20</sub>).

Some studies indicated a superior performance for lighter solvents. For example, Govind et al. (2008) reported an additional improvement in the oil production rate when C<sub>4</sub> is coinjected with steam over those obtained from coinjection of C<sub>5</sub> and heavier hydrocarbons at the operating pressure of 4000 kPa. Ardali et al. (2010) studied coinjection of n-alkenes from C<sub>3</sub> to C<sub>7</sub> with steam and concluded that C<sub>4</sub> was suitable for coinjection at Cold Lake at the operating pressure of 3400 kPa, and heavier solvents were suitable for Athabasca reservoirs at the operating pressure of 2100 kPa.

Many proposals also exist for coinjection procedures with different concentrations of coinjected solvents (Gates and Chakrabarty 2008; Gupta and Gittins 2007ab; Edmunds et al. 2010; Jiang et al. 2012). Some of the research considered how to minimize solvent retention in the reservoir (or solvent loss). The experimental and simulation results of Jiang et al. (2012) suggested the maximization of solvent loading in the injection stream during the coinjection

period and then continuing the process under the SAGD mode after a certain period of coinjection. This procedure was favorable for solvent recovery while maintaining comparable oil production. Gates and Gutek (2008) and Gupta and Gittins (2007b) investigated the effects of heavy and light solvents sequencing on the optimization of coinjection. They showed that progressing from heavy solvents to lighter ones had the advantage of recovering the most expensive solvents.

The diversity of prior proposals described above indicates the need for a systematic workflow for designing solvent and its injection procedure. In the subsequent sections, we first discuss condensation behavior of steam and solvent in coinjection chamber, which can significantly affect the oil production rate. Selection of solvent will then be made mainly to optimize the oil production rate. An injection procedure for the selected solvent will also be presented to maximize ultimate oil recovery while minimizing solvent retention in situ. Finally, we apply the systematic workflow to two actual field cases, EnCana's SAP pilot in Senlac (Gupta et al. 2005; Gupta and Gittins 2006) and Nexen's ES-SAGD pilot in Long Lake (Nexen 2007; Orr et al. 2010).

### **Condensation Behavior of Steam and Solvent in Coinjection**

Coinjection can exhibit a chamber-edge temperature that is substantially lower than that in SAGD (Keshavarz et al. 2012). Dong (2012) explained this unfavorable temperature distribution in coinjection using simplified representation of binary phase behavior of water and a single-component solvent. In our opinion, the analysis of Dong (2012), although simple, is useful in explaining the condensation behavior of steam and solvent in the coinjection chamber. This section presents an application of Dong's analysis for estimation of the chamber-edge temperature for a wide variety of solvents and operating conditions. The estimations are then compared with results from numerical flow simulations, where some of assumptions made in the estimation are relaxed.

Assumptions are made as follows: (1) binary mixtures of water and a single-component solvent, (2) Raoult's law for phase equilibrium, (3) no mutual solubility between water and solvent, and (4) a negligible pressure gradient in

the chamber. The phase equilibrium relation for component  $i$  can then be written as

$$P_i^{\text{vap}} = y_i P, \quad (3-1)$$

where  $P_i^{\text{vap}}$  is the vapor pressure of component  $i$ ,  $P$  is the system pressure,  $y_i$  is the mole fraction of component  $i$  in the gaseous phase, and  $i$  is the component index (i.e.,  $i = \{\text{water, solvent}\}$ ). Equation 3-1 is for the aqueous (W) and gaseous (V) phases for  $i$  of water, and is for the oleic (L) and gaseous (V) phases for  $i$  of solvent. By definition,  $\sum_i y_i = 1.0$ , or  $\sum_i y_i P = P$ . Using Equation 3-1, we have

$$P = \sum_i P_i^{\text{vap}}. \quad (3-2)$$

Vapor pressure curves for the water and solvent compounds can be expressed as functions of temperature using an EOS or correlations such as Antoine's correlation tabulated in National Institute of Standard and Technology Chemistry WebBook. Equation 3-2 can then be solved for the temperature for the L-V-W equilibrium ( $T_{3p}$ ) at a given pressure. Once we obtain  $T_{3p}$ , Equation 3-1 gives the component mole fractions in the V phase at that pressure and  $T_{3p}$ . The L and W phases with the complete immiscibility are present at  $T < T_{3p}$  at this pressure. Two phases are present at  $T > T_{3p}$  at this pressure, and are either V and L or V and W, depending on the overall composition. Details of relevant phase diagrams can be found in Dong (2012).

$T_{3p}$  corresponds to the chamber-edge temperature for coinjection of steam and a certain solvent compound under consideration. Ahead of the chamber edge, temperature is lower than  $T_{3p}$ , and there exist two immiscible liquid phases (i.e., the L and W phases). Inside the chamber, temperature is higher than  $T_{3p}$ , and the two equilibrium phases consist of either V and L or V and W. Note that bitumen is not considered in the system here due to assumption 1. As stated by Dong (2012), the temperature and partial pressure of steam or solvent at the chamber edge are independent of the initial concentration of solvent in the injectant under the assumptions made.

**Figure 3-1** shows the solutions of Equation 3-2 at an injection pressure  $P_{\text{inj}}$  for binaries of water and a few different hydrocarbons.  $T_{3p}$  at  $P_{\text{inj}}$  is where

$(P_{inj} - P_{water}^{vap})$  intersects  $P_{solvent}^{vap}$ . **Figure 3-2** summarizes the  $T_{3p}$  solutions for different solvents at different injection pressures. These plots should be interpreted only for temperature above the initial reservoir temperature. Coinjection of a more volatile solvent results in a lower temperature at the chamber edge. Coinjection of a given solvent at a lower pressure gives a smaller reduction in the chamber-edge temperature.

**Figure 3-3** shows the water component mole fractions in the V phase at the chamber edge for different solvents at different injection pressures. Coinjection of a more volatile solvent results in a lower concentration of water in the V phase near the chamber edge. This concentration profile is not very sensitive to the injection pressure in **Figure 3-3**.

Some of prior studies explained that reduction of the chamber-edge temperature in coinjection occurs due to a reduced partial pressure of water in the V phase (i.e.,  $y_{water} < 1.0$ ). However, the most fundamental reason is the deviation of  $T_{3p}$  from the steam temperature at a given injection pressure as shown in the sequential solution of Equations 3-1 and 3-2 and in **Figure 3-1**.

Some of the assumptions made above are invalid for many practical applications. For example, oil and solvent always have mutual solubility. Some of the reservoir oil components also can exist in the V phase. Also, actual phase behavior of water-hydrocarbon mixtures will deviate from Raoult's law. We use the STARS simulator (Computer Modelling Group 2011) to see how much the assumptions, especially assumptions 1 and 2, can affect the accuracy of the chamber-edge temperature estimation based on Dong (2012).

A 2-D homogeneous reservoir of  $70.0 \text{ m} \times 37.5 \text{ m} \times 20.0 \text{ m}$  with gravity is considered with a uniform grid-block size of  $1.0 \text{ m} \times 37.5 \text{ m} \times 1.0 \text{ m}$ . The injector and producer are located at the left boundary at depths of 16 m and 20 m from the top, respectively. Reservoir/fluid properties used are presented in **Table 3-1**. Capillarity and physical diffusion/dispersion are not considered in this research. A typical viscosity-temperature relation for Athabasca bitumen is estimated using Equation 3-3 (Mehrotra and Syrczek 1986)

$$\ln\mu = \exp(A + B\ln T), \quad (3-3)$$

where  $\mu$  is bitumen viscosity in cp and  $T$  is the absolute temperature in Kelvin. The constants  $A$  and  $B$  used are 22.8515 and -3.5784, respectively. The bitumen considered here is a dead oil; i.e., only solvent and water can exist in the V phase. Fluid phase behavior is represented using constant-K flash with the Rachford-Rice equations (1952). Tabulated K-values are generated by performing a series of flash calculations using the Peng-Robinson (PR) equation of state (1976) with the van der Waals mixing rules for hydrocarbons. Raoult's law is used for K values for the water component. Detailed instructions on K-value tables generation is provided in Appendix A. Possibilities of mutual solubility of water and hydrocarbons and asphaltene precipitation are not considered in this study.

The injection and production wells are constrained to constant bottom-hole pressures of 2730 kPa and 1500 kPa, respectively. Injected steam with a quality of 0.9 is at 228.7°C according to steam table (228.1°C according to Antoine's correlation with the coefficients used in this study) at 2730 kPa. A maximum flow rate of 1.0 m<sup>3</sup>/day is assigned to steam at the producer to prevent significant steam breakthrough during the simulation. Preheating of the reservoir is performed for six months.

Simulations are performed for steam-only injection and steam-solvent coinjection with different single-component solvents from C<sub>3</sub> to C<sub>8</sub> for five years. The solvent concentration in the injection stream is 2 mol% in all cases unless otherwise stated. A sample STARS's data file for the simulation of C<sub>5</sub>-steam coinjection is presented in Appendix 2.

**Figure 3-4** presents variations of temperature and the V phase saturation simulated along the sixth row from the top of the reservoir model at two years for the C<sub>4</sub> and C<sub>8</sub> coinjection cases, respectively. The chamber edge is defined where the V phase saturation becomes zero on the phase transition between three and two phases. The temperature in the grid block just before the grid blocks without the V phase is considered to be the chamber-edge temperature. The chamber-edge temperature is 85°C lower for the C<sub>4</sub> coinjection case than for the

C<sub>8</sub> coinjection case. Figure 3-4a also indicates that condensation of water starts deep inside the chamber.

**Figure 3-5** compares the chamber-edge temperatures estimated from Equation 3-2 and those from simulation for coinjection of C<sub>4</sub> and steam. The estimation from Equation 3-2 gives an error range of  $\pm 15^{\circ}\text{C}$ , compared to the simulation results. **Figure 3-6** presents a similar comparison for the water mole fractions in the V phase at the chamber edge. The accuracy of the component mole fractions calculated from Equation 3-1 is affected by an error in estimation of the chamber-edge temperature. Figure 3-6 shows that Equation 3-1 systematically overestimates the water mole fractions in the V phase at the chamber edge for the case studied. The deviations observed in Figures 3-5 and 3-6 indicate that the mutual solubility between the dead oil and solvent and fluids' non-idealities can affect physical properties at the chamber edge and oil recovery predictions in coinjection.

**Figure 3-7** presents the water molar fluxes in steam-only injection and the C<sub>4</sub> and C<sub>8</sub> coinjection cases. Arrows represent the direction and the magnitude of water molar fluxes. Note that lengths of arrows cannot be compared among different coinjection cases since they have different scales. The effect of gravity on the water flux comes mainly from the condensed W phase; thus, downward fluxes in the C<sub>4</sub> coinjection in Figure 3-7a indicate that steam condensation occurs deep inside the chamber. This effect is more pronounced for lighter solvents, for which less energy is transported to the chamber-edge by steam.

Assumption 1 leads to a simplification that only water and the single-component solvent can exist in the gaseous phase. This assumption does not consider a third component in the gaseous phase. This will be invalid when multi-component solvent is considered and when some components in the reservoir oil can be present in the V phase at high concentrations.

### **Solvent Selection**

Coinjection attempts to enhance the oil production rate through two main measures; i.e., heat and dilution of oil with solvent. The main concern of coinjection is whether coinjection can achieve a higher oil production rate than

SAGD. In the previous section, however, we explained that coinjection can substantially lower the chamber-edge temperature, which adversely affects the oil production rate. In general, coinjection of a more volatile solvent tends to result in a lower chamber-edge temperature for given operation conditions. A less volatile solvent, however, results in a more viscous mixture when mixed with bitumen at a given mixing ratio at a temperature and pressure. Thus, an optimum volatility of solvent is expected to exist in terms of the oil production rate for given operation conditions.

In this section, simple simulations of coinjection are performed with different single-component solvents to see if such an optimum solvent volatility can be observed. Reservoir properties used are the same as in the previous section. The following mixing rule is used in the simulations to estimate the viscosity of phase  $j$  ( $\mu_j$ ):

$$\ln\mu_j = \sum_{i=1}^{N_C} x_{ij} \ln\mu_{ij}, \quad (3-4)$$

where  $N_C$  is the number of components,  $x_{ij}$  is the mole fraction of component  $i$  in phase  $j$ , and  $\mu_{ij}$  is the viscosity of component  $i$  in phase  $j$ .

**Figure 3-8** shows oil recoveries simulated with different solvents. The amount of produced solvent is excluded in the calculation of the oil production rate. **Figure 3-9** shows the average oil production rates for these cases. The average production rate is calculated for the first 2.5 years when reservoir boundary effects on chamber propagation are insignificant. Most of the coinjection cases result in higher average production rates for the first 2.5 years than steam-only injection, but coinjection of  $C_3$  yields no improvement in the average production rate.

The average bitumen production rate increases as the coinjected solvent becomes less volatile up to  $C_6$ . The  $C_6$  and  $C_8$  coinjection cases result in the chamber-edge temperatures of 188°C and 211°C, respectively. This temperature difference causes only a few centipoises of difference in the bitumen viscosity; however, the viscosity of  $C_8$  is greater than that of  $C_6$  at their respective chamber-edge temperatures. Considering significant accumulation of solvent in the L phase in this region, a higher viscosity of this phase can occur for

coinjection of  $C_8$ , compared to that of  $C_6$  (**Figure 3-10**). This has resulted in the break-over point in Figure 3-9.

The low oil production rate in the  $C_3$  coinjection case is mainly because the temperature near the chamber edge is much lower than that in the steam-only injection case. The chamber-edge temperature estimated from the previous section is  $72^\circ\text{C}$  for the  $C_3$  coinjection case. The reservoir oil and  $C_3$  have viscosities of approximately 1060 cp and 0.09 cp at this temperature, respectively. In the steam-only injection case, however, the chamber-edge temperature is  $228^\circ\text{C}$ , at which the oil viscosity is only 6 cp. Thus, depending on temperature and solvent distributions ahead of the chamber, it is highly conceivable that the L phase in the  $C_3$  coinjection case becomes more viscous than that in steam-only injection (Figure 3-10). This negative effect will be more severe if lighter solvents (such as  $C_2$  or  $C_1$ ) are coinjected with steam as reported in literature (Jiang et al. 1998; Serhat et. al 2002; Hosseininejad Mohabati et al. 2010; and Li and Mamora 2011a). Coinjection of non-condensable gases with steam into a bitumen reservoir can lead to extremely slow chamber propagation.

Figure 3-9 indicates a simple way to find an optimum volatility range of coinjection solvent in terms of the bitumen production rate. An optimum solvent in this type of figure will occur when the effects of heating and solvent dilution on oil viscosity take a balance. Although it is not our objective to single out a specific solvent as an optimum, Figure 3-9 indicates that solvents lighter than  $C_4$  and heavier than  $C_6$  are not recommended for the simple simulation case studied here.

Reliable selection of an optimum solvent in terms of the bitumen production rate also requires accurate prediction of viscosities for bitumen/solvent mixtures at different temperatures, which in itself is a technical issue to be addressed. Also, diffusion and dispersion in the L phase can affect the viscosity profile of the L phase near the chamber edge. The bitumen studied here is a dead oil with no initial gas-oil ratio (GOR). Non-zero initial GOR will also shift the break-over point in Figure 3-9 due to a lower bitumen viscosity at the initial conditions and multiple hydrocarbon components in the V phase.

Sensitivity analyses of the oil production rate to these additional factors should be considered. Nevertheless, the simple procedure presented above and in Figure 3-9 captures the primary effects on the oil mobility in coinjection, and can be extended to other cases considering additional engineering factors.

### **Design of Solvent Concentration**

Coinjection of steam and solvent can achieve oil saturation lower than the residual saturation in the chamber (Redford and McKay 1980; Li and Mamora 2010; Ardali et al. 2012a; Mohammadzadeh et al. 2012; Jha et al. 2012). Keshavarz et al. (2012) presented that the oil saturation reduction results mainly from two processes; solvent accumulation in the L phase outside the chamber and phase transition at the chamber edge between the W-L equilibrium and the W-L-V equilibrium. The solvent accumulation lowers the oil-component concentrations. The diluted oil is then redistributed in the V and L phases in the presence of the W phase on the phase transition. The equilibrium L phase contains a fair amount of oil components; however, the amount of the L phase can be significantly small, resulting in low oil saturations in the coinjection chamber.

Accumulation of coinjected solvent occurs due to a higher solvent injection rate than its drainage rate. In this section, we show that it is possible to maximize oil recovery while minimizing solvent retention in situ by controlling the concentration of a given coinjection solvent. We continue to use the simulation case in the previous sections with  $C_5$  as a coinjection solvent, which resulted in an improved oil production rate in Figure 3-9.

**Figure 3-11** compares oil recovery predictions for different concentrations of  $C_5$  in the injectant. The concentration is constant with time for each simulation case. As the solvent concentration increases, the oil production rate and oil recovery are more improved compared to the steam-only injection case. The use of a higher solvent concentration expedites the accumulation of solvent outside the chamber edge, and oil recovery can be enhanced earlier in the process. Thus, a greater portion of the swept area by chamber, including regions closer to the well pair, can exhibit lowered oil saturation compared to the steam-

only injection case. A secondary effect of a thicker solvent-rich bank ahead of the chamber edge is a slight improvement in the bitumen drainage rate.

**Figure 3-12** shows distributions of the solvent-rich bank at the chamber edge and the L phase saturation inside the chamber for 1 mol% and 8 mol% C<sub>5</sub> coinjections. Figure 3-12 confirms that a higher concentration of solvent in the injectant promotes solvent accumulation in the L phase right ahead of the chamber edge. This results in improved local displacement efficiency in the region closer to the well pair and a thicker solvent-rich bank during the process.

Coinjection at a higher solvent concentration can achieve a higher oil production rate and oil recovery, but recovery of the solvent also is of practical importance. It would not be feasible to continuously inject a solvent at a high concentration throughout the project period. **Figure 3-13** shows that the solvent concentration of 16% results in a cumulative solvent injection of 40,000 Sm<sup>3</sup>, which is approximately four times the cumulative bitumen production. **Figure 3-14** shows the solvent volumes retained in the reservoir for simulations with different solvent concentrations. The solvent retention at a given time is defined as the standard volume of solvent injected less the standard volume of solvent produced. The volume of solvent retention can be more than 20% of the cumulative bitumen production for continuous coinjection of a fixed solvent concentration.

Retention of solvent inside the reservoir mainly occurs in three places; (1) the V phase inside the chamber, (2) the L phase inside the chamber and at the chamber edge, and (3) the L phase in the un-swept region. Solvent retention in place 2 can be efficiently minimized by maximizing oil recovery. That is, a higher oil recovery can also reduce solvent costs in coinjection. Solvent retention in place 1 can be significant depending on reservoir conditions and the solvent coinjected as is shown in the next section. Solvent retention in place 3 can occur owing to diffusion and dispersion of solvent through the L phase, which is difficult to model accurately in the conventional finite-difference simulation. In this section, our focus is on maximizing oil recovery while

minimizing the solvent loss in place 2 by controlling the concentration of solvent in the injectant.

A thicker solvent-rich bank is beneficial for oil recovery, but the main portion of oil drainage occurs within a few meters of the chamber edge, where both heat and solvent dilution effects contribute (Keshavarz et al. 2012; see also Figure 3-10). Also, accumulation of solvent in the V phase in the chamber unfavorably lowers the temperature there as explained in the section on Condensation Behavior of Steam and Solvent in Coinjection. That is, solvent accumulation early in the process is beneficial, but a very thick region of solvent accumulation in the L and V phases is unfavorable later in the process.

We test the following coinjection procedure:

1. Start coinjection of solvent with a high solvent concentration after the thermal communication between the wells is established.
2. Gradually decrease the solvent concentration in the injectant to avoid a very thick solvent-rich region in situ.
3. Inject only steam for the final period of the process; e.g., after the chamber reaches the outer boundary for the well pair.

Initiation of coinjection with a high solvent concentration in step 1 expedites accumulation of solvent near the chamber edge early in the process. This contributes to higher oil recovery because of enhanced local displacement efficiency. A declining trend of the solvent concentration in step 2 is to control the thickness of the solvent-rich bank near the chamber edge when the chamber is still developing. Termination of solvent coinjection in step 3 is to prevent the accumulated solvent from being trapped in the L phase along the chamber edge.

**Figure 3-15** compares the injection and production volumes of  $C_5$  in coinjection simulations using two different injection procedures. One is to coinject  $C_5$  at a constant concentration of 2 mol% in the injectant throughout the entire process. The other is to vary the solvent concentration in the injectant in a step-wise manner as shown in **Figure 3-16**. Due to high concentrations of  $C_5$  for the first year of coinjection, the cumulative volume of  $C_5$  injected rapidly increases in Figure 3-15. However, a significant portion of the injected volume

is recovered subsequently. The variable-concentration case results in 58% less volume of  $C_5$  retention in situ at five years.

**Figure 3-17** shows the volumes of  $C_5$  left in the reservoir and the L phase saturation distributions after five years of operation for the two cases. The variable-concentration case achieves enhanced displacement efficiency in the chamber while reducing solvent retention at the end of the process. The constant-concentration case yields significant accumulation of  $C_5$  near the outer boundary at the end of the process. Results show that the L phase in this region consists of almost 100%  $C_5$ . The cumulative oil production at five years is  $10147 \text{ Sm}^3$  for the constant-concentration case, and  $9995 \text{ Sm}^3$  for the variable-concentration case. The solvent retention at five years is  $1293 \text{ Sm}^3$  for the constant-concentration case and  $533 \text{ Sm}^3$  for the variable-concentration case. The variable-concentration case results in improved local displacement efficiency in the swept region, but its swept region is smaller at five years. This is why the variable-concentration case results in 1.3% lower ultimate recovery of bitumen, which is worth a fraction of the improved  $C_5$  recovery.

### **Simulation Case Studies**

In this section, we investigate two coinjection pilots, the Senlac SAP pilot by EnCana and the Long Lake ES-SAGD pilot by Nexen. It is indicated in the literature that the results of the former were more encouraging than those of the latter. The main objective here is to clarify the reasons for these mixed results on the basis of limited information available in the literature. We also discuss any further improvements that could have been made for these pilots.

#### **Senlac SAP Pilot**

EnCana's Senlac SAP pilot was successfully conducted in 2002 and located 100 kilometers south-east of Lloydminster, Alberta. The entire project consisted of three phases; A, B, and C. Phase C had two well pairs, C1 and C2, with a horizontal section of 750 m and an inter-well-pair spacing of 120 m. A short period of SAP was tested for the C1 pair. The average vertical spacing between

the injector and producer is 5 m. The reservoir is approximately 16 m thick with minimal exposure to bottom water (Boyle et al. 2003).

Pre-heating was performed by injecting high pressure steam into the producer for 10 days, and then the well was shut in for five days to soak. The producer was then flowed back for three days to enhance the injectivity for the next cycle. Three cycles of injection, soaking, and production were used to establish thermal communication between the injector and producer (Boyle et al. 2003). After seven months of SAGD, the SAP pilot began in January 2002 with coinjection of a small amount of C<sub>4</sub> with steam with no significant change in the operational conditions. Gupta et al. (2005) reported a significant increase in the bitumen production rate from an average of 302 m<sup>3</sup>/day (1900 bbl/day) during SAGD to an average of 477 m<sup>3</sup>/day (3000 bbl/day) during the SAP pilot. Also, the SOR decreased from an average of 2.6 to 1.6 for the same periods.

We first conduct history matching for the bitumen production rate and the SOR for the periods of SAGD and SAP using the STARS simulator (Computer Modelling Group 2011). Reservoir/fluid properties and recurrent data are taken from Boyle et al. (2003) and Gupta et al. (2003) as listed in **Table 3-2**. The dimensions of the reservoir model are 120 m, 750m, and 16 m in the x, y, and z directions, respectively. A uniform grid-block size of 2 m × 750 m × 1 m is used. The reservoir oil is assumed to be a dead oil. Phase equilibrium calculations are conducted based on K-values tabulated prior to the simulation. The K-values are generated using the PR EOS for hydrocarbon components, and using Raoult's law for the water component.

The injector and producer are constrained to constant bottom-hole pressures. Steam is injected at 260 °C with a quality of 90%. A minimum of 25 °C subcool is considered for the producer to prevent steam production.

Adjustments are made on the oil-viscosity/temperature relation, permeabilities in the horizontal and vertical directions, and the solvent concentration in the injectant for SAP. **Table 3-3** shows the adjusted oil viscosity. A fixed concentration of 12% (on the mass basis) of C<sub>4</sub> is selected to match data for the SAP period. Simulation results after history matching are

presented in **Figure 3-18** along with data taken from the literature. Reasonable agreements can be observed for the oil production rate and the SOR between data and simulations. Simulations also exhibited that coinjection of  $C_4$  and steam can significantly increase the production rate from an average of 1900 bbl/day to 3000 bbl/day as reported by Gupta et al. (2005). Due to the scarcity of the field data available, no further adjustment of parameters is conducted for the discussion below.

We then test other solvents based on the simulation model developed above. The solvent of  $C_4$  for the SAP period is replaced with  $C_3$ ,  $C_5$ , or  $C_6$ . A molar concentration of solvent is fixed at 4%, which is equivalent to 12% of  $C_4$  on the mass basis in the original SAP case. We assume that all coinjections, including the  $C_4$  case, are continued for approximately three years after the initiation of the SAP pilot in January 24, 2002. **Figure 3-19** presents the average oil production rates for different solvents after eight months of coinjection (i.e., the SAGD period is not included in calculation of the average production rate). The original solvent selection of  $C_4$  corresponds to the break-over point in Figure 3-19, resulting in the highest average oil production rate. The reservoir oil in this project is not an extra-heavy oil, and its viscosity exhibits less sensitivity to temperature than the typical bitumen viscosity. The optimum volatility of coinjection solvent is shifted to the more volatile side, compared to the case of Athabasca bitumen.

We now compare two scenarios; scenario 1 is the original operation in the Senlac SAP pilot, and scenario 2 uses the modified injection procedure presented in the previous section. The two scenarios use  $C_4$  as the coinjected solvent. In scenario 1, solvent coinjection is started after the peak production rate is achieved in SAGD, and is stopped shortly after the oil production rate starts decreasing (Gupta and Gittins 2006). Thus, coinjection starts at January 24, 2002 with a  $C_4$  concentration of 4 mol%, and continues until April 1, 2002. After that, steam is the only injectant until January 2005. In scenario 2, coinjection starts with a  $C_4$  concentration of 4 mol% right after thermal communication is achieved between the wells. The  $C_4$  concentration is then

gradually decreased until it becomes zero for the last 1.5 years of the coinjection period.

**Figure 3-20** compares the two scenarios in terms of the oil production history and the L phase saturation distribution at the end of the process. Scenario 2 results in approximately 14% more oil recovery than scenario 1 at the end of the simulations. Also, the oil recovery in scenario 2 is 4% more than that in scenario 1 at April 1, 2002, when coinjection is terminated in scenario 1. Scenario 2 exhibits enhanced oil displacement (i.e.,  $S_o < S_{or}$ ) in a wider portion of the reservoir. This is because of earlier accumulation of the solvent near the chamber edge, which is a key requirement for enhanced oil displacement (Keshavarz et al. 2012). These results indicate that it is beneficial to achieve solvent accumulation near the chamber edge as early in the process as possible.

**Figure 3-21** presents the solvent injection and production amounts in scenario 2. Although the variable solvent concentration in scenario 2 attempts to minimize the amount of solvent retention in the L phase, solvent recovery is not as successful as the case studied in the previous section. Solvent recovery is only about 31% because solvent retention in the V phase is quite significant in this case. The solvent retained in the V phase is more difficult to recover than that in the L phase during the project, but would be partly recovered when winding down the project at reduced temperature.

Comparison of scenario 2 with the steam-only injection process shown in Figure 3-18 indicates that the cumulative oil production can be improved from 251,400 Sm<sup>3</sup> to 330,200 Sm<sup>3</sup> for four years of operation. Scenario 2 also can reduce the cumulative SOR from 3.92 to 2.22. Scenario 2 shows that the C<sub>4</sub> retention is 48,391 tones at the end of simulation.

#### **Long Lake ES-SAGD Pilot**

Long Lake in Athabasca Oil Sands is located approximately 40 km southeast of Fort McMurray. Nexen conducted a SAGD pilot at the Long Lake project site from May 2003 until August 2006. An ES-SAGD test was performed for well-pair 3 from February 13 to April 16, 2006. This ES-SAGD coinjected Jet B, a mixture of petroleum fractions from C<sub>7</sub> to C<sub>12</sub>, at a volumetric concentration of

5% except for an initial short period (Orr et al. 2010). The ES-SAGD pilot did not show significant changes in oil production rate compared to SAGD (Nexen 2007). Orr et al. (2010) performed a simulation study of this two-month ES-SAGD pilot. Their simulation showed that the oil rate was increased by 6% and the SOR was decreased by 7% compared to the prior SAGD.

A uniform gridblock size of  $2 \times 650 \times 1 \text{ m}^3$  is used to model a reservoir with dimensions of  $100 \times 23 \times 650 \text{ m}^3$  in x, y and z directions, respectively. The injector and producer are located on a side boundary of the reservoir at the depths of 15 m and 20 m from the top, respectively. **Table 3-4** shows rock and fluid data taken from Nexen's annual report for the Long Lake project (2007, 2012) and Orr et al. (2009). K-values are generated using the PR EOS for hydrocarbon components and using Raoult's law for water. Since details of Jet B are unavailable in literature, we assume that Jet B behaves similarly to  $C_{10}$  for simplicity. Using this assumption, 5 vol% of Jet B is equivalent to 0.5 mol% of  $C_{10}$  for the coinjection simulation in this subsection. Bitumen viscosities at different temperatures were taken from Orr et al. (2009) as given in **Table 3-5**.

The injection and production pressures are adjusted to match the SAGD production data from May 2003 to February 2006. The injection pressure is initially 2800 kPa and follows a declining trend as reported by Nexen (2007). They are stabilized at approximately 1500 kPa for the ES-SAGD period and afterwards. The steam quality is 90% in the simulation. A minimum subcool of  $10^\circ\text{C}$  is considered. **Figure 3-22** shows history matching results for the SAGD production rate.

Based on the history-matched reservoir/fluid models, the ES-SAGD pilot is simulated with a  $C_{10}$  concentration of 0.5 mol% in the injectant between February 13, 2006 and April 16, 2006. An improvement of 10% in oil production rate, compared to SAGD, is observed approximately five months after the termination of solvent coinjection (Figure 3-22). A sufficient accumulation of solvent near the chamber edge is one of the keys to successful coinjection as explained in Keshavarz et al. (2012), which was not achieved within two months in this ES-SAGD simulation.

We implement the procedure presented in this chapter for selecting a single-component solvent. Here, we assume coinjection is initiated on February 13, 2006, and continued for four years. The same reservoir model is used with different single-component solvents at a concentration of 2.0 mol%. **Figure 3-23** presents that the average bitumen production rate for 1.5 years of coinjection exhibits a break-over point at  $C_5$ . Therefore, Jet B used in Nexen's ES-SAGD pilot is likely a sub-optimum solvent due to its low volatility. Ardali et al. (2012b) speculated that the low volatility of Jet B is the reason for the less encouraging results of the Long Lake ES-SAGD pilot. Figure 3-23, however, shows that  $C_{10}$ , a single-component solvent equivalent to Jet B, can exhibit a higher oil production rate than SAGD once a sufficient amount is injected.

Comparisons are made between two scenarios. Scenario 1 attempts to follow the actual operation by Nexen. Coinjection of  $C_{10}$  is conducted with a constant concentration of 0.5 mol% after the initial SAGD period between May 2003 and February 2006. This coinjection is continued only for two months. After that, only steam is injected until January 2010. In scenario 2, coinjection of  $C_5$  is started after the inter-well communication is achieved in July 2003. The injector is constrained to a maximum bottom-hole pressure of 1500 kPa, and the producer is constrained to a minimum bottom-hole pressure of 1100 kPa throughout the process. The solvent concentration is initially 6.0 mol%, and then reduced in a step-wised manner. Coinjection is stopped at approximately 3.6 years when the chamber reaches the other boundary of the reservoir model. Only steam is injected for the last three years of the project to recover part of the solvent accumulated in the chamber.

**Figure 3-24** compares the two scenarios in terms of oil production and local displacement efficiency. Scenario 2 yields 34% higher oil recovery than scenario 1 at January 2010. The steam chamber in scenario 2 propagates faster than that in scenario 1 by exploiting the effects of solvent accumulation near the chamber edge from the early stage of the process. This is the main reason for the significant improvement observed in the cumulative oil production in Figure 3-24. Another reason is that scenario 2 gives higher local displacement efficiency

in the chamber (regions in red in Figure 3-24b) than scenario 1. Since enhancement of local displacement efficiency requires a sufficient amount of solvent accumulation near the chamber edge (Keshavarz et al. 2012), scenario 1 results in lower displacement efficiency than scenario 2.

**Figure 3-25** presents the cumulative amounts of solvent injected and produced in scenario 2. Results show that 92% of the coinjected solvent volume can be recovered by the end of the process.

Comparison of scenario 2 with the steam-only injection process shown in Figure 3-22 indicates an improvement of the cumulative oil production from 123,100 Sm<sup>3</sup> to 215,500 Sm<sup>3</sup> after 6.7 years of operation. The cumulative SOR is also reduced from 7.47 to 2.78. Scenario 2 results in the C<sub>5</sub> retention of 72,938 tones at the end of the simulation.

## Conclusions

We presented a systematic workflow for selecting an optimum solvent and its concentration in coinjection of a single-component solvent with steam. The optimization considered the oil production rate, ultimate oil recovery, and solvent retention in situ. Conclusions are as follows:

1. Reduction of the chamber-edge temperature in coinjection can be qualitatively explained using a simplified representation of water-solvent binary phase behavior. The temperature reduction can occur as a direct consequence of deviation of the three-phase temperature from the steam temperature at the injection pressure in water-solvent binary phase behavior.
2. Numerical simulation was conducted to quantitatively examine the accuracy of the simplified estimation of the chamber-edge temperature. Results show that the mutual solubility between the dead oil and solvent and fluids' non-idealities can substantially affect physical properties at the chamber edge.
3. The chamber-edge temperature reduction becomes more significant for coinjection of a more volatile solvent with steam for given operation conditions. A less volatile solvent, however, results in a more viscous

mixture when mixed with bitumen at a given mixing ratio at a temperature and pressure. Thus, an optimum volatility of solvent can be typically observed in terms of the oil production rate for given operation conditions. Different reservoir/fluid properties result in different optimum solvents.

4. A key to enhanced oil recovery in coinjection is accumulation of solvent in the oleic phase outside the chamber. It is possible to maximize oil recovery while minimizing solvent retention in situ by controlling the concentration of a given coinjection solvent. Initiation of coinjection right after achieving the inter-well communication enables to enhance oil recovery early in the process. Subsequently, the solvent concentration should be gradually decreased until it becomes zero for the final period of the coinjection. This coinjection procedure can minimize solvent retention in the oleic phase in situ while keeping oil recovery.
5. The proposed workflow was successfully applied to simulation of the Senlac SAP pilot project, which is one of the successful field applications of solvent-steam coinjection. Results indicate that the original solvent selection of C4 is the optimum solvent in terms of the oil production rate for this project. Although local displacement efficiency and solvent recovery can be further improved by modifying the coinjection procedure, the incremental oil recovery is insignificant.
6. The proposed workflow was also applied to simulation of the Long Lake ES-SAGD project. The main reason for this less successful ES-SAGD is likely because two months of coinjection at a low solvent concentration gave an insufficient amount of solvent accumulation near the chamber edge. Also, Jet B seems to be a sub-optimum solvent for this ES-SAGD. The proposed workflow indicates that C5 is the optimum solvent in terms of oil production rate. Simulation results for coinjection of C5 with a variable solvent concentration show that oil recovery can be enhanced by 34% compared to the original operation

scheme and that 92% of injected solvent can be recovered by the end of the process.

### **Nomenclature**

L:	Oleic phase
$N_C$ :	Number of components
P:	Pressure, kPa or bar
$P_{inj}$ :	Injection pressure, kPa or bar
$P^{vap}$ :	Vapor pressure, kPa or bar
T:	Absolute temperature, K
V:	Gaseous phase
W:	Aqueous phase
$x$ :	Molar concentration
$\mu$ :	Viscosity, cp

### *Subscripts*

$i$ :	Component index
$j$ :	Phase index

### *Abbreviations*

CN:	Carbon number
ES-SAGD:	Expending-solvent steam assisted gravity drainage
LASER:	Liquid addition to steam enhanced recovery
PR:	Peng and Robinson
SAGD:	Steam assisted gravity drainage
SAP:	Solvent aided process
SAS:	Steam alternating solvent
SOR:	Steam-oil ratio
SA-SAGD:	Solvent aided steam assisted gravity drainage

**Table 3-1. Reservoir and field properties used in numerical simulations**

<b>Properties</b>	<b>Values</b>
Porosity	33%
Horizontal permeability	4000 md
Vertical permeability	3000 md
Initial reservoir pressure at depth of 500 m	1500 kPa
Initial reservoir temperature	13°C
Initial oil saturation	0.75
Initial water saturation	0.25
Three-phase relative permeability model (CMG, 2011)	STARS internal correlations
Formation compressibility	1.8E-5 1/kPa
Rock heat capacity (Butler, 1997)	2600 kJ/m <sup>3</sup> °C
Rock thermal conductivity (Butler, 1997)	660 kJ/m day °C
Over/underburden heat capacity (Butler, 1997)	2600 kJ/m <sup>3</sup> °C
Over/underburden thermal conductivity (Butler, 1997)	660 kJ/m day °C
Bitumen thermal conductivity (Butler, 1997)	11.5 kJ/m day °C
Gas thermal conductivity (Yazdani et al., 2011)	2.89 kJ/m day °C
Water thermal conductivity	1500 kJ/m day °C
Bitumen molecular weight (Mehrotra and Syrczek, 1987)	594.6 kg/kgmole
Bitumen specific gravity (Mehrotra and Syrczek, 1987)	1.077

**Table 3-2. Reservoir and fluid properties used in simulation of Senlac SAP pilot**

<b>Properties</b>	<b>Values</b>
Porosity (Boyle et al. 2003)	33%
Horizontal permeability (Boyle et al. 2003)	7000 md
Vertical permeability (Boyle et al. 2003)	5000 md
Initial reservoir pressure at depth of 500 (Boyle et al. 2003)	5200 kPa
Initial reservoir temperature (Boyle et al. 2003)	29°C
Initial oil saturation (Boyle et al. 2003)	0.85
Initial water saturation (Boyle et al. 2003)	0.15
Residual oil saturation	0.13
Irreducible water saturation	0.15
Three-phase relative permeability model (CMG 2011)	STARS internal correlations
Total pay thickness (Boyle et al. 2003)	16 m
Oil density (Boyle et al. 2003)	985 kg/m <sup>3</sup>
Minimum sub-cool (Gupta et al. 2003)	25 °C
Injector bottom hole pressure (maximum)	5250 kPa
Producer bottom hole pressure (minimum)	5000 kPa
Injection temperature (Gupta et al. 2003)	260 °C
Steam quality	0.9

<b>Table 3-3. Viscosity-temperature for simulation of Senlac SAP pilot</b>	
<b>Temperature, °C</b>	<b>Viscosity, cp</b>
0	115330.00
60	260.00
120	4.28
180	0.50
240	0.15
300	0.09

<b>Table 3-4. Reservoir and fluid data for simulation of Long Lake ES-SAGD pilot</b>	
<b>Properties</b>	<b>Values</b>
Porosity	31%
Horizontal permeability	6300 md
Vertical permeability	4900 md
Initial reservoir pressure at depth of 200	1050 kPa
Initial reservoir temperature	7°C
Initial oil saturation	0.68
Initial water saturation	0.32
Residual oil saturation	0.13
Irreducible water saturation	0.25
Three-phase relative permeability model	STARS internal correlations
Total pay thickness	23 m
Oil density	930 kg/m <sup>3</sup>
Minimum sub-cool	10°C
Steam quality	0.9

<b>Table 3-5. Viscosity -temperature behavior for simulation of Long Lake ES-SAGD pilot</b>	
<b>Temperature, °C</b>	<b>Viscosity, cp</b>
0	7708500.00
75	2691.00
150	68.19
225	9.94
300	3.30

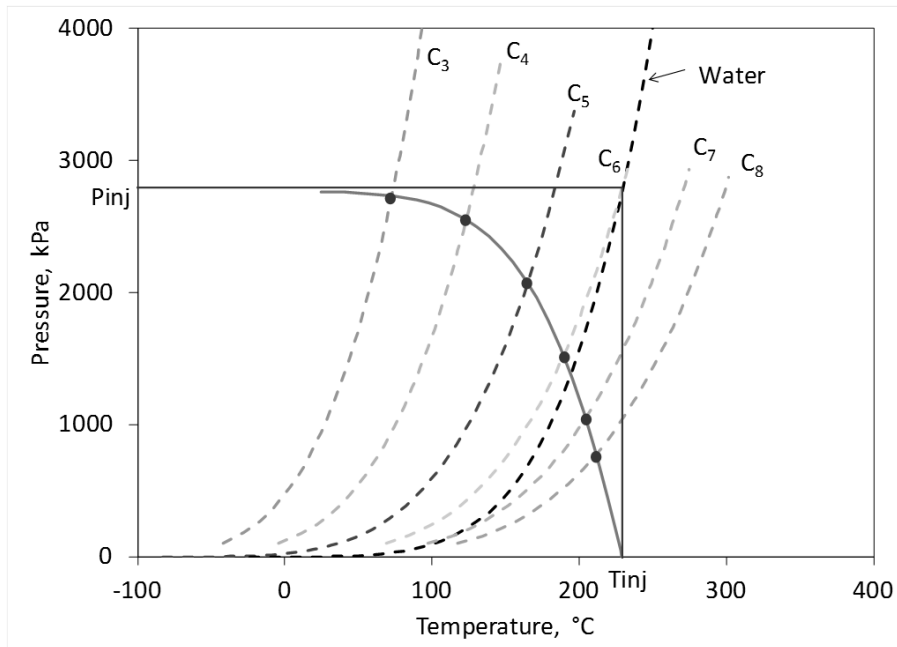


**Figure 3-1. Example for solutions of Equation 3-2 for a few different single-component solvents at an injection pressure  $P_{inj}$ .**

Dashed curves are vapor pressures of water and a few solvent components. The bold solid curve shows  $P_{inj} - P_{water}^{vap}$ , where  $P_{water}^{vap}$  is the vapor pressure of water. The dot on the vapor pressure curve of each solvent represents the solution of Equation 3-2 for  $T_{3p}$  when that solvent is coinjected with steam.  $T_{3p}$  corresponds to the chamber-edge temperature.

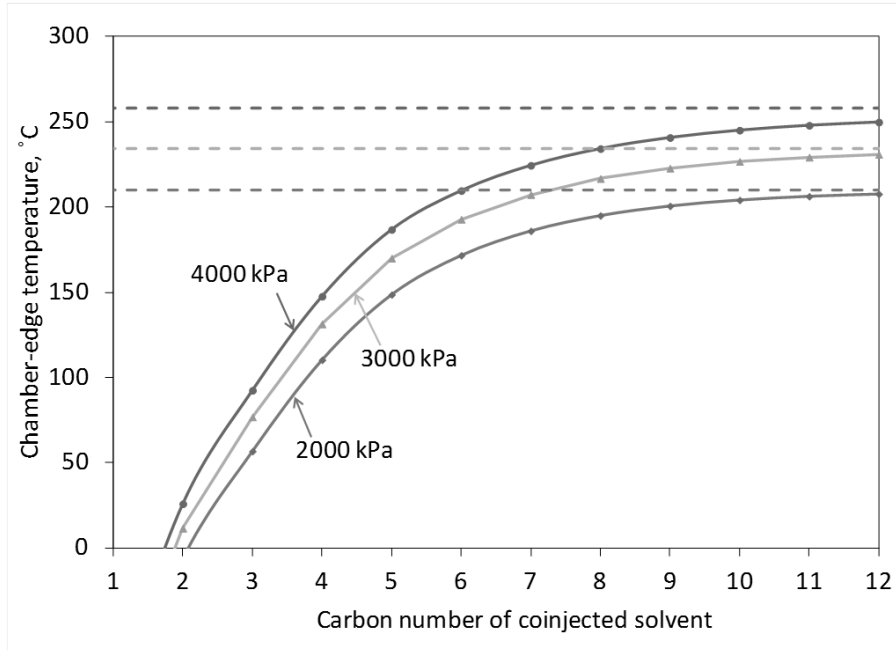


**Figure 3-2. Chamber-edge temperatures estimation using Equation 3-2 for single-component solvents from  $C_1$  to  $C_{12}$  for injection pressures of 2.0 MPa, 3.0 MPa, and 4.0 MPa.**

The horizontal asymptote of each curve is shown by a dashed line, which is the chamber-edge temperature for steam-only injection at that pressure. The vertical distance between each data point and its respective horizontal asymptote is the temperature reduction at the chamber edge with respect to  $T_{inj}$ . This reduction is more severe as the solvent becomes more volatile for a given injection pressure and as the injection pressure increases for a given single-component solvent. The plots are used for temperature above the original reservoir temperature.

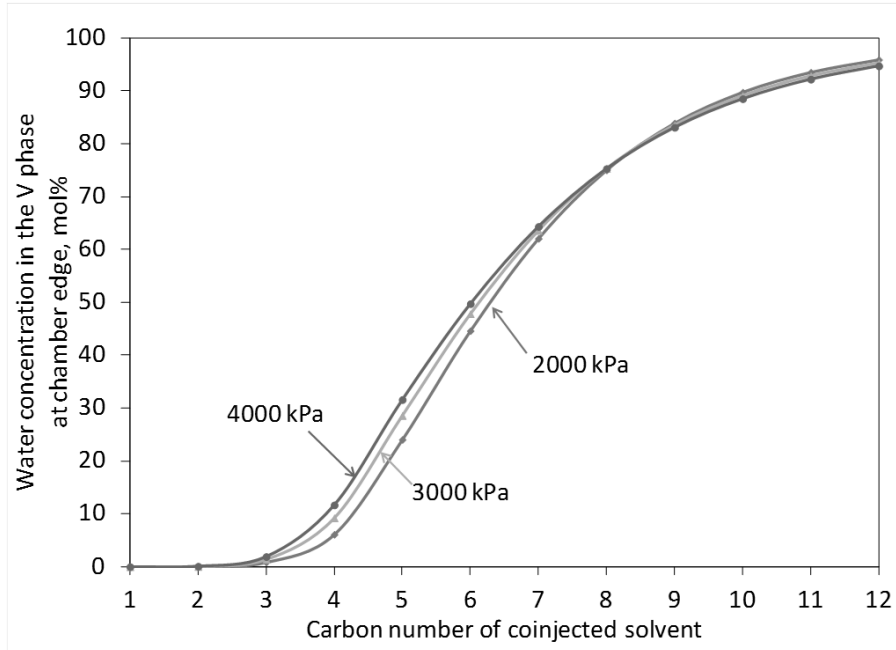
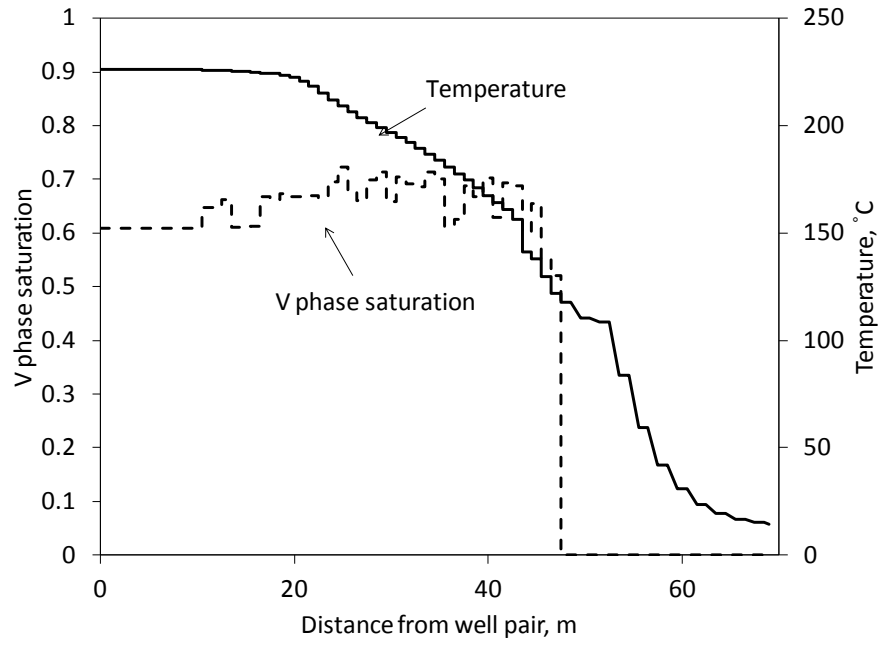
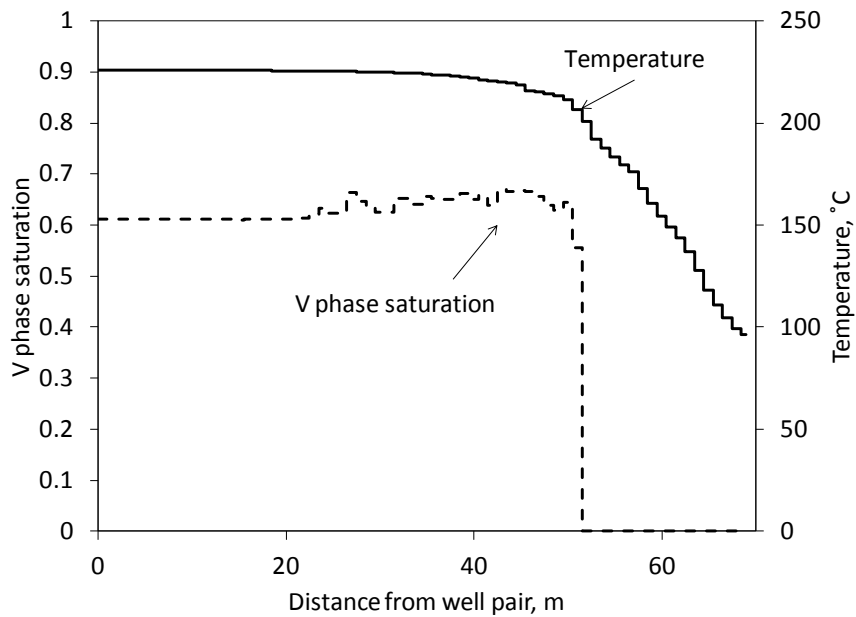


**Figure 3-3. Water mole fraction in the V phase at the chamber edge edge for coinjection of a single-component solvent and steam.**

Dots are solutions of Equation 3-1 after solving Equation 3-2 for  $T_{3p}$ . Coinjection of a more volatile solvent results in a lower concentration of water in the V phase near the chamber edge.



(a) C<sub>4</sub> and steam coinjection



(b)  $C_8$  and steam coinjection

**Figure 3-4. Variations of temperature and the V phase saturation simulated along the sixth row from the top of the reservoir model at two years.**

The chamber edge is defined where the V phase saturation becomes zero on the phase transition between three and two phases. The temperature in the gridblock just before the gridblocks without the V phase is considered to be the chamber-edge temperature. The chamber-edge temperature is 122°C in (a), where  $C_4$  is coinjected with steam at 2730 kPa, and it is 207°C in (b), where  $C_8$  is coinjected with steam at 2730 kPa.

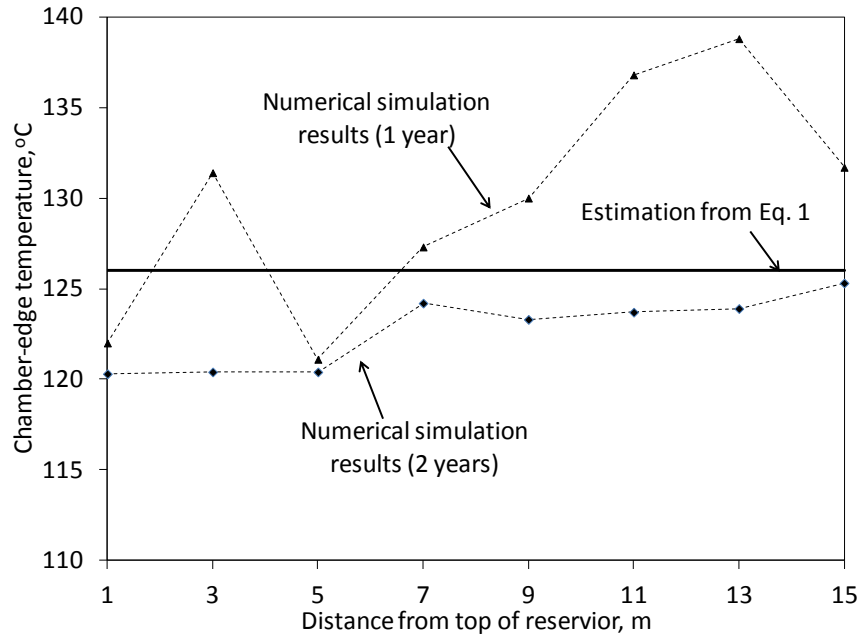


**Figure 3-5. Comparison of numerical simulation results and estimations from Equation 3-2 for the chamber-edge temperature**

$C_4$  is the coinjected solvent here. Results are presented for different rows of the reservoir model at 1 year and 2 years. The assumptions made for Equation 3-2 result in an error range of  $\pm 15^\circ\text{C}$  in the cases studied.

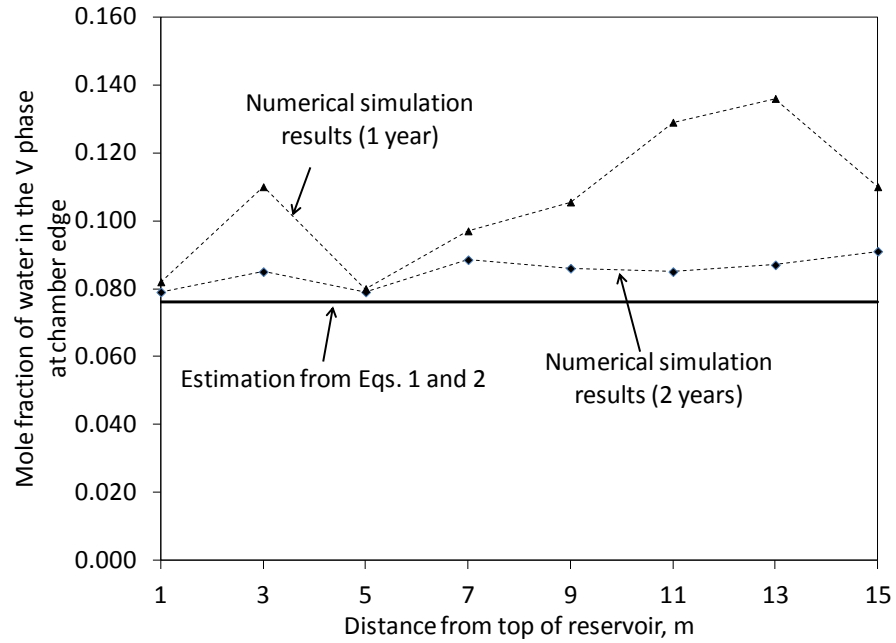
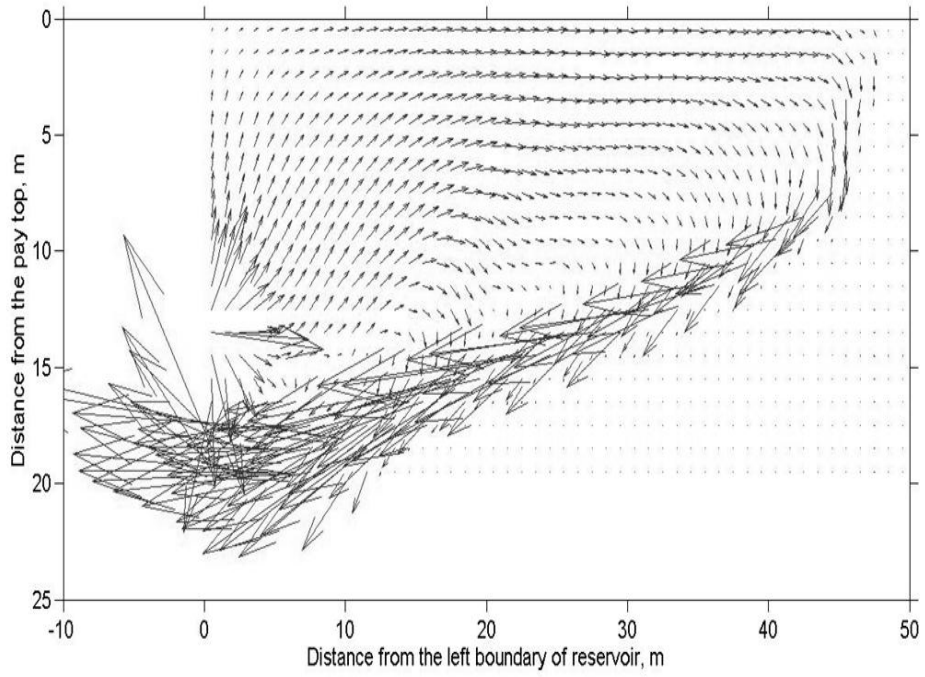
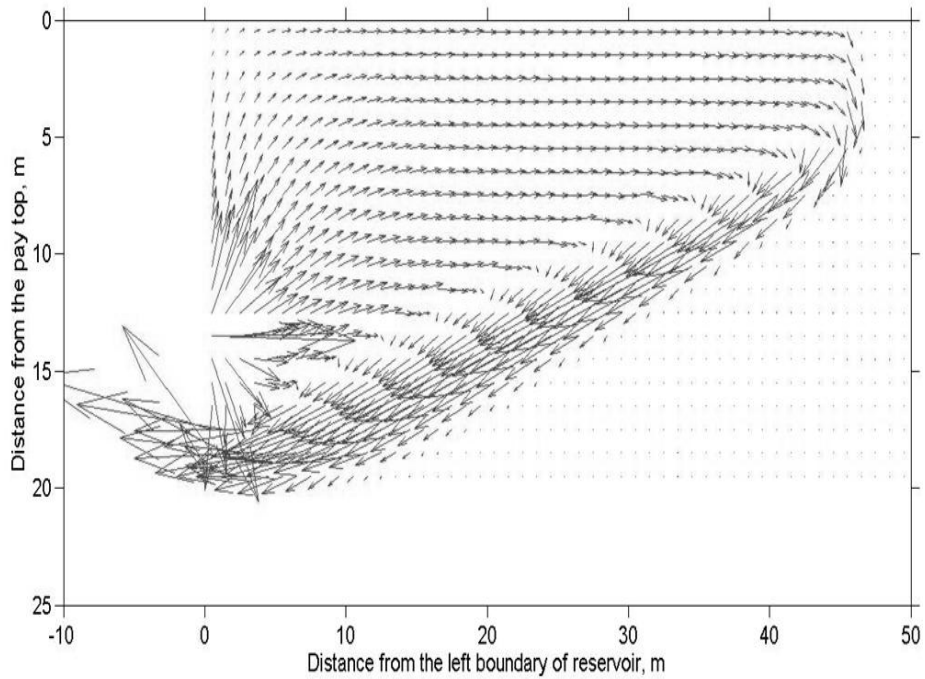


**Figure 3-6. Comparison of numerical simulation results and estimations from Equation 3-1 for the water mole fraction in the V phase at the chamber edge.**

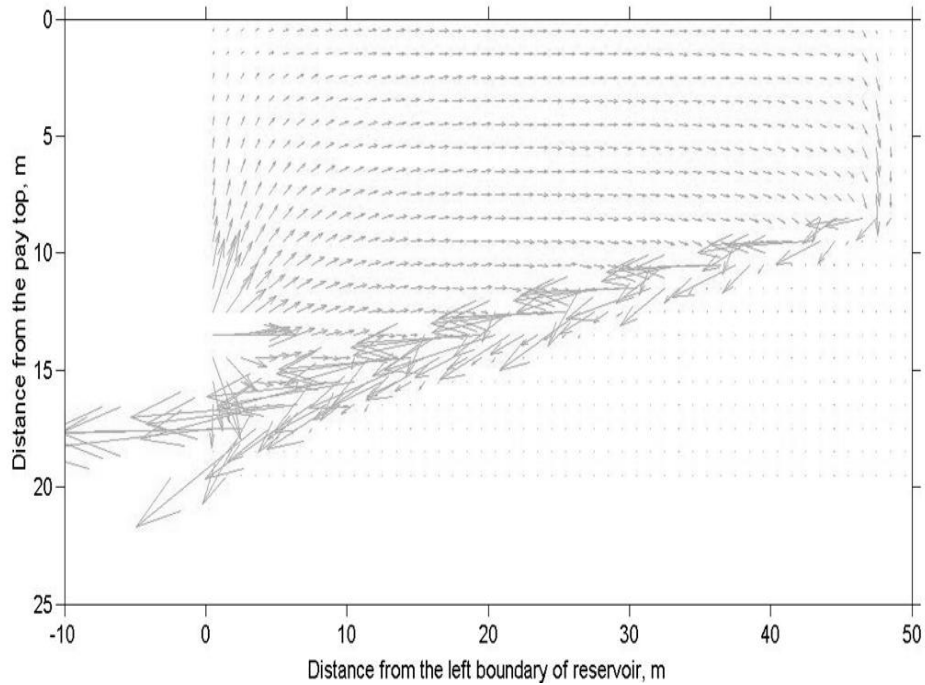
$C_4$  is the coinjected solvent here. Results are presented for different rows of the reservoir model at 1 year and 2 years.



(a)  $C_4$  and steam coinjection, 23 months from the start of simulation.



(b)  $C_8$  and steam coinjection, 17 months from the start of simulation.



(c) Steam-only injection, 23 months from the start of simulation.

**Figure 3-7. Water molar fluxes in steam-only injection and the C<sub>4</sub> and C<sub>8</sub> coinjection cases.**

The well pair is located at the left boundary of the reservoir. Horizontal axis shows the distance from the left boundary, and the vertical axis shows the distance from the top of the reservoir model. Arrows represent the direction and the magnitude of water molar fluxes. Lengths of arrows cannot be compared among different cases since they have different scales. Downward deviation of fluxes indicates gradual condensation of steam along the temperature gradient in the chamber. As the coinjected solvent becomes more volatile, condensation of steam starts deeper in the chamber. This reduces the efficiency of heat flow to the chamber edge.

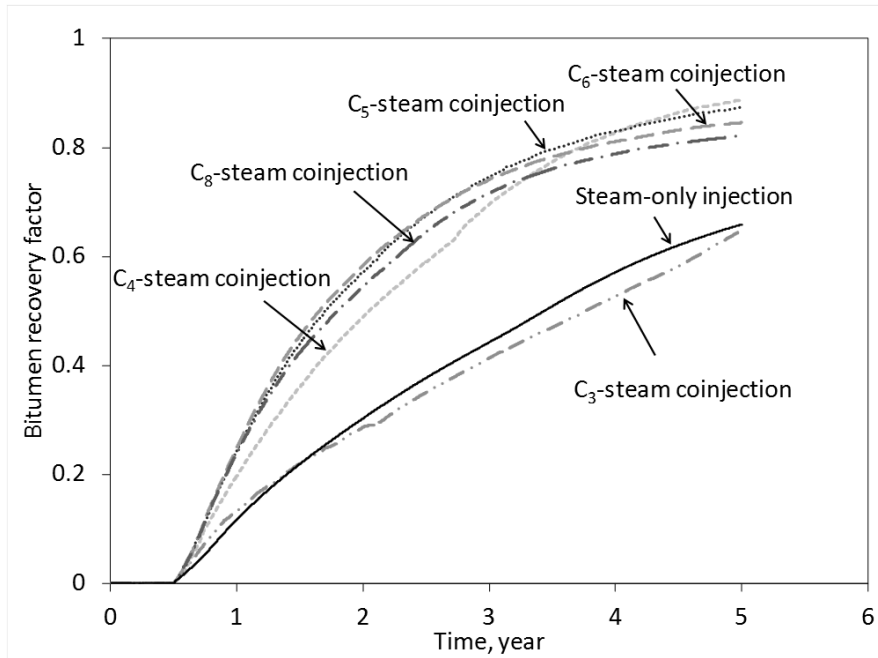


**Figure 3-8. Oil recoveries for the steam-only injection and coinjection cases.**

Solvent production is excluded in the oil recovery calculation. Reservoir and fluid properties used are given in Table 3-1. The solvent concentration in the coinjection stream is 2.0 mol%.

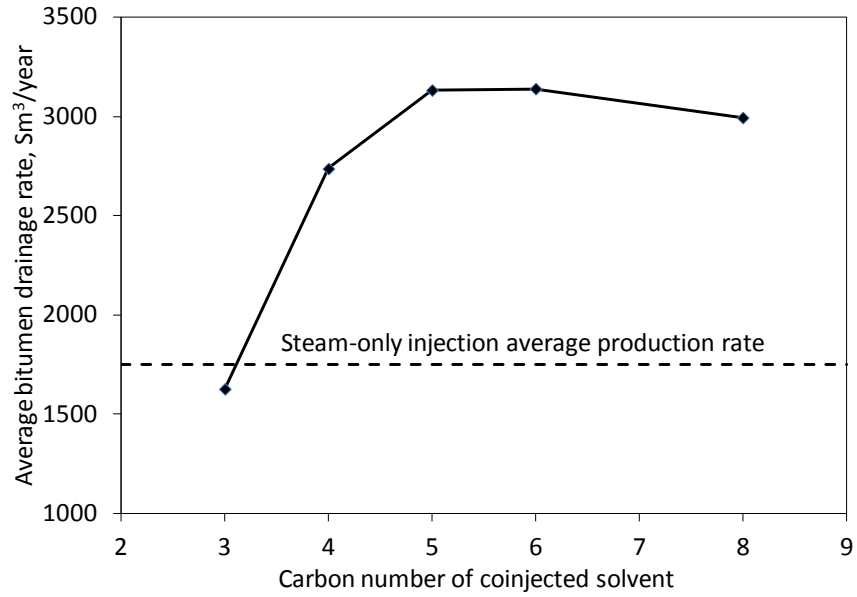


**Figure 3-9. Average bitumen production rates for the first 2.5 years in Figure 3-8**

The bitumen production rate is affected by coupled effects of heat and solvent dilution on the mobility of the draining L phase near the chamber edge. The break-over point in this figure occurs when these two effects take a balance. The average production rate for steam-only injection is shown with a horizontal line.

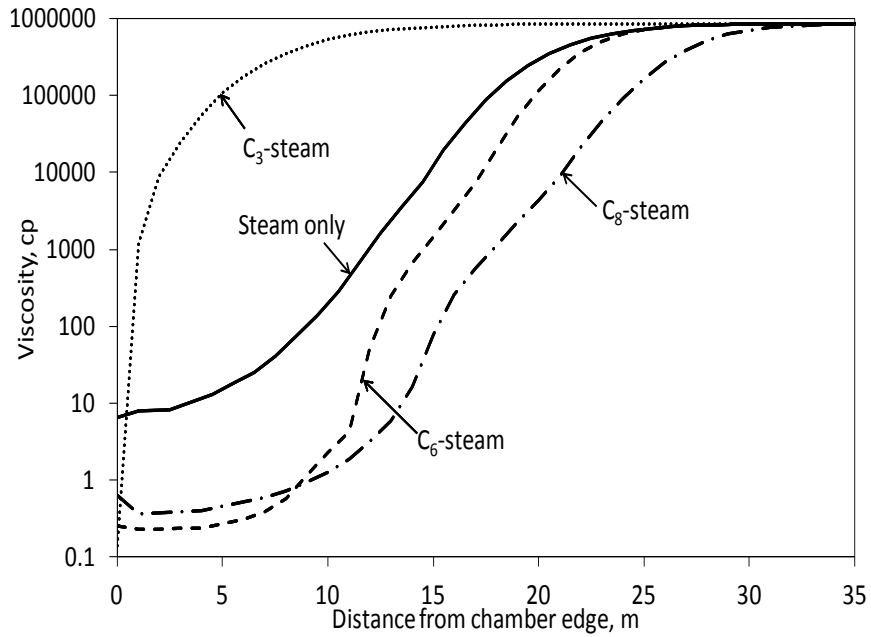


**Figure 3-10. Profiles of the L phase viscosities in the 12<sup>th</sup> row of the reservoir model at 1.5 years.**

The main portion of oil drainage occurs within a few meters of the chamber edge. Thus, the L phase viscosity in this region has a significant effect on the drainage rate. Solvent dilution effects cannot offset the negative effects of a lowered temperature at the chamber edge for the C<sub>3</sub> coinjection case. The L phase viscosity right ahead of the chamber edge is higher in C<sub>3</sub>-steam coinjection compared to that in steam-only injection.

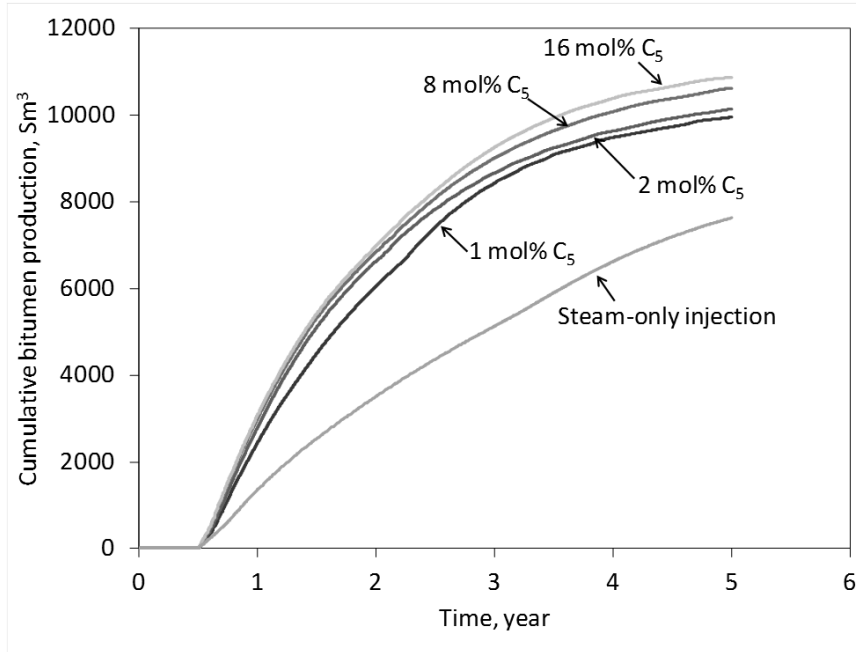
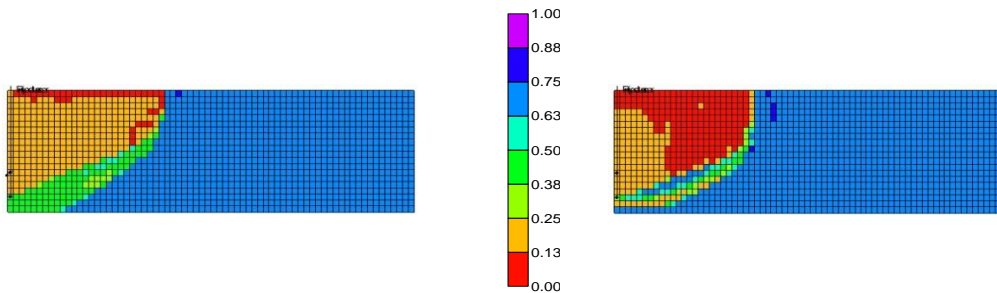
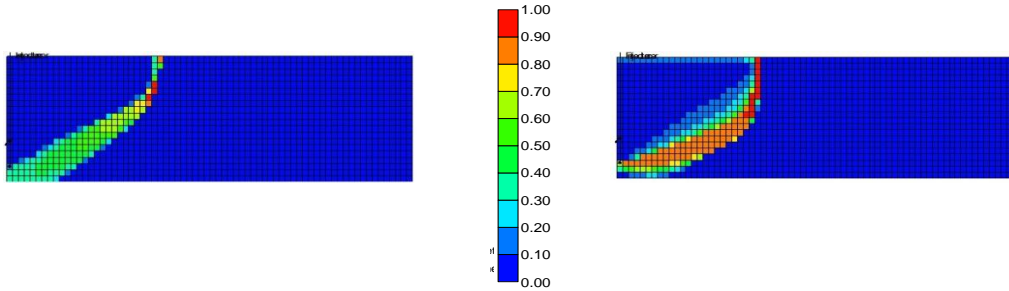


**Figure 3-11. Comparison of cumulative oil production**

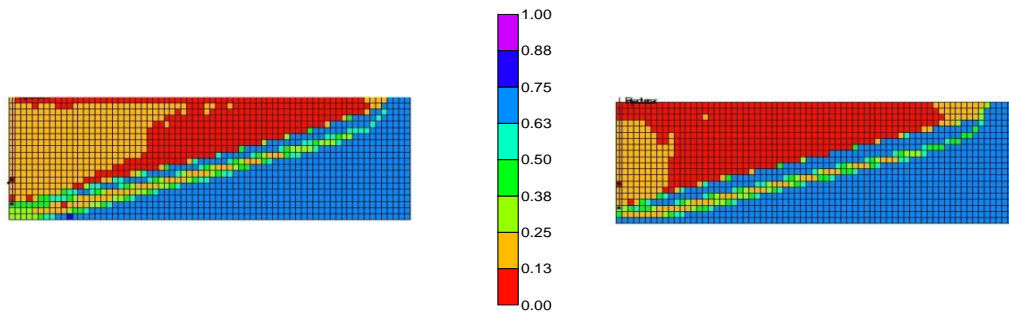
Comparison of cumulative oil production for steam-only injection and  $C_5$ -steam coinjection with different molar concentrations. Increasing the concentration of solvent in the injectant improves oil production rate.



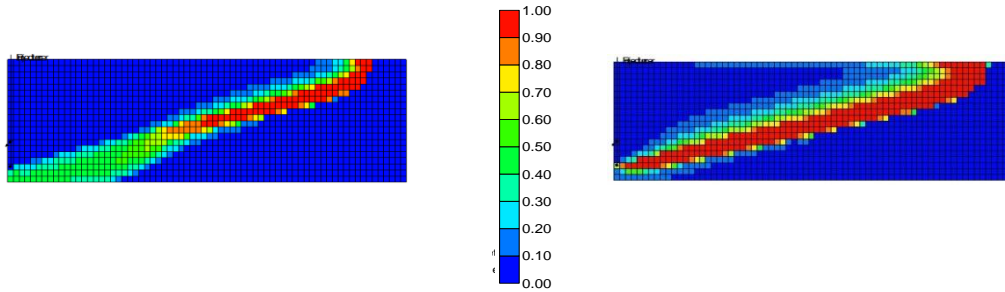
(a) Profiles of the L phase saturation in  $C_5$ -steam coinjection at 1 year; Left:  $C_5$  concentration of 1 mol%, Right:  $C_5$  concentration of 8 mol%. Regions in red indicate enhanced local displacement efficiency with the L phase saturations below  $S_{or}$ . The higher  $C_5$  concentration gives higher local displacement efficiency.



(b) Profiles of the  $C_5$  mole fraction in the L phase for  $C_5$ -steam coinjection at 1 year; Left:  $C_5$  concentration of 1 mol%, Right:  $C_5$  concentration of 8 mol%. The higher  $C_5$  concentration gives a thicker region of solvent accumulation near the chamber edge.



(c) Profiles of the L phase saturation in  $C_5$ -steam coinjection at 2 years; Left:  $C_5$  concentration of 1 mol%, Right:  $C_5$  concentration of 8 mol%. Regions in red indicate enhanced local displacement efficiency with the L phase saturations below  $S_{or}$ . Local displacement efficiency is improved in the near-well region for the higher concentration case. The reason for the displacement efficiency not being improved in the small region at the top corner edge of chamber is that temperature has not risen up sufficiently due to accumulation of solvent in this region.



(d) Profiles of the  $C_5$  mole fraction in the L phase for  $C_5$ -steam coinjection at 2 years; Left:  $C_5$  concentration of 1 mol%, Right:  $C_5$  concentration of 8 mol%. Continuous coinjection of a high-concentration solvent results in an unfavorably thick region of solvent accumulation. This can lead to a significant amount of solvent being trapped near the chamber edge by the end of process.

**Figure 3-12. Profiles of the L phase saturation and solvent ( $C_5$ ) mole fraction in the L phase in solvent/steam coinjection simulations at 1 and 2 years.**

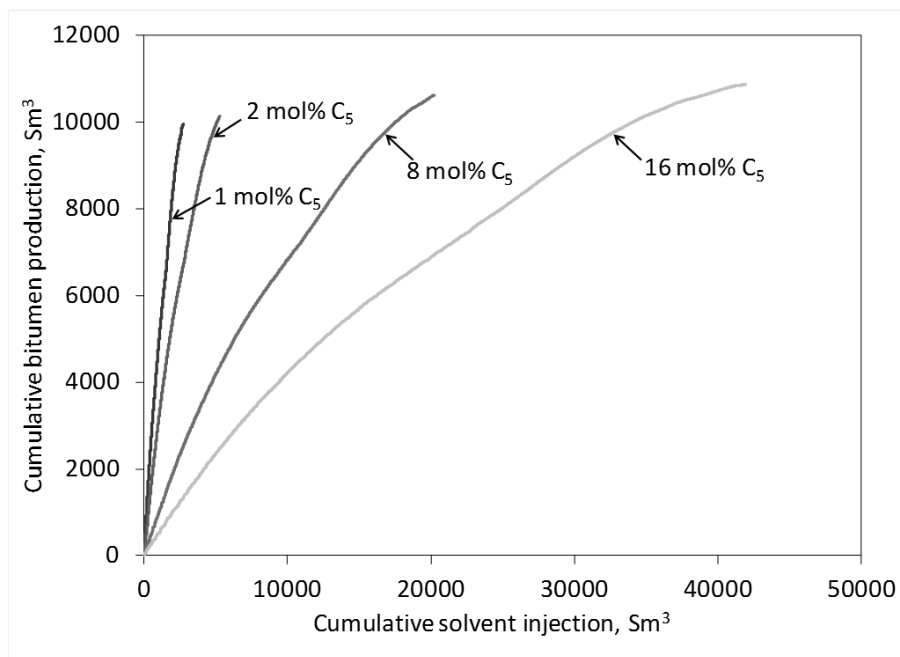


**Figure 3-13. The cumulative oil production with respect to the cumulative volume of  $C_5$  coinjected with steam.**

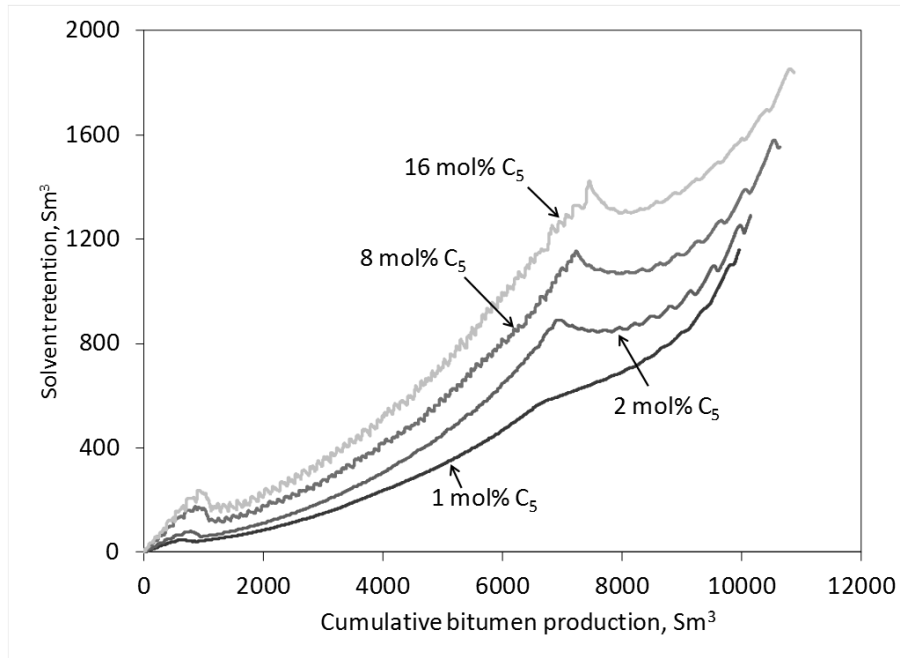


**Figure 3-14. Solvent volumes retained in the reservoir for C<sub>5</sub>-steam coinjection simulations with different solvent concentrations.**

C<sub>5</sub> is continuously coinjected with a constant concentration in the cases in this figure. A molar concentration of C<sub>5</sub> in the injection stream is shown beside each curve. Solvent retention in the reservoir increases as the solvent concentration increases.

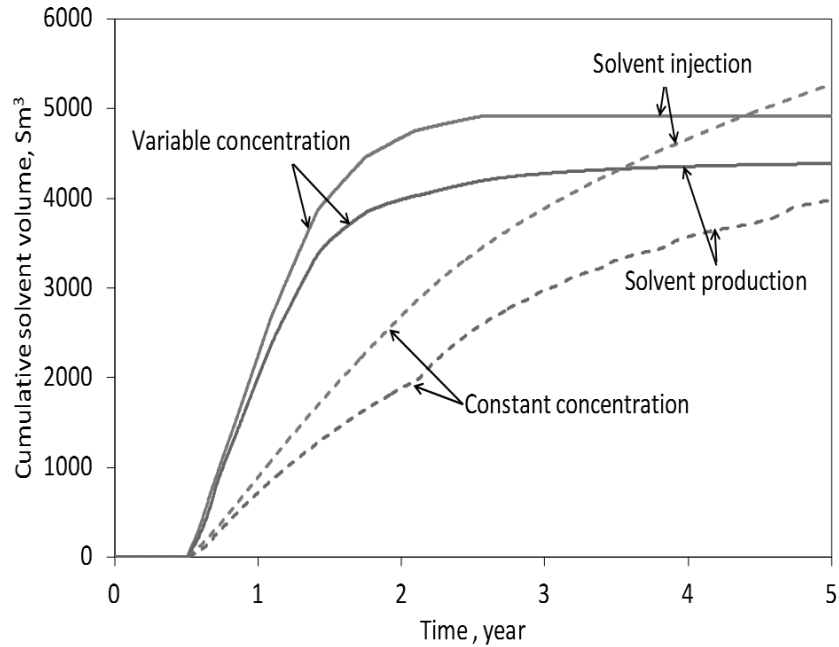


**Figure 3-15. Injection and production volumes of  $C_5$  in coinjection simulations using two different injection procedures.**

The solid line corresponds to the modified coinjection procedure given in the Design of Solvent Concentration section. The dashed line corresponds to a constant solvent concentration of 2.0 mol%. Solvent recovery is improved from 75.5% in the constant-concentration case to 89.2% in the modified coinjection procedure.

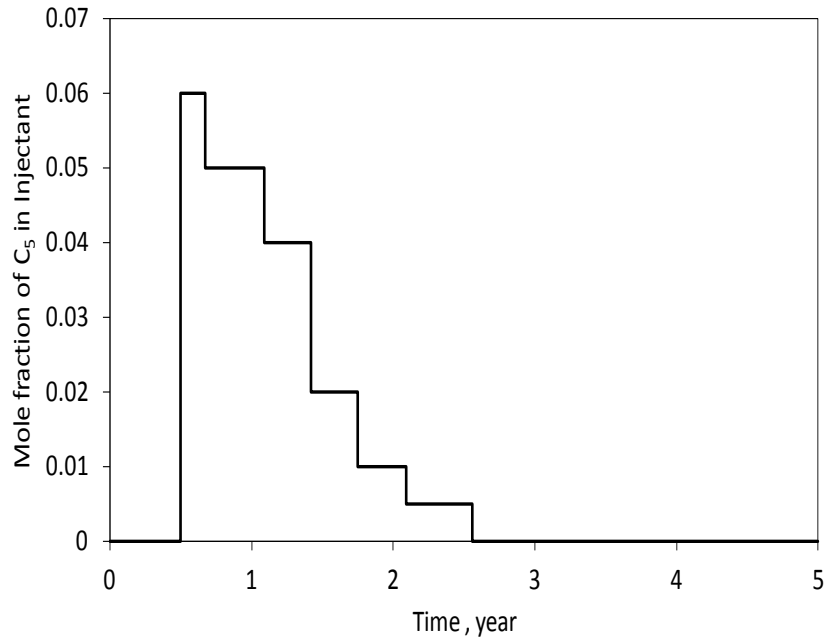
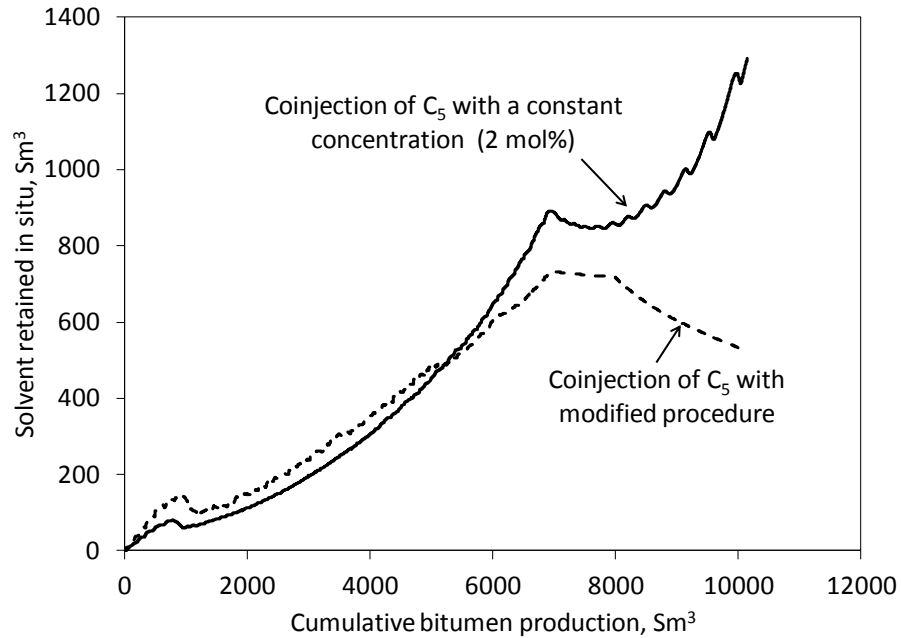
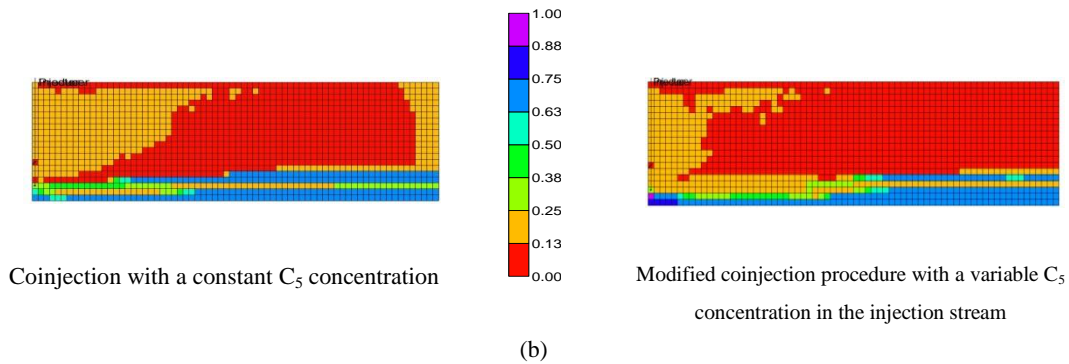


**Figure 3-16. Variation of the solvent concentration in the injectant during the modified coinjection procedure.**

C<sub>5</sub> is used as the solvent here. Coinjection is initiated with a high solvent concentration after the inter-well thermal communication is established. Coinjection is continued with a declining trend of the solvent concentration and is terminated at 2.6 years when the chamber reaches the lateral boundary for the well pair.



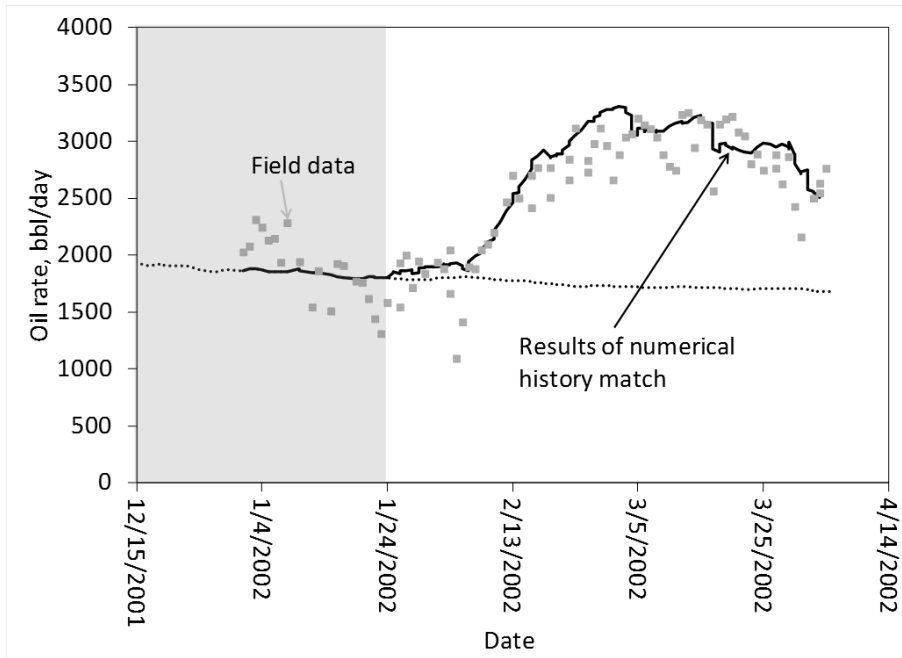
(a)



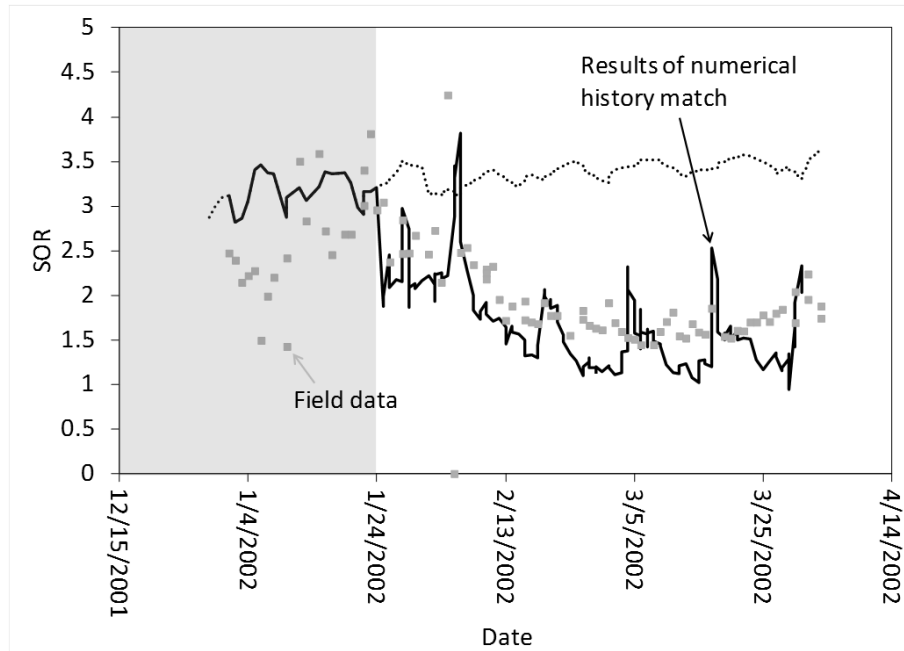
(b)

**Figure 3-17. Volumes of C<sub>5</sub> left in the reservoir and the L phase saturation distributions after five years of operation for the two injection procedures; one with a constant C<sub>5</sub> concentration of 2.0 mol% and the other with a variable C<sub>5</sub> concentration.**

Red regions in the L phase saturation profiles show enhanced local displacement efficiency. The variable-concentration case can enhance local displacement efficiency in a wider region.



(a)



(b)

**Figure 3-18. Field data and results of simulation history matching for well pair C1 in the Senlac SAP project in 2002.**

(a) the bitumen production rate and (b) the steam-oil ratio. Scattered points are field data reported by Gupta et al. (2005). The period before the SAP test is shaded. The dotted line shows the expected trend of the SAGD performance without SAP. The oil production rate is reported in bbl/day for simplicity of comparison with results reported by Gupta et al.

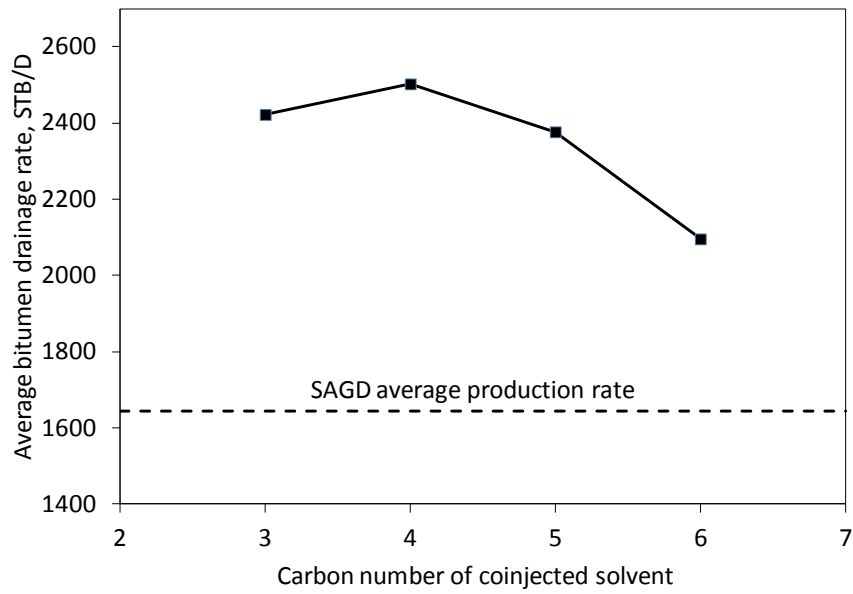
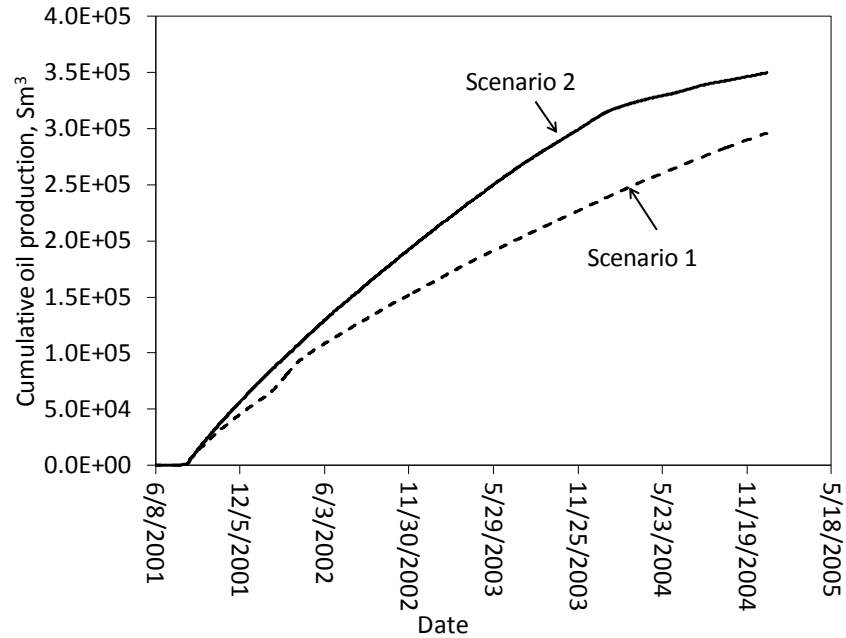
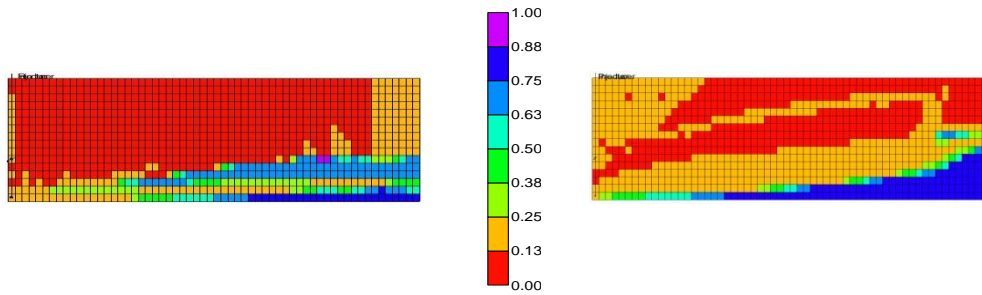


**Figure 3-19. The average oil production rates after 8 months of SAP in simulations with different single-component solvents.**

The average oil production rate for steam-only injection is shown with a horizontal line. The break-over point occurs at  $C_4$  where there is an optimum balance between the heat transfer effect and the solvent diluting effect on the oil drainage rate.



(a)



(b)

**Figure 3-20. Comparison of EnCana’s original operation (scenario 1) and a modified coinjection process (scenario 2) for the Senlac SAP pilot.**

(a) Cumulative oil production histories. (b) Profiles of the L phase saturation at the end of two SAP cases; scenario 2 is given on the left and scenario 1 is given on the right.  $C_4$  is used as an optimum solvent here. Regions in red exhibit enhanced displacement efficiency;  $S_o < S_{or}$ . The modified coinjection procedure results in 14% additional oil recovery and improves local displacement efficiency in the near-well region.

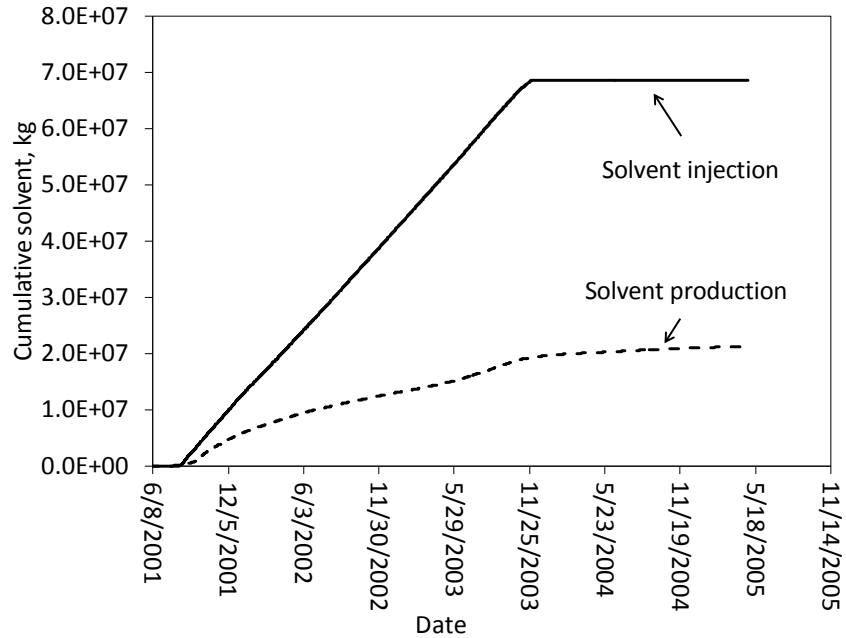


**Figure 3-21. Cumulative solvent injection and production during SAP with scenario 2.**

Coinjection starts with a  $C_4$  concentration of 4 mol% right after thermal communication is achieved between the wells. Solvent concentration decreases gradually until it becomes zero for the last 1.5 years of simulation. The  $C_4$  amounts are reported on the mass basis since  $C_4$  is produced in the L and V phases. Although scenario 2 attempts to lower solvent retention in the L phase by the end of process, the overall solvent recovery is not as successful as the case studied earlier. This is because the main retention of solvent in this case occurs in the V phase due to the high volatility of  $C_4$ .

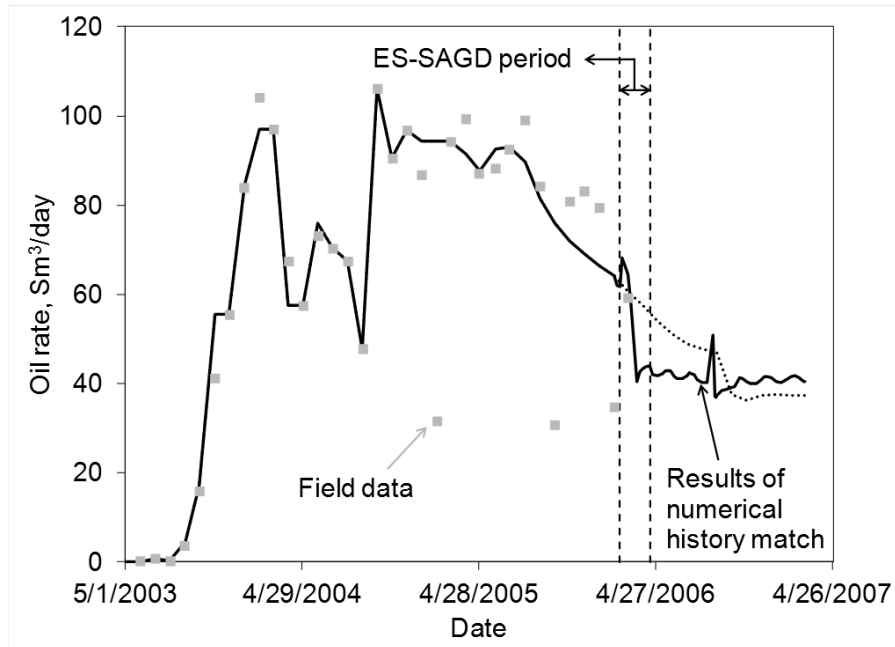


**Figure 3-22. Field data and results of history matching for oil production rate from well pair 3 for the Long Lake SAGD/ES-SAGD project.**

Scattered points are field data reported by Orr et al. (2007). The bold curve shows simulated bitumen production rate. ES-SAGD is conducted in February and March 2006.  $C_{10}$  is continuously coinjected with steam with a  $C_{10}$  concentration of 0.5 mol% for this period. The dashed curve shows the forecasted trend of oil production in SAGD with no ES-SAGD.

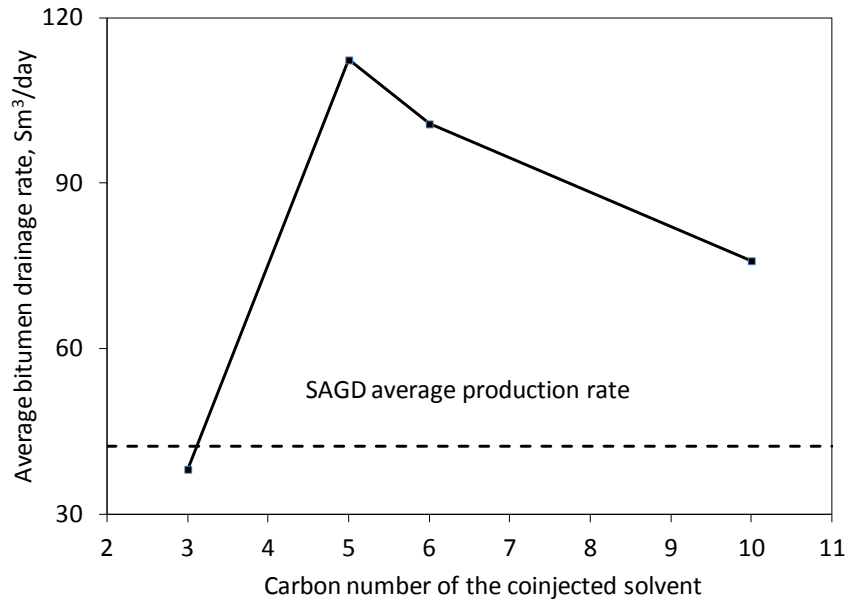
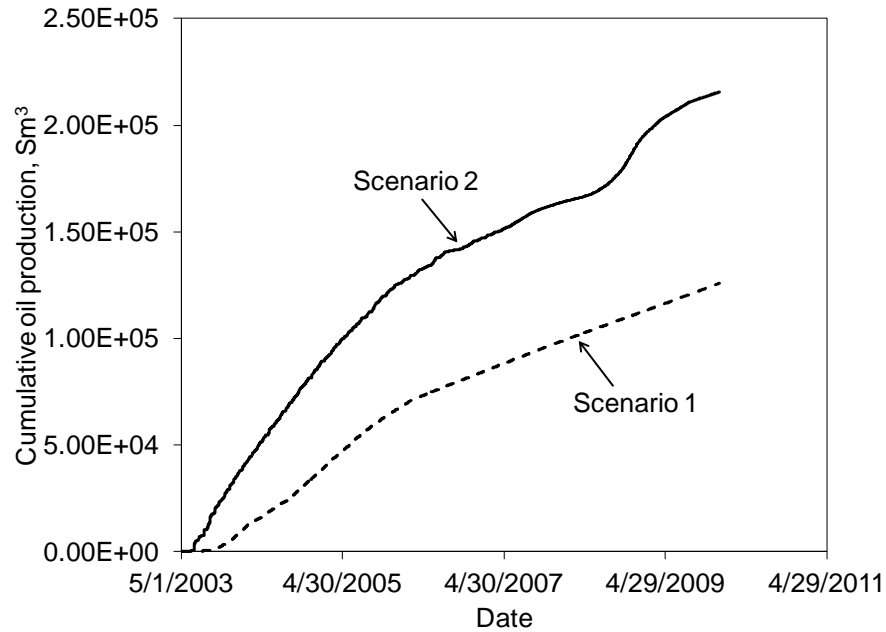
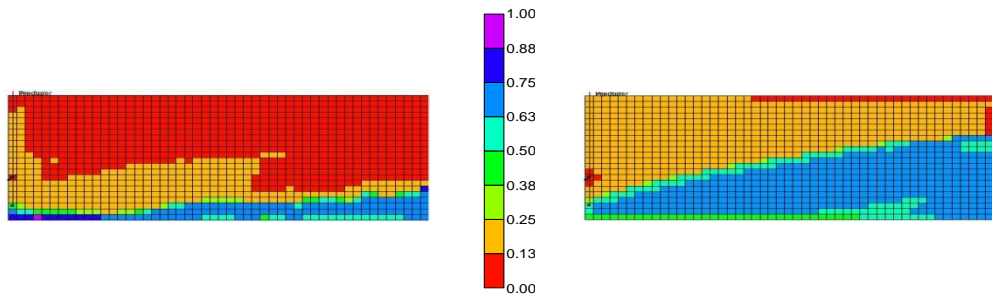


**Figure 3-23. Average oil production rates for 1.5 years of the Long Lake ES-SAGD with different single-component solvents.**

The average oil production rate for steam-only injection (i.e., SAGD) is shown as a horizontal line. The break-over point is observed at C<sub>5</sub>, where there is an optimum balance between the heat transfer effect and the solvent diluting effect on the oil drainage rate.



(a)



(b)

**Figure 3-24. Comparison between Nexen’s original process (scenario 1) and the modified coinjection (scenario 2) for the Long Lake ES-SAGD pilot.**

(a) Cumulative bitumen production histories. (b) Profiles of the L-phase saturation at 6.6 years. Scenario 2 is given on the left, and scenario 1 on the right. Solvent production as part of the L phase is excluded in calculations of cumulative productions. Results indicate that scenario 2 yields 34% more oil recovery than scenario 1 by January 2010. Scenario 2 exhibits faster chamber propagation and a wider region of local displacement efficiency improvement. Regions in red in Figure 3-24b exhibit enhanced displacement efficiency, where the L-phase saturation is lower than the input residual oil saturation.

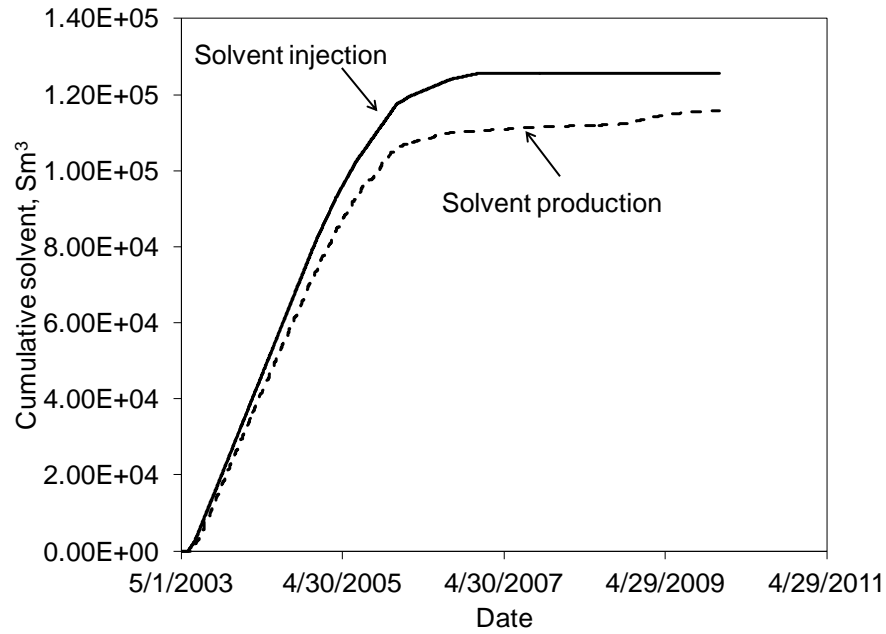


**Figure 3-25. Injection and production volumes of C<sub>5</sub> for scenario 2 for the Long Lake ES-SAGD simulation.**

Coinjection starts with 6 mol% of solvent in the injectant. Solvent concentration is then decreased in a step-wised manner. Part of the accumulated solvent in the chamber is recovered after the termination of solvent coinjection in January 2007. Results indicate that more than 90% of the injected solvent is recovered.

## References

- Ardali, M., Barrufet, M.A., Mamora, D.D., Qiu, F., 2012b. A Critical Review of Hybrid Steam/Solvent Processes for the Recovery of Heavy Oil and Bitumen. Paper SPE 159257 presented at SPE Annual Technical Conference and Exhibition, San Antonio, Texas, USA, October 8-10.
- Ardali, M., Barrufet, M., and Mamora, D.D. 2012a. Laboratory Testing of Addition of Solvents to Steam to Improve SAGD Process. Paper SPE 146993 presented at SPE Heavy Oil Conference Canada, Calgary, Alberta, Canada, June 12-14.
- Ardali, M., Mamora, D.D., and Barrufet, M. 2010. A Comparative Simulation Study of Addition of Solvents to Steam in SAGD Process. CSUG/SPE Paper 138170 presented at Canadian Unconventional Resources and International Petroleum Conference, Calgary, Alberta, Canada, October 19-21.
- Boyle, T.B., Gittins, S.D. and Chakrabarty, C. 2003. The Evolution of SAGD Technology at East Senlac. *Journal of Canadian Petroleum Technology* **42** (1): 58-61.
- Butler, R.M. 1997. *Thermal Recovery of Oil and Bitumen*. Prentice Hall.
- Computer Modelling Group (CMG) Ltd. STARS User Manual. Version 2011. Calgary, Alberta, Canada, 2011.
- Deng, X. 2005. Recovery Performance and Economics of Steam/Propane Hybrid Process. Paper SPE/PS-CIM/CHOM 97760 presented at the 2005 SPE International Thermal Operations and Heavy Oil Symposium, Calgary, Alberta, Canada, November 1-3.
- Deng, X., Huang, H., Zhao, L., Law, D.H.-S., and Nasr, T.N. 2010. Simulating the ES-SAGD Process with Solvent Mixture in Athabasca Reservoirs. *Journal of Canadian Petroleum Technology* **49** (1): 38-46.
- Dong, L. 2012. Effect of Vapor-Liquid Phase Behavior of Steam-Light Hydrocarbon Systems on Steam Assisted Gravity Drainage Process for bitumen recovery. *Fuel* **95**: 159-168.
- Edmunds, N. and Moini, B. 2010. Advanced Solvent-Additive Processes by Genetic Optimization. *Journal of Canadian Petroleum Technology* **49** (9): 34-41.
- Gates, I.D. 2007. Oil Phase Viscosity Behavior in Expanding-Solvent Steam-Assisted Gravity Drainage. *Journal of Petroleum Science and Engineering* **59** (1-2): 123-134.
- Gates, I.D. and Chakrabarty, N. 2008. Design of Steam and Solvent Injection Strategy in Expanding Solvent Steam-Assisted Gravity Drainage. *Journal of Canadian Petroleum Technology* **47** (9): 12-19.
- Gates, I.D. and Gutek, A.M.H. 2008. Process for In Situ Recovery of Bitumen and Heavy Oil. U.S. Patent 7464756.
- Govind, P.A., Das, S.K., Srinivasan, S., and Wheeler, T.J. 2008. Expanding Solvent SAGD in Heavy Oil Reservoirs. Paper SPE/PS/CHOA presented at the 2008 SPE International

- Thermal Operations and Heavy Oil Symposium, Calgary, Alberta, Canada, October 20-23.
- Gupta, S.C. and Gittins, S.D. 2007b. Effect of Solvent Sequencing and Other Enhancements on Solvent Aided Process. *Journal of Canadian Petroleum Technology* **46** (9): 57-61.
- Gupta, S. and Gittins, S. 2007a. Optimization of Solvent Aided Process. Paper 2007-022 presented at the Petroleum Society's 8th Canadian International Petroleum Conference, Calgary, Alberta, Canada, June 12-14.
- Gupta, S. and Gittins, S.D. 2006. Christina Lake Solvent Aided Process Pilot. *Journal of Canadian Petroleum Technology* **45** (9), 15-18.
- Gupta, S., Gittins, S., and Picherack, P. 2005. Field Implementation of Solvent Aided Process. *Journal of Canadian Petroleum Technology* **44** (11): 8-13.
- Gupta, S., Gittins, S., and Picherack, P. 2003. Insights into Some Key Issues with Solvent Aided Process. *Journal of Canadian Petroleum Technology* **43** (2): 54-61.
- Hosseininejad Mohebati, M., Maini, B.B. and Harding, T.G. 2010. Optimization of Hydrocarbon Additives with Steam in SAGD for Three Major Canadian Oil Sand Deposits. Paper CSUG/SPE 138151 presented at the Canadian Unconventional Resources and International Petroleum Conference, Calgary, Alberta, Canada, October 19-21.
- Ivory, J., Zheng, R., Nasr, T., Deng, X., Beaulieu, G., and Heck, G. 2008. Investigation of Low Pressure ES-SAGD. Paper SPE 117759 presented at 2008 SPE International Thermal Operations and Heavy Oil Symposium, Calgary, Alberta, Canada, October 20-23.
- Jha, R.K., Kumar, M., Benson, I., and Hanzlik, E. 2012. New Insights into Steam-Solvent Co-Injection Process Mechanism. Paper SPE 159277 presented at 2012 SPE Annual Technical Conference and Exhibition, San Antonio, Texas, October 8-10.
- Jiang, H., Deng, X., Huang, H., Beaulieu, G., Heck, G., Akinlade, O.G., and Nasr, T.N. 2012. Study of Solvent Injection Strategy in ES-SAGD Process. Paper SPE 157838 presented at SPE Heavy Oil Conference, Calgary, Alberta, Canada, June 12-14.
- Jiang, Q., Butler, R., and Yee, C.T. 1998. The Steam and Gas Push (SAGP)-2: Mechanism Analysis And Physical Model Testing. Petroleum Society's 49th Annual Technical Meeting, Calgary, Alberta, Canada, June 8-10.
- Keshavarz, M., Okuno, R., and Babadagli, T. 2012. Efficient Oil Displacement Near the Chamber Edge in ES-SAGD. Submitted for publication to *Journal of Petroleum Science and Engineering* on July 27, 2012.
- Leaute, R.P. 2002. Liquid Addition to Steam for Enhancing Recovery of Bitumen with CSS: Evolution of Technology from Research Concept to a Field Pilot at Cold Lake. SPE/Petroleum Society of CIM/CHOA Paper 79011, Calgary, Alberta, Canada, November 4-7.

- Leaute, R.P. and Carey, B.S. 2005. Liquid Addition to Steam for Enhancing Recovery (LASER) of Bitumen with CSS: Results from the First Pilot Cycle. Paper 2005-161 presented at the 56<sup>th</sup> Canadian International Petroleum Conference, Calgary, Alberta, Canada, June 7-9.
- Li, W., Mamora, D.D., and Li, Y. 2011b. Solvent-Type and -Ratio Impacts on Solvent-Aided SAGD Process. *SPE Reservoir Evaluation and Engineering* **14** (3): 320-331.
- Li, W., Mamora, D.D., and Li, Y. 2011a. Light-and Heavy-Solvent Impacts on Solvent-Aided-SAGD Process: A Low-Pressure Experimental Study. *Journal of Canadian Petroleum Technology* **50** (4): 19-30.
- Li, W. and Mamora, D.D. 2010. Phase Behavior of Steam with Solvent Coinjection under Steam Assisted Gravity Drainage (SAGD) Process. Paper SPE 130807 presented at the SPE EUROPEC/EAGE Annual Conference and Exhibition, Barcelona, Spain, June 14-17.
- Mehrotra, A.K. and Svrcek, W.Y. 1987. Corresponding States Method for Calculating Bitumen Viscosity. *Journal of Canadian Petroleum Technology* **26** (5): 60-66
- Mehrotra, A.K. and Svrcek, W.Y. 1986. Viscosity of Compressed Athabasca Bitumen. *Canadian Journal of Chemical Engineering* **64** (5): 844-847.
- Mohammadzadeh, O., Rezaei, N., and Chatzis, I. 2012. More Insight into the Pore-Level Physics of the Solvent-Aided SAGD (SA-SAGD) Process for Heavy Oil and Bitumen Recovery. Paper SPE 157776 presented at SPE Heavy Oil Conference Canada, Calgary, Alberta, Canada, June 12-14.
- Nasr, T.N., Beaulieu, G., Golbeck, H., and Heck, G. 2003. Novel Expanding Solvent-SAGD Process “ES-SAGD”. *Journal of Canadian Petroleum Technology* **42** (1): 13-16.
- Nasr, T. and Isaacs, E. 2001. Process for Enhancing Hydrocarbon Mobility Using a Steam Additive. U.S. Patent 6230814.
- Nexen Inc., 2012. Long Lake 2011-Subsurface Performance Presentation. ERCB’s database, <http://www.ercb.ca/data-and-publications/activity-and-data/insitu-progress> (accessed 18 April 2013).
- Nexen Inc., 2007. Annual Performance Presentation for Long Lake Oil Sand Scheme & Long Lake annual Resource Management Report. ERCB’s database, <http://www.ercb.ca/data-and-publications/activity-and-data/insitu-progress> (accessed 18 April 2013).
- Linstorm, P.J., and Mallard, W.G., *NIST Chemistry WebBook: NIST Standard Reference Database Number 69*, National Institute of Standards and Technology (NIST), Gaithersburg MD, 20899, <http://webbook.nist.gov> (accessed 1 October 2012).
- Orr, B. 2009. ES-SAGD; Past, Present and Future. Paper SPE-129518-STU presented at the 2009 SPE International Student Paper Contest at the SPE Annual Technical Conference and Exhibition, New Orleans, Louisiana, USA, October 4-7.
- Orr, B.W., Srivastava, P., Sadetsky, V., and Stefan, B.J. 2010. Reducing Steam Oil Ratio in Steam-Assisted Gravity Drainage. CSUG/SPE Paper 136851 presented at the Canadian

- Unconventional Resources and International Petroleum Conference, Calgary, Alberta, Canada, October 19-21.
- Peng, D.-Y. and Robinson, D.B. 1976. A New Two-Constant Equation of State. *Industrial and Engineering Chemistry Fundamentals* **15** (1): 59-64.
- Rachford, Jr., H.H. and Rice, J.D. 1952. Procedure for Use of Electronic Digital Computers in Calculating Flash Vaporization Hydrocarbon Equilibrium. *Petroleum Transactions, AIME* **195**: 327-328.
- Redford, D.A. and McKay, A.S. 1980. Hydrocarbon-Steam Processes for Recovery of Bitumen from Oil Sands. Paper SPE 8823 presented at SPE/DOE Enhanced Oil Recovery Symposium, Tulsa, Oklahoma, USA, April 20-23.
- Canbolat, S. and Akin, S. 2002. A Study of Steam-Assisted Gravity Drainage Process in the Presence of Noncondensable Gases. Paper SPE 75130 presented at SPE/DOE Improved Oil Recovery Symposium, Tulsa, Oklahoma, USA, April 13-17.
- Sharma, J. and Gates, I.D. 2010. Steam-Solvent Coupling at the Chamber Edge in an In Situ Bitumen Recovery Process. Paper SPE 128045 presented at the SPE Oil and Gas India Conference and Exhibition, Mumbai, India, January 20-22.
- Shu, W.R. and Hartman, K.J. 1988. Effect of Solvent on Steam Recovery of Heavy Oil. *SPE Reservoir Engineering* **3** (2): 457-465.
- Yazdani, A., Alvestad, J., Kjonsvik, D., Gilje, E., and Kowalewski, E. 2011. A Parametric Simulation Study for Solvent Co-injection Process in Bitumen Deposits. Paper SPE 148804 presented at the Canadian Unconventional Resources Conference, Calgary, Alberta, Canada, November 15-17.

## **CHAPTER 4 : A SEMI-ANALYTICAL SOLUTION TO OPTIMIZE SINGLE-COMPONENT SOLVENT COINJECTION WITH STEAM**

A version of this chapter has been submitted to SPE Reservoir Evaluation & Engineering for publication.

## **Introduction**

Steam assisted gravity drainage (SAGD) has been the most widely commercialized process for the recovery of bitumen and heavy oil in western Canada. In this process, steam propagates into the reservoir from a horizontal injection well in the form of a chamber called steam chamber. The heated bitumen in contact with steam chamber drains under the effect of gravity towards the production well located a few meters below the injection well. The draining oil is typically produced in conjunction with the condensed water in the form of emulsion (Butler 1977).

High energy demands as well as environmental concerns associated with SAGD have entailed emerging alternative processes. Solvent-steam coinjection (referred to as “coinjection” from this point on) is one of these alternatives and has been tested as field scale pilot applications under different commercial names. In almost all of coinjection processes, a small amount of hydrocarbon solvent is coinjected with steam in order to further reduce the viscosity of bitumen as a result of dilution in conjunction with heat transfer.

Successful applications of coinjection at the field and lab scale have reported improved oil production rates and ultimate recovery factors as well as reduced steam-oil ratio (SOR) in comparison with steam-only injection (Nasr et al. 2003; Ivory et al. 2008; Gupta et al. 2005; Gupta and Gittins 2006; Leaute 2002; Leaute and Carey 2005; Redford and McKay 1980; Li and Mamora 2010; Ardali et al. 2012; Mohammadzadeh et al. 2012).

Besides promising results of steam-solvent coinjection, there are also evidences that coinjection of solvents with steam has resulted in no improvement or an even worse performance compared to steam-only injection (Jiang et al. 1998; Canbolat et. al 2002; Hosseininejad-Mohabati et al. 2010; and Li and Mamora 2011; Shu and Hartman 1988). Therefore, when the high costs of solvents are taken into account, a proper choice of solvent becomes a vital issue for the practicality of coinjection processes.

Several studies investigated the effects of different solvents and/or their concentrations on various aspects of the coinjection process and, in particular, on

oil production rates. These studies have led to several proposals for optimum solvent selection and coinjection strategies. These proposals, however, are very specific to their experimental conditions or reservoir properties and are not necessarily consistent with each other. This implies that the current level of understanding of the key mechanisms of the coinjection process is not fully satisfactory.

A number of analytical efforts were made to better understand the fundamental physics and mechanisms involved during coinjection. Sharma and Gates (2010a) used a simple analytical model to predict the length scales of mass and heat transfer beyond the edge of a coinjection chamber. They identified two distinct regions beyond the edge of chamber; one in which solvent mass transfer is dominant with a length scale of 10 cm, and the other which is mainly controlled by heat transfer whose length scale is of order of 10 m. They concluded that both enhanced temperature and solvent distribution in the oil phase contribute to the reduction of oil viscosity and slight improvement of oil relative permeability.

In a subsequent study, Sharma and Gates (2011) developed a stability theory for the interface at the edge of steam or steam-solvent chamber. They identified three fundamental mechanisms that contribute to improved production rates by steam-solvent processes: 1) Reduction of oleic phase viscosity, 2) local enhancement of oil saturation at the edge of chamber, and 3) instability of vapor/oil interface which promotes more mixing and heat transfer. They explain the pick oil production rate observed for intermediate solvent as a result of maximized interface instability for these solvents. According to their results, this physically is due to the balance between solubility and viscosity reduction capability of solvent.

Sharma et al. (2011) derived a simple analytical model to predict oil production rates when methane is coinjected with steam. According to the results of their analytical model and numerical runs, methane coinjection with steam in SAGD is generally unfavorable. This, they state, is due to

accumulation of non-condensable gas at the steam condensation front which reduces the heat transfer rate to the bitumen beyond.

Keshavarz et al. (2012) conducted a numerical and theoretical study on C<sub>5</sub>-steam coinjection. They demonstrated that the production rate enhancement depends mainly on three factors; i.e., solvent accumulation, temperature distribution, and bitumen dilution with solvent near the chamber edge. They also demonstrated how SAGD residual oil saturation ( $S_{or}$ ) can be further reduced via coinjection.

Existence of a temperature gradient inside the coinjection chamber was also discussed by Dong (2012). He used a simplistic theoretical model involving a binary mixture of water and solvent only to describe the condensation behavior of steam and solvent in a coinjection chamber.

Keshavarz et al. (2013) verified the results of chamber edge estimation based on Dong's analysis against the results of numerical simulation in which some of the simplifying assumptions were relaxed. Existence of the reservoir oil as a third component as well as non-idealities are the most important relaxed assumptions that can result in deviating temperature and thus component accumulation at the chamber edge in numerical simulations. They also showed that an optimum volatility can be expected for the coinjected solvent as result of the balance between two factors affecting the oil mobility along the chamber edge; i.e., reduction of the chamber-edge temperature and superior dilution of oil in coinjection of more volatile solvent with steam.

In this work, a simple calculation algorithm is presented for estimation of temperature at the vapor/liquid interface in a system of water, solvent and oil. Solvent and oil are assumed to be single component for simplicity. Then a semi-analytical approach is taken to predict temperature and solvent distribution profiles beyond the chamber edge as a function of solvent accumulation at the chamber edge.

The sensitivity of the proposed model to different parameters is also analysed. This is achieved by applying the model to several solvent-steam coinjection processes. Results show that the oil production rate is a function of

the mobility as well as the reservoir oil content of the draining oleic phase. These two, in turn, depend on temperature profile, solvent diluting capabilities and its distribution in the vicinity of chamber edge.

This semi-analytical model is believed to enhance the current level knowledge of the key mechanisms of the coinjection process. This improved knowledge is used to interpret the effects of operating pressure as well as oil viscosity-temperature behavior on the production rates through two case studies.

Eventually, predictions of the semi-analytical method are validated against the results from numerical simulations. Validations show that the proposed semi-analytical method can be reliable for a preliminary screening of solvents for coinjection with steam. This is much more convenient and time-saving than running full simulations of mass and energy flow in the reservoir. The need for running unnecessary numerical simulations of multiple processes can be eliminated when a meaningful contrast in their performances is predicted by the semi-analytical method.

### **Solution for Chamber Edge Conditions**

Coinjection of solvent with steam will result in a temperature gradient inside the chamber. The temperature at the chamber interface will be substantially lower than the injection temperature (Keshavarz et al. 2012 and 2013). Earlier attempts estimated this temperature drop using simplified representation of binary phase behavior of water and a single-component solvent (Dong 2012). In his analysis, Dong applied Raoult's law for phase equilibrium calculations assuming no mutual solubility between water and solvent and a negligible pressure gradient inside the chamber. Some of these assumptions, however, may not be realistic for many practical applications.

Keshavarz et al. (2013) showed the effects of simplifying assumptions, particularly binary consideration of mixture and using Raoult's law for equilibrium calculations, on the accuracy of predictions in comparison with results from numerical simulations. A more accurate estimation of temperature at the chamber edge is crucial for a more reliable prediction of oil drainage rate.

For a three-phase equilibrium problem in a binary system, consisting of water and a single-component hydrocarbon solvent only, the degree of freedom (DF) is one. Thus, for an assumed constant pressure corresponding to the injection pressure ( $P_{inj}$ ), the 3-phase equilibrium temperature ( $T_{3P}$ ) is unique. The  $T_{3p}$  can be used as a rough estimation of chamber edge temperature under that injection pressure; however, if the reservoir oil is added to the above system as a second hydrocarbon component, the DF is two. This implies that for a fixed pressure, the temperature at which three equilibrium phases coexist cannot be identified uniquely. In this section, we demonstrate how the existence of reservoir oil as a third component will affect the estimations of chamber edge temperature. In this attempt, the following assumptions are made: 1) No mutual solubility between water and hydrocarbon components, 2) constant pressure inside the chamber, and 3) Raoult's law is used for equilibrium calculations.

Water, oil and solvent components are labeled with indices  $i=1, 2$  and  $3$ , respectively. The aqueous (W), oleic (L) and gaseous (V) phases are identified with indices  $j=1, 2$  and  $3$ , respectively.  $x_{ij}$  is the mole fraction of component  $i$  in phase  $j$ .

Equilibrium calculations in a system of three components and three phases, are conducted with the system of equations below:

$$\begin{aligned}
 P_1^{vap} &= x_{13}P, \\
 x_{22}P_2^{vap} &= x_{23}P, \\
 x_{32}P_3^{vap} &= x_{33}P, \\
 x_{22} + x_{32} &= 1, \\
 x_{13} + x_{23} + x_{33} &= 1,
 \end{aligned} \tag{4-1}$$

where  $P_i^{vap}$  is the vapor pressure of component  $i$ , and  $P$  is the pressure. The first equation describes V-W equilibrium; the second and the third equations describe V-L equilibrium; and, the last two equations result from mass balance.

Partitioning of components between phases is expressed through the K-values defined as below:

$$K_{ij} = \frac{x_{ij}}{x_{iN_p}} \quad (i = 1, \dots, 3; j = 1, \dots, 3), \quad (4-2)$$

where  $x_{iN_p}$  is the mole fraction of component  $i$  in the reference phase  $N_p$ .

For an assumed overall composition, up to three equilibrium phases can be calculated at a given pressure and temperature. Constant K-flash with the Rachford-Rice (RR) equations (1952) is used to conduct these calculations:

$$f_j(\beta) = \sum_{i=1}^3 \frac{(1-K_{ij})z_i}{1-\sum_{j=1}^3 (1-K_{ij})\beta_j}$$

$$\sum_{j=1}^3 \beta_j = 1 \quad (j = 1, \dots, 3), \quad (4-3)$$

with the constraint  $0 \leq \beta_j \leq 1$  where  $\beta_j$  is the mole fraction of phase  $j$ .

After solving the RR equations for  $\beta_j$ , the compositions of the L and V phases can be calculated as follows:

$$x_{iN_p} = \frac{z_i}{1-\sum_{j=1}^3 (1-K_{ij})\beta_j}$$

$$x_{ij} = K_{ij}x_{iN_p} \quad (i = 1, \dots, 3; j = 1, \dots, 3; j \neq N_p). \quad (4-4)$$

Three phases are present inside the steam chamber. Also, temperature will gradually drop from the injection end to the edge of chamber. The chamber edge temperature ( $T_{\text{edge}}$ ) is dependent on the overall composition. For a given overall composition, the chamber edge temperature by definition is the highest temperature at which no stable V phase can be identified.

A step-wised procedure is presented in the flowchart given in **Figure 4-1** to estimate this temperature for a given pressure and overall composition at the chamber edge. In this algorithm, temperature decreases from the saturated steam temperature at the specified pressure in a step-by-step manner. At each temperature step the possibility of a three phase equilibrium ( $0 \leq \beta_j \leq 1$ ) is searched for by solving Equation 4-3. The highest temperature at which no stable V phase is found, i.e.  $\beta_3 \leq 0$  for all acceptable solutions, is identified as the chamber edge temperature. Then, the procedure is repeated for another assumed overall composition. The accuracy of these estimations is controlled by the magnitude of the temperature steps taken.

The chamber edge is schematically illustrated in composition space for water, solvent and oil in **Figure 4-2**. Note that, due to zero mutual solubility

assumption between water and hydrocarbon components, the tie line connecting the W phase and the L phase will cross the whole height of the triangle as shown in Figure 4-2. Therefore, the chamber edge temperature is calculated to be the same for all overall compositions on this tie line.

**Figures 4-3** presents the results of the calculations at the pressures of 2000 kPa and 5000 kPa. Typical dead-oil properties for Athabasca bitumen taken from Mehrotra and Syrczek (1987) are considered for the oil component. The properties of the components in these calculations are listed in **Table 4-1**.

The K-values of water and solvent components are generated using the following correlation based on Raoult's law:

$$K_i(P, T) = \frac{P_i^{vap}}{P} = \frac{a}{P} \times e^{\frac{b}{T-c}} \quad (i = 1, \dots, 3) , \quad (4-5)$$

where  $P$  is pressure,  $T$  is temperature and  $P_i^{vap}$  is the vapor pressure of component  $i$  at temperature  $T$ .  $a, b$  and  $c$  are the correlation coefficients corresponding to the units of pressure and temperature. They are taken from Reid et al. (1977) and listed in Table 4-1. Due to unavailability of these coefficients for the bitumen component, its vapor pressure was calculated by Peng-Robinson (PR) equation of state (1976). The following transformation of variables should be considered before applying the K-values in Equation 4-5 into Equation 4-3:

$$\begin{aligned} K_1 &= \frac{1}{K_{11}} , \\ K_2 &= \frac{1}{K_{22}} , \\ \text{and } K_3 &= \frac{1}{K_{32}} , \end{aligned} \quad (4-6)$$

The accuracy of estimations is improved if the EOS generated K-values are used. Temperature step in the solution algorithm is taken as 0.1°C.

Figure 4-3 presents that for the same operating pressure and molar concentration of solvent in the L phase, a lower  $T_{edge}$  is expected as the solvent becomes more volatile. The two ends of the horizontal axis correspond to two limiting cases of calculations. At the left end, where there is no solvent component present, all the curves converge to water saturation temperature.

This is the expected temperature at the edge of the chamber during a steam-only injection process such as SAGD. Accumulation of solvent results in reduction of  $T_{\text{edge}}$  until a minimum is reached at the right end of plot.

$T_{\text{edge}}$  at the right end, where there is no bitumen component present, corresponds to the estimations from the binary mixture consideration in Dong (2012). Such conditions may occur at certain stages of chamber propagation when the local oleic phase at the chamber edge is composed of 100% solvent. This would be beneficial in terms of displacement efficiency enhancement. The mechanisms of displacement efficiency enhancement are discussed by Keshavarz et al. (2012) in details. V-L phase transition following further propagation of chamber and local temperature increment can leave residual oil saturation of zero.

Due to non-zero mutual solubility between hydrocarbon components, some partitioning of the lighter solvent into the bitumen/heavy oil is always expected to occur. Therefore, the transition from three-phase (V-W-L) to two-phase (W-L) equilibrium occurs at a higher temperature compared to the transition from V-W to W-L equilibrium in the binary mixture of water-solvent. Thus, the latter transition temperature can be considered as a minimum for the former transition temperature.

As mentioned above, these two transition temperatures merge as the solvent concentration in the L phase approaches unity. For solvent concentrations smaller than unity, the V-W-L to W-L phase transition temperature ranges from its minimum to water saturation temperature at the operating pressure. For a fixed solvent concentration in the L phase, the deviation of phase transition temperature in a three-component system compared to water-solvent binary becomes more pronounced for lighter solvents. This deviation can result in erroneous predictions of oil production rates as will be shown in the next section.

### **Oil Drainage Flux Index beyond the Chamber Edge**

A critical challenge in coinjection processes is the selection of proper solvent. There are field and laboratory evidences in which little improvement in oil

production rate has been observed as a result of coinjecting specific solvents with steam.

In this section, a semi-analytical approach is proposed for preliminary screening for an optimum solvent in terms of oil production rates. Results of the earlier section for chamber edge temperature estimation are used to predict temperature and solvent distributions beyond the edge of chamber by using correlations available in the literature.

Darcy's law for the L phase flow parallel to the chamber edge in a 2-D reservoir can be written as:

$$u_l = - \frac{kk_{rl}}{\mu_l} \frac{\partial \Phi_l}{\partial \eta}, \quad (4-7)$$

where  $k$  is the absolute permeability,  $k_{rl}$  is the relative permeability for the L phase,  $\mu_l$  is the viscosity of the L phase,  $\Phi_l$  is the potential for the L phase flow and  $\eta$  is the direction parallel to the chamber edge.

The oil-component molar flux in the L phase  $j_l$  [mole/L<sup>2</sup>-T] can be obtained from equation 4-8 as below:

$$j_l = - \frac{kk_{rl}}{\mu_l} \frac{\partial \Phi_l}{\partial \eta} \rho_l x_o, \quad (4-8)$$

where  $\rho_l$  is the molar density of the L phase and  $x_o$  is the mole fraction of the reservoir oil component(s) in the L phase.  $x_o$  is 1.0 for a steam-only injection process such as SAGD.

If potential gradient and relative permeability with respect to the L phase beyond the chamber edge are assumed to be similar for steam-only injection and different steam-solvent coinjection processes in the same reservoir,  $j_l$  would be proportional to the ratio of  $\frac{\rho_l}{\mu_l} x_o$ .

This assumption, however, may not be accurate when a steam-only injection and a coinjection process are compared. Sharma and Gates (2010b) showed that oil saturation in the flowing oil zone beyond the edge of a SAGD chamber ranges from the residual oil saturation at the chamber edge up to the original oil saturation of the reservoir. Accumulation of solvent in the L phase beyond the edge of a coinjection chamber contributes to local improvement of oil saturation and thus, oil relative permeability, compared to steam-only

injection. Therefore, the ratios of relative permeabilities with respect to L phase may significantly deviate from unity due to dissimilar distributions of the L phase saturation beyond the edge of steam-only and coinjection chambers as shown by Keshavarz et al. (2012). This study does not consider the local improvement in L phase saturation beyond the edge of coinjection chamber. This does not violate the core discussion of this chapter in terms of relative performance for different coinjection processes. However, it might cause a slight underestimation of the relative performance of coinjection when compared with steam-only injection.

A single component oil and solvent are used in this study. Viscosity and density of *L* phase are calculated using the following mixing rules:

$$\ln(\mu_l) = x_o \ln(\mu_o) + x_s \ln(\mu_s), \quad (4-9)$$

$$\frac{1}{\rho_l} = \frac{x_o}{\rho_o} + \frac{x_s}{\rho_s}, \quad (4-10)$$

where  $x_s$  is the mole fraction of solvent component in the *L* phase,  $\rho_o$  and  $\rho_s$  are the molar densities of oil and solvent components, respectively and  $\mu_o$  and  $\mu_s$  are the viscosities of oil and solvent components, respectively.

The following correlations are used to estimate the viscosity of oil and solvent components as functions of temperature:

$$\ln\mu_o(\text{cp}) = \exp(A + B\ln T), \quad (4-11)$$

$$\mu_s(\text{cp}) = A \cdot \exp\left(\frac{B}{T}\right), \quad (4-12)$$

where  $A$  and  $B$  in Equation 4-11 are taken from Mehrotra and Svrcek (1984) to generate a viscosity-temperature profile that is typical for an Athabasca bitumen.  $A$  and  $B$  for solvent components are taken from Reid et al. (1977). These coefficients for both equations are listed in **Table 4-2**.

Densities of the oil and solvent components are considered to be functions of both pressure and temperature through the following correlation:

$$\rho_i = \rho_i^0 \cdot \exp(\alpha_c(P - P_r) - \alpha_1(T - T_r) - 0.5\alpha_2(T^2 - T_r^2)), \quad (4-13)$$

where  $P_r$  is the reference condition pressure,  $T_r$  is the reference condition temperature and  $\rho_i^0$  is the reference condition molar density of component  $i$ .  $P_r$  and  $T_r$  are taken as 101.3 kPa and 15°C, respectively, in this work.  $\alpha_c$ ,  $\alpha_1$  and

$\alpha_2$  are compressibility, first and second thermal expansion coefficients, respectively, and are also listed with their units in Table 4-2.

Assuming the oil drainage rate to come from the regions beyond the chamber edge only, it will be proportional to the infinite integral below:

$$I = \int_0^{\infty} \left( \frac{\rho_l}{\mu_l} x_o \right) d\xi, \quad (4-14)$$

where  $\xi$  is the distance from the chamber edge normal to its interface. Profiles of both  $\rho_l$  and  $\mu_l$  are functions of temperature and solvent concentration beyond the chamber edge.

Based on Butler's equation for 1-D quasi-steady state conductive heat transfer ahead of a steam chamber, whose translation velocity through the oil sand and normal to its edge is  $U$ , temperature profile ahead of the chamber edge is given by:

$$\frac{T - T_R}{T_{edge} - T_R} = e^{\frac{-U\xi}{\alpha}}, \quad (4-15)$$

where  $T_R$  is the original reservoir temperature, and  $\alpha$  is the thermal diffusivity of the reservoir material (Butler 1985).

For a typical Athabasca oil sand, thermal diffusivity ranges from  $2 \times 10^{-7}$  m<sup>2</sup>/s to  $9 \times 10^{-7}$  m<sup>2</sup>/s (Butler 1985; Farouq Ali 1997). In a typical SAGD operation, chamber propagates at a velocity of about  $2.315 \times 10^{-7}$  m/s to  $2.315 \times 10^{-8}$  m/s in a typical Athabasca reservoir (Gotawala and Gates 2008). In this study, values of  $U$  and  $\alpha$  were taken as  $10^{-7}$  m/s and  $8 \times 10^{-7}$  m<sup>2</sup>/s, respectively. A more accurate model may consider a different chamber propagation velocity for each steam-only injection or steam-solvent coinjection process.

The exact profile of solvent concentration beyond the chamber edge requires simultaneous solution of mass transfer, heat transfer and fluid flow equations. In their theoretical model of VAPEX, Dun et al. (1989) assumed the solvent-bitumen diffusion coefficients to be constant. Thus, solvent distribution beyond the vapor-liquid interface will decline exponentially from a maximum at the interface towards its concentration in the original reservoir at infinite distance from the interface.

In reality, the diffusion is inversely proportional to viscosity or viscosity to some power and proportional to temperature or temperature to some power (Sharma and Gates 2010a; Reid et al. 1977). As a result, the observed concentration profiles in diffusion experiments exhibit the abrupt front-end profiles (Okazawa 2009; Oballa and Butler 1989). In this work, we assume solvent is only distributed within a finite distance from the interface of coinjection chamber in the form:

$$\frac{x_s}{x_s^{edge}} = \left(1 - \frac{\xi}{\xi_t}\right)^m, \quad (4-16)$$

where  $\xi_t$  is the thickness of the solvent-rich zone and  $m$  is a factor that determines the shape of profile. If  $m$  is smaller than unity, the profile is convex upward with an abrupt advancing front at  $\xi_t$  which is also consistent with the results of laboratory experiments.

Such profile has also been used by Okazawa (2009) to describe solvent distribution beyond the vapor-liquid interface in VAPEX. The only difference is the replacement of volumetric concentrations in his work by molar concentrations here. **Figure 4-4** compares the profiles of solvent distribution obtained from Equation 4-16 with arbitrary but similar values of  $\xi_t$  and  $x_s^{edge}$ , and different values of  $m$ .

Gupta and Gittins (2012) reported the need for diffusion coefficients that are three orders of magnitude greater than the reported values from laboratory experiments, to match the experimental and field data of solvent aided process (SAP). Use of a greater diffusion coefficient is equivalent to a thicker region of solvent mass transfer into the unswept reservoir oil, if the oil production is assumed to come only from beyond the vapor-liquid interface. Gupta and Gittins (2012) also suggested an alternative model; i.e., considering a solvent-vapor blanket layer inside the chamber and close to its edge which contributes to oil drainage in addition to oil drainage from beyond the chamber edge. As they stated, in either of these two approaches, using a greater diffusion coefficient or considering a vapor blanket layer, the overall effect is equivalent to a thicker layer of solvent accumulation around the vapor-liquid interface.

Here we assumed  $\xi_t$  to be a function of a critical reservoir oil/bitumen viscosity,  $\mu_{crit}$ , beyond which solvent and reservoir oil/bitumen mixing will be negligible due to the resistance imposed by the viscous reservoir oil. The region from the chamber edge to  $\xi_t$  in which the mixing of solvent and reservoir oil occurs is referred to as the solvent mixing zone from this point on in this work.  $m$  and  $\mu_{crit}$  are assumed to be 0.25 and 500 cp, respectively, for all coinjection cases in this study. The value of  $m$  is chosen to capture the abrupt front end of solvent distribution profile. The value for  $\mu_{crit}$  is chosen based on our experience of the observed thickness for the solvent mixing zone in numerical simulations. The method should apply equally well if a more reliable solvent distribution profile is available.

### **Algorithm of Solution**

The following steps are followed in the algorithm for estimation of the oil drainage flux index in Equation 4-14:

1. For a given operating pressure, P, profiles of chamber edge temperature vs. local solvent concentration in the L phase ( $x_s^{edge}$ ) are calculated using the algorithm described in the previous section.
2. For a fixed  $x_s^{edge}$ , chamber edge temperature will be fixed in each process. Thus, profiles of temperature beyond the chamber interface can be determined using Equation 4-15.
3. Profiles of bitumen and solvent viscosities and densities are generated using Equations 4-11 to 4-13.
4. Solvent distribution profile is then calculated using Equation 4-16.
5. The profiles of the L phase viscosity and density are generated using mixing rules in Equations 4-9 and 4-10.
6. Eventually the oil drainage flux index introduced in Equation 4-14 is evaluated numerically by replacing  $\infty$  in the upper limit of the integral with a sufficiently high value. An upper limit of 200 m is used here. Considering that the integrand in Equation 4-14 becomes negligible only over a few meters from the chamber edge

with the data used in this study, the expected error would be negligible. Numerical evaluation of this integral is much more convenient than the analytical evaluation due to the complex forms of  $\rho_l$  and  $\mu_l$  when expressed as functions of the integral variable,  $\xi$ .

7. Then the whole calculation procedure is repeated for another value of  $x_s^{edge}$ . The two limiting cases of calculations are  $x_s^{edge} = 0$  and  $x_s^{edge} = 1$ . All the required input data for the calculations in this study are listed in Tables 4-1 and 4-2.

## Sensitivity Analysis

### Effect of Solvent Accumulation at the Chamber Edge

Due to a DF of 2 for a system of three components and three phases, equilibrium phase compositions cannot be uniquely identified by fixing the operating pressure alone. The oil molar flux index is strongly dependent on three-phase equilibrium conditions at the chamber edge. Thus, it is studied over the entire mixing line from 0% up to 100% solvent concentration in the L phase.

**Figure 4-5** presents the variations of the  $\frac{\rho_l}{\mu_l} x_o$  ratio at the chamber edge vs. local solvent concentration in the L phase for steam-only injection and three solvent-steam coinjection processes. The reservoir oil is a typical Athabasca bitumen with properties listed in Tables 4-1 and 4-2. The operating pressure is 2000 kPa.

Variations of  $\frac{\rho_l}{\mu_l} x_o$ , can be better interpreted if it is considered as a product of two factors:  $(\rho_l \cdot x_o)$ , which is a representative for the reservoir oil content of the draining L phase and  $1/\mu_l$ , which is a representative for the draining L phase mobility. The former is affected by solvent distribution profile and the latter is affected by both solvent dilution and temperature profile. The break-over point for each solvent in Figure 4-5, occurs as a result of the balance between these two factors. For lower solvent concentrations, the temperature and the reservoir oil content of the draining L phase  $(\rho_o \cdot x_o)$  are higher; however, it is not sufficiently mobile due to less dilution. For higher solvent concentrations,

although temperature at the chamber interface is higher, but the L phase is sufficiently mobile due to considerable dilution by solvent; however, it contains a very small amount of reservoir oil due to significant accumulation of solvent.

**Figure 4-6** presents the values of the oil component molar flux integral in Equation 4-14 vs.  $x_s^{edge}$ . Figure 4-6 deserves a fair amount of discussion. Coinjection of C<sub>3</sub> with steam has deteriorated the oil production rate. Temperature profile beyond the edge of C<sub>3</sub>-steam chamber falls considerably below that of steam-only chamber due to solvent accumulation effects.

For  $x_s^{edge} < 0.4$ , solvent accumulation is not sufficient for its diluting effects to compensate the negative effects of unfavorable temperature profile on the L phase viscosity. The overall effect results in the profile of bitumen molar flux integrand for C<sub>3</sub>-steam coinjection to remain below that in steam-only injection within this range of  $x_s^{edge}$ . This is shown in **Figure 4-7** for  $x_s^{edge} = 0.25$ .

For  $x_s^{edge} > 0.4$ , values of the bitumen molar flux integrand in C<sub>3</sub>-steam coinjection are higher than that in steam-only injection right at the chamber interface. But this superiority is maintained only within a few centimeters from the chamber edge as shown in **Figure 4-8** for  $x_s^{edge} = 0.7$ . Significant accumulation of a volatile solvent such as C<sub>3</sub> has resulted in more than 125 °C temperature drop at the interface of C<sub>3</sub>-steam chamber with respect to that in steam-only. This lowered temperature results in a much more viscous oil which also limits the thickness of the solvent mixing zone beyond the chamber edge. Therefore, the profile of the bitumen flux integrand of coinjection exhibits a sharp decline to values below that in steam-only injection after the solvent diluting effects disappear within a few centimeters from the chamber interface (Figure 4-8). Based on this discussion, coinjection of C<sub>3</sub> with steam is not economical for this reservoir and operating pressure.

Note that the negative effects of unfavorable temperature distribution beyond the chamber edge are not as severe when C<sub>5</sub> or C<sub>8</sub> are coinjected with steam. This is due to their less volatility as also shown in by Figure 4-3 in.

Lower viscosities of bitumen close to the chamber edge are expected as the solvent becomes less volatile, which in turn provides more room for solvent-reservoir oil mixing beyond the chamber edge.

Solvent diluting effects become less effective as the solvent becomes less volatile. This is the main reason for better performance of the process under C<sub>5</sub> coinjection compared to C<sub>8</sub> coinjection when  $x_s^{edge}$  is maintained higher than approximately 0.88.

This point becomes clearer with the profiles of temperature, solvent distribution and the values of bitumen flux integrand vs.  $\xi$  presented in **Figure 4-9** for  $x_s^{edge} = 0.95$  during C<sub>5</sub>- and C<sub>8</sub>-steam coinjections. The strong non-linearity observed in the profiles of the integrand is due to the balance between the bitumen content of the L phase and its mobility which is achieved at some distance from the chamber interface.

According to Figure 4-6, the coinjection of C<sub>5</sub> or C<sub>8</sub>, regardless of  $x_s^{edge}$ , will most likely result in improved oil production rates compared to steam-only injection. The optimum rate is achieved if the coinjection scenario is designed such a way that the average solvent concentration at the chamber edge is maintained at  $x_s^{edge} = 0.95$  for C<sub>5</sub> coinjection and at  $x_s^{edge} = 0.90$  for C<sub>8</sub> coinjection with steam. These values correspond to  $T_{edge} = 151^\circ\text{C}$  and  $T_{edge} = 198^\circ\text{C}$ , respectively.

Controlling  $x_s^{edge}$  may be challenging since it is variable with both time and the distance from the chamber ceiling. According to Figure 4-6, if C<sub>5</sub> and C<sub>8</sub> are coinjected with similar mole numbers of solvent in the injectant, they will have approximately similar performances in terms of oil production rate.

As stated earlier, using a binary mixture of water and solvent only will underestimate the chamber edge temperatures for  $x_s^{edge}$  smaller than unity. This in turn will underestimate the expected oil drainage rates. The deviation becomes more severe as the solvent becomes more volatile.

**Figure 4-10** presents the results of another version of calculations for numerical evaluation of the oil drainage flux index in Equation 4-14 vs.  $x_s^{edge}$ .

In this version of calculations, the estimated values of  $T_{3p}$  for a binary mixture of water and solvent are used in the place of  $T_{edge}$  for all  $x_s^{edge}$ . The relative performances of C<sub>3</sub>-steam and C<sub>5</sub>-steam coinjections are underestimated compared to C<sub>8</sub>-steam coinjection. This may not seem to be important for the C<sub>3</sub>-steam coinjection case since its performance falls significantly short of being optimum; however, one may erroneously pick C<sub>8</sub> as the optimum solvent based on the results of this version of calculations. Considering much higher costs of C<sub>8</sub> compared to C<sub>5</sub>, the economical profits of the process with C<sub>8</sub> coinjection may not be maximum.

#### **Effect of Operating Pressure and Oil Viscosity**

Besides the coinjected solvent, the operating pressure and the viscosity-temperature behavior of the reservoir oil are expected to affect the profiles of the oil component flux integrand significantly. The operating pressure has a direct effect on the chamber edge temperature which in turn alters the temperature profile, and thus viscosity, density and solvent distribution beyond the vapor-liquid interface. The viscosity-temperature behavior of the bitumen affects the mobility of the draining L phase as well as the thickness of the solvent mixing zone. This section discusses these effects with the same approach as the last section through two different case studies.

#### **Case 1: Effect of Higher Operating Pressure**

Typically, there are many practical limitations for the range of the operating pressure such as formation depth, geomechanical characteristics of formation, existence of bottom water, and so on. These factors sometimes require using higher operating pressures as in the cases of deep formations. The same approach as in the previous section is applied to evaluate the performance of three solvent-steam coinjections under a higher operating pressure in this section.

**Figure 4-11** presents the results of numerical evaluation of the integral in Equation 4-14 for steam-only injection and three solvent-steam coinjection

cases. The operating pressure is 5000 kPa. All other input data remain the same as in the previous section.

Comparison of this figure with Figure 4-6 reveals a significant improvement in the performance of C<sub>3</sub>-steam coinjection. This is conceivable due to exponential behavior of viscosity vs. temperature. Increasing operating pressure from 2000 kPa to 5000 kPa will result in approximately 50° C increase in the chamber edge temperature for all solvents-steam coinjection cases studied here. The same amount of temperature increment, however, will yield much higher viscosity reduction at lower temperatures, which is the case at the chamber interface of more volatile solvents-steam. This, in turn, will result in considerable improvement in the thickness of more volatile solvents mixing zone beyond the chamber interface. Overall, improved oil production rates with all solvents, including C<sub>3</sub>, are observed compared to steam-only injection. The best performance will likely occur when  $\chi_s^{edge}$  is maintained at around 0.95.

The key finding of this section is that the coinjection of volatile solvents such as C<sub>3</sub> with steam into an Athabasca type of reservoir may be economical at high operational pressures (such as 5000 kPa). Even at operational pressures in this range, detailed economical analysis of incremental oil production rates are required to justify the additional costs imposed as a result of solvent introduction to the injectant or solvent loss.

Similar to the previous section, the performances of C<sub>5</sub>- and C<sub>8</sub>-steam coinjections in terms of oil production rates are more promising than C<sub>3</sub>-steam coinjection and are expected to be close to each other. C<sub>5</sub> coinjection with steam has a higher potential to be the optimum solvent of these 3 cases, if  $\chi_s^{edge}$  is maintained at values greater than 0.7.

#### **Case 2: Effect of a Less Viscous Oil**

The viscosity of bitumen falls into the range of 10<sup>6</sup> cp to 10<sup>7</sup> cp at typical reservoir conditions. Heavy oil shows much lower viscosity on the order of 10<sup>3</sup> cp to 10<sup>5</sup> cp at the same temperature but yet too viscous for conventional recovery techniques. This section presents a qualitative evaluation of the

performance under different solvent-steam coinjection processes for a less viscous oil compared to Athabasca bitumen.

The same calculation procedure is followed as in the two previous sections. Operating pressure is 2000 kPa. All input data are kept unchanged except for the reservoir oil molar density which is increased to  $1.950 \text{ kg-mole/m}^3$  and viscosity-temperature behavior which is presented in **Table 4-3**. The viscosity-temperature behavior of oil is taken from Hosseininejad et al. (2012) and represents a Lloydminster type of heavy oil. The faster propagation of chamber through a less viscous oil is also taken into account by increasing the value of  $U$  to  $1.5 \times 10^{-7} \text{ m/s}$ . The volatility of oil at these operating conditions is negligible. Therefore, using the same  $T_{\text{edge}}$  vs.  $x_s^{\text{edge}}$  profile as the one used for Athabasca bitumen will result in negligible error.

**Figure 4-12** presents the results of numerical evaluation of oil drainage flux index in Equation 4-14 for steam-only injection and three solvent-steam coinjection cases. Similar to the effect of higher operating pressure, a less viscous oil also increases the potential for  $C_3$  coinjection with steam to result in improved oil production rates, compared to steam-only injection but only for greater values of  $x_s^{\text{edge}}$ .

The reason for improved performance of lighter solvents can be sought in the effect of chamber edge temperature reduction as a result of solvent introduction into the injectant. The effects of temperature reduction on the viscosity of a heavy oil is not as drastic as bitumen. This is due to weaker temperature dependency of the heavy oil viscosity compared to bitumen; however, still if the accumulation of  $C_3$  at the chamber edge is not sufficiently high, its diluting effects are not capable of compensating the negative effects of unfavorable temperature distribution on the L phase viscosity beyond the chamber interface.

Similar to the last two case studies, coinjections of  $C_5$  or  $C_8$  with steam, both are more promising than  $C_3$  in terms of oil production rates.  $C_5$  is still the most likely solvent to be the optimum among these three.

## Validation of the Results Using Numerical Simulations

In this section, predictions of the proposed semi-analytical approach are validated against the results from fine-scale numerical simulations using CMG's thermal reservoir simulator STARS (2012). Note that the objective of the semi-analytical model was a qualitative comparison of performance in different steam-only or steam-solvent coinjection processes rather than an exact quantitative match on the values of oil drainage flux index.

A 2-D homogeneous reservoir of 70.0 m × 37.5 m × 20.0 m with gravity is considered resulting in model dimensions of 70.0 m, 37.5 m, and 20.0 m in the x, y, and z directions, respectively. The injector and producer are located at the left boundary at depths of 16 m and 20 m from the top, respectively. Thus the simulations are performed for one half of the chamber only. Homogeneous reservoir properties are presented in **Table 4-4**. The relative permeability curves are shown in **Figure 4-13**. Capillarity, asphaltene precipitation and physical diffusion/dispersion are not considered in the simulations.

Three series of simulations are performed for steam-only injection (SAGD) and different single component solvent-steam coinjections. They correspond to the following case studies:

Case 1 (base case): SAGD/Coinjection at 2000 kPa operating pressure into a reservoir with an Athabasca type of bitumen. Oil properties are taken from Tables 4-1 and 4-2.

Case 2: SAGD/Coinjection at 5000 kPa operating pressure into a reservoir with an Athabasca type of bitumen. Oil properties are taken from Tables 4-1 and 4-2.

Case 3: SAGD/Coinjection at 2000 kPa operating pressure into a reservoir with a less viscous oil than the Athabasca bitumen. Oil properties are taken similar to those presented in Tables 4-1 and 4-2 except for its molar density which is increased to 1.950 kg-mole/m<sup>3</sup> and viscosity-temperature behavior which is presented in Table 4- 3.

Producer is constrained to a constant bottom hole pressure of 1500 kPa in Case 1 and Case 3 and to 4500 kPa in Case 2. Also, a maximum flow rate of 1.0

m<sup>3</sup>/day is assigned to steam at the production well to prevent steam losses from chamber. A quality of 90% is assigned to the injected steam at sandface. Solvent concentration in the injectant is 1 mol% in all coinjection simulations. Preheating of the reservoir is also performed for six months. Properties of solvent and water components in all simulation cases are taken from Tables 4-1 and 4-2.

**Figure 4-14** presents the results of the numerical simulation for the average bitumen production rates from the 9<sup>th</sup> month of coinjection until the 20<sup>th</sup> month in the base case. This time interval falls into the period of lateral expansion of chamber before it arrives to the boundary of reservoir model. The solvent portion of the produced L phase is excluded from oil production rates. Average production rate of steam-only injection within this period is shown by a horizontal line.

As expected through semi-analytical calculations, the coinjection of C<sub>3</sub> with steam deteriorated the oil production rate compared to steam-only injection. The C<sub>5</sub> and C<sub>8</sub> coinjection cases exhibit almost similar average production rates. They both resulted in significant improvements of oil production rate compared to steam-only injection. C<sub>5</sub>-coinjection yielded slightly greater average production rate and is likely to be the optimum solvent among these three.

**Figures 4-15** and **4-16** present the average oil production rate for case 2 and case 3, respectively. The time interval in each case is chosen within the period of lateral expansion of the chamber before it arrives to the other boundary of the reservoir model. Unlike in the base case, the coinjection of C<sub>3</sub> with steam in both Cases 2 and 3 resulted in improved oil production rates compared to steam-only injection. This was predicted by the semi-analytical model in Case 2 regardless the solvent accumulation at the chamber edge. For Case 3, however, a solvent accumulation resulting in  $x_s^{edge} > 0.4$  is required. This corresponds to a chamber edge temperature of 110° C or lower. According to the results of numerical simulation, the average values of  $x_s^{edge}$  vary from 0.45 to 0.7 within the time period considered for oil production rate averaging.

Coinjection of  $C_5$  or  $C_8$  with steam showed almost similar average production rates which are considerably higher than that of steam-only injection.  $C_5$  coinjection in Case 3 resulted in slightly higher average production rates and is likely to be the optimum solvent of the three studied here.

## Conclusions

This work proposed a step-wised semi-analytical approach for preliminary screening of the relative performance of different solvent-steam coinjection processes in terms of oil production rates. Detailed discussions of the effects of solvent type, operating pressure and reservoir oil viscosity-temperature behavior were presented. Specific conclusions withdrawn from this analysis are as follows:

1. An algorithm was proposed to calculate the temperature at the chamber edge as a function of solvent molar concentration in the L phase for a three component system with certain simplifying assumptions. Chamber edge temperature in a solvent-steam coinjection may vary from steam saturation temperature at the operating pressure to the dew point of binary mixture of water and solvent. Solvent volatility and accumulation both act to reduce the chamber edge temperature.
2. A semi-analytical method was proposed to qualitatively compare the performance of different solvent-steam coinjection processes in terms of oil production rate. The analytical method gives a more detailed understating of the factors affecting the oil drainage rate beyond the chamber edge; such as :
  - Oil drainage rate is a function of the oil component content of the L phase as well as its mobility. During a specific solvent-steam coinjection process, solvent accumulation up to an optimum amount improves the dilution efficiency. Further accumulation, however, is not beneficial as it reduces the temperature, thickness of the solvent mixing zone, and the oil content of the draining L phase beyond the vapor-liquid interface. The best performance of

a specific coinjection process in terms of oil production rate is expected to occur when the average solvent accumulation at the chamber edge is maintained at this optimum.

- Among solvents of different volatilities, a less volatile solvent results in a more favorable temperature and a thicker solvent mixing zone ahead of the chamber edge. However, diluting effects are expected to be less effective. Thus an optimum solvent volatility is theoretically expected in terms of oil production rates when the above mentioned factors balance each other.
3. The proposed semi-analytical model was applied to three case studies. The results indicate that coinjection of a very volatile solvent such as C<sub>3</sub> at low operating pressures will not be economical for an Athabasca type of bitumen. A higher operating pressure or a less viscous reservoir oil increase the practicality of coinjecting more volatile solvents with steam. C<sub>5</sub> was observed to be the optimal when compared to C<sub>3</sub> and C<sub>8</sub> for the cases studied in this work.
  4. Predictions of the semi-analytical model were qualitatively validated with the results of numerical simulations. The results indicate that the semi-analytical approach can be used as a preliminary screening method for the coinjection solvent when the contrast between the performances is meaningful. This can be much faster and more convenient than running full numerical simulations of flow and eliminate the need to run unnecessary simulations.

### **Nomenclature**

A,B,C: Viscosity correlation constants

a,b,c: K-value correlation constants

C<sub>3</sub>: Normal Propane

C<sub>5</sub>: Normal Pentane

C<sub>8</sub>: Normal Octane

I: Oil drainage flux index defined by equation 4-14

$j_o$ :	Oil-component molar flux in the oleic phase
$K$ :	K-value as defined by Equation 4-6
$K_{ij}$ :	K-value as defined by Equation 4-2
$k$ :	Permeability
$k_r$ :	Relative permeability
$L$ :	Oleic phase
$m$ :	Solvent distribution correlation constant
$P$ :	Pressure
$P_{inj}$ :	Injection pressure
$P_r$ :	Reference condition pressure
$P^{vap}$ :	Vapor pressure
$S_{or}$ :	Residual oil saturation
$T$ :	Temperature
$T_{3p}$ :	Three-phase equilibrium temperature
$T_{edg}$ :	Chamber edge temperature
$T_r$ :	Reference condition temperature
$U$ :	Chamber propagation velocity
$u$ :	Velocity
$V$ :	Gaseous phase
$W$ :	aqueous phase
$x$ :	Mole fraction
$x_{ij}$ :	Mole fraction of component $i$ in phase $j$
$x_s^{edge}$ :	Mole fraction of solvent in the L phase at the chamber edge
$z_i$ :	Overall composition of component $i$
$\alpha$ :	Thermal diffusivity of reservoir
$\alpha_c$ :	Compressibility
$\alpha_1$ :	First thermal expansion coefficients
$\alpha_2$ :	Second thermal expansion coefficients
$\beta$ :	Phase mole fraction
$\rho$ :	Molar density
$\rho^0$ :	Reference condition molar density in L phase

$\mu$ : Viscosity  
 $\mu_{\text{crit}}$ : Critical viscosity as defined by Equation 4-16  
 $\Phi$ : Potential  
 $\eta$ : Distance parallel to the chamber interface  
 $\xi$ : Distance perpendicular to the chamber interface  
 $\xi_t$ : Thickness indicator of solvent rich bank

#### *Subscripts*

$i$ : Component index  
 $j$ : Phase index  
 $l$ : Oleic phase  
 $N_p$ : Phase index for the reference phase  
 $o$ : oil component  
 $s$ : solvent component  
 $w$ : water component

#### *Abbreviations*

DF: Degree of freedom  
EOS: Equation of state  
RR: Rachford-Rice  
SAGD: Steam assisted gravity drainage  
SAP: Solvent aided process  
SOR: Steam oil ratio

<b>Table 4-1. Properties of components used in chamber edge temperature estimation calculations</b>						
<b>Component</b>	<b>T<sub>c</sub>, °C</b>	<b>P<sub>c</sub>, kPa</b>	<b>ω</b>	<b>a, kPa</b>	<b>b, °C</b>	<b>c, °C</b>
Water	374.15	22088.850	0.344	1.1860×10 <sup>7</sup>	-3816.44	-227.02
C <sub>3</sub>	96.65	4245.518	0.152	9.0085×10 <sup>5</sup>	-1872.46	-247.99
C <sub>5</sub>	196.45	3374.120	0.251	1.0029×10 <sup>6</sup>	-2477.07	-233.21
C <sub>8</sub>	295.65	2482.463	0.394	1.1187×10 <sup>6</sup>	-3120.29	-209.52
Oil	817.75	785.980	1.361	$K_o = \frac{P_o^{vap}}{P}$ where $P_o^{vap}$ is calculated using PR EOS		

<b>Table 4-2. Properties of oil and solvent components used in calculation of oil component drainage flux index</b>						
<b>Component</b>	<b>A</b>	<b>B</b>	<b>ρ<sub>i</sub><sup>0</sup>,kgmol/m<sup>3</sup></b>	<b>α<sub>c</sub>,1/kPa</b>	<b>α<sub>1</sub>,1/°C</b>	<b>α<sub>2</sub>,1/°C<sup>2</sup></b>
C <sub>3</sub>	0.021425	512.72	11.7234	2.54×10 <sup>-6</sup>	5.84×10 <sup>-4</sup>	3.41×10 <sup>-6</sup>
C <sub>5</sub>	0.0191041	722.23	8.7360	1.69×10 <sup>-6</sup>	2.32×10 <sup>-4</sup>	2.82×10 <sup>-6</sup>
C <sub>8</sub>	0.0131342	1090.70	6.1690	1.17×10 <sup>-6</sup>	1.02×10 <sup>-4</sup>	2.19×10 <sup>-6</sup>
Oil	22.851500	-3.57840	1.8060	3.24×10 <sup>-7</sup>	2.25×10 <sup>-5</sup>	6.31×10 <sup>-7</sup>

**Table 4-3. Viscosity-temperature for  
Lloydminster heavy oil**

<b>Temperature, °C</b>	<b>Viscosity, cp</b>
19.53	5201.51
29.33	2175.88
39.61	1004.96
49.40	428.80
59.67	227.50
69.45	133.27
79.72	75.04
89.97	50.49
99.74	33.31
109.51	24.26
119.28	17.67
130.02	13.13
139.78	10.56
150.03	8.16
160.27	6.83
170.03	5.60
179.79	4.88
189.55	4.16
200.28	3.62
209.55	3.15
219.79	2.75
230.03	2.54
239.80	2.00
250.04	1.78
259.31	1.61
270.03	1.49
279.79	1.40
299.78	1.24

**Table 4-4. Properties of the reservoir model used in numerical simulations**

<b>Properties</b>	<b>Values</b>
Porosity	0.33
Horizontal permeability	4000 md
Vertical permeability	3000 md
Initial reservoir pressure at depth of 500 m - case 1 and 3	1500 kPa
Initial reservoir pressure at depth of 500 m - case 2	4500 kPa
Initial reservoir temperature	13°C
Initial oil saturation	0.75
Initial water saturation	0.25
Formation compressibility	1.8E-5 1/kPa
Rock heat capacity	2600 kJ/m <sup>3</sup> °C
Rock thermal conductivity	660 kJ/m day °C
Over/underburden heat capacity	2600 kJ/m <sup>3</sup> °C
Over/underburden thermal conductivity	660 kJ/m day °C
Bitumen thermal conductivity	11.5 kJ/m day °C
Gas thermal conductivity	2.89 kJ/m day °C
Water thermal conductivity	1500 kJ/m day °C

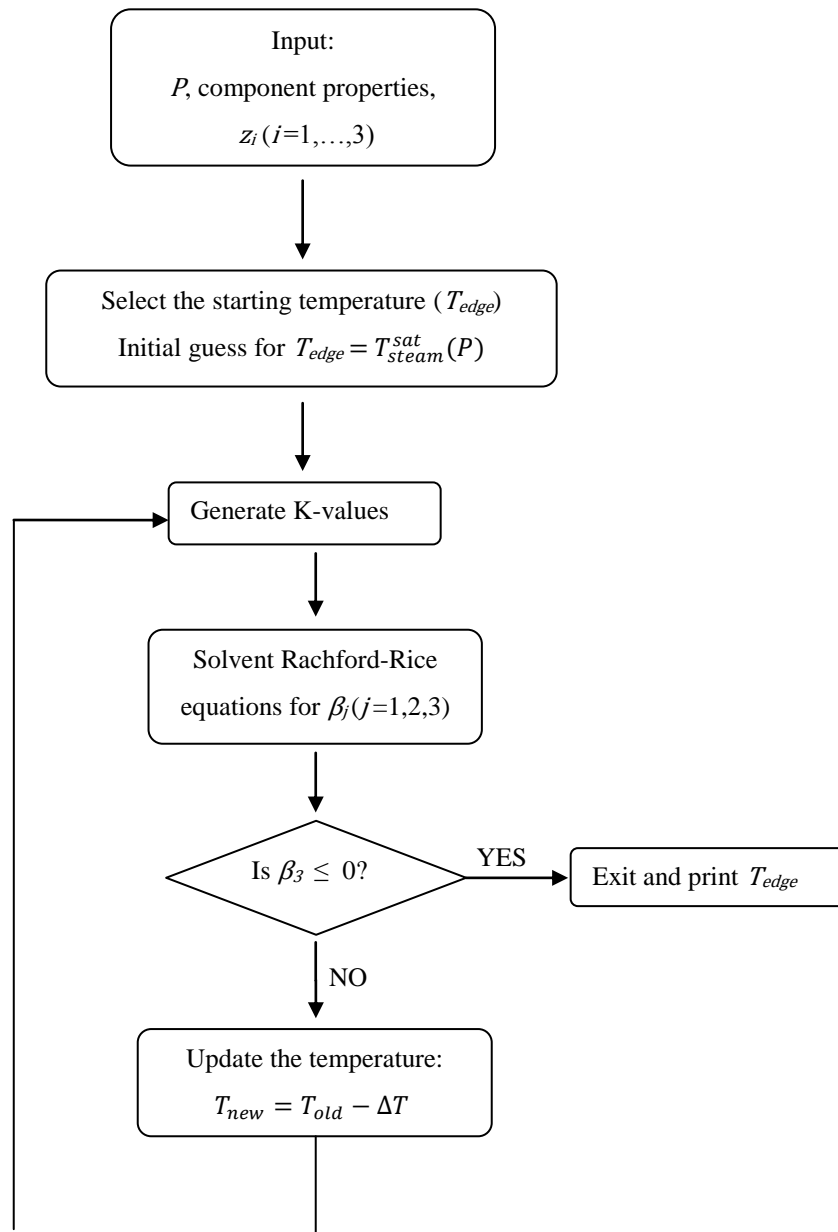


**Figure 4-1. Flowchart of the algorithm used for estimation of  $T_{edge}$  for a given pressure and an assumed overall composition.**

The accuracy of estimations is increased by picking a smaller  $\Delta T$  as the temperature update step.

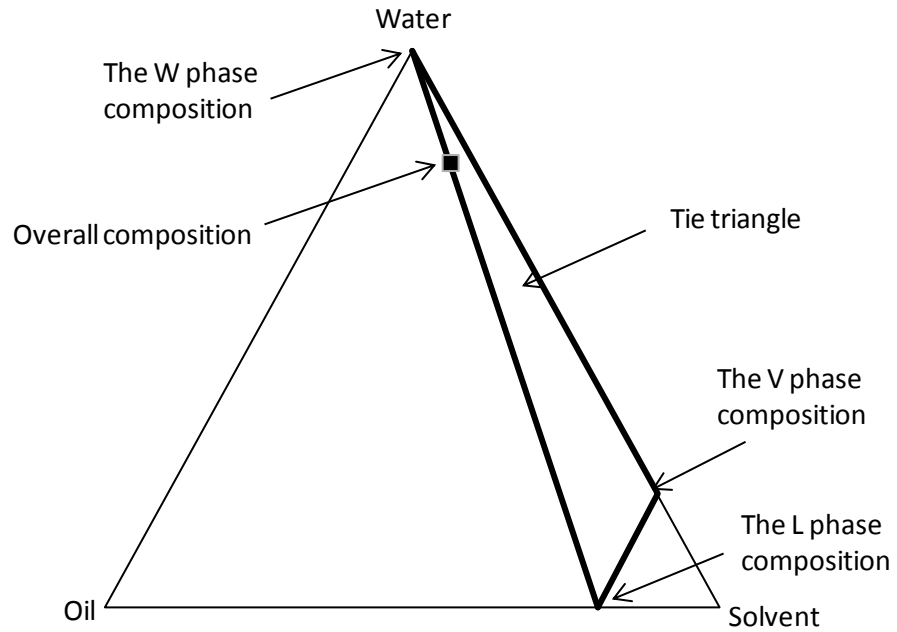
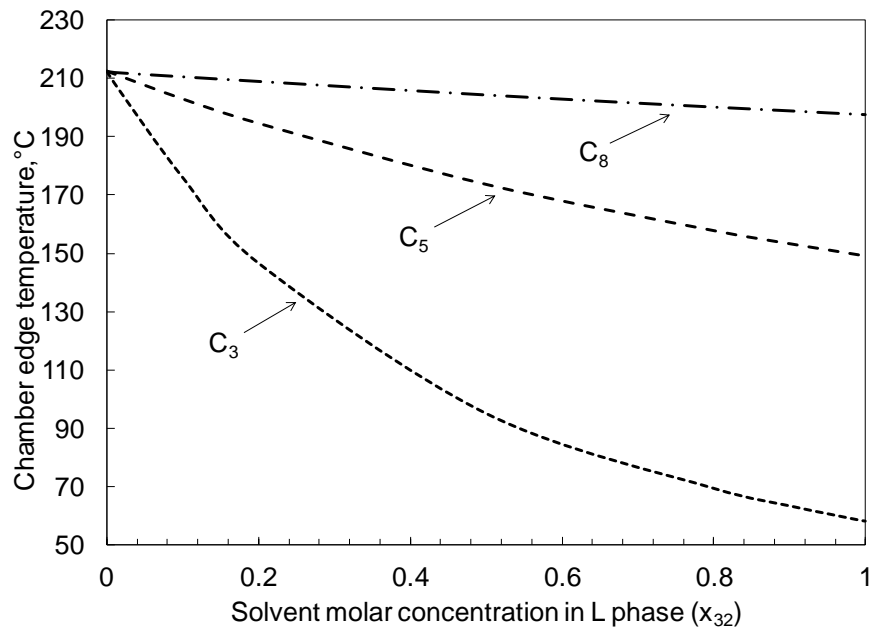
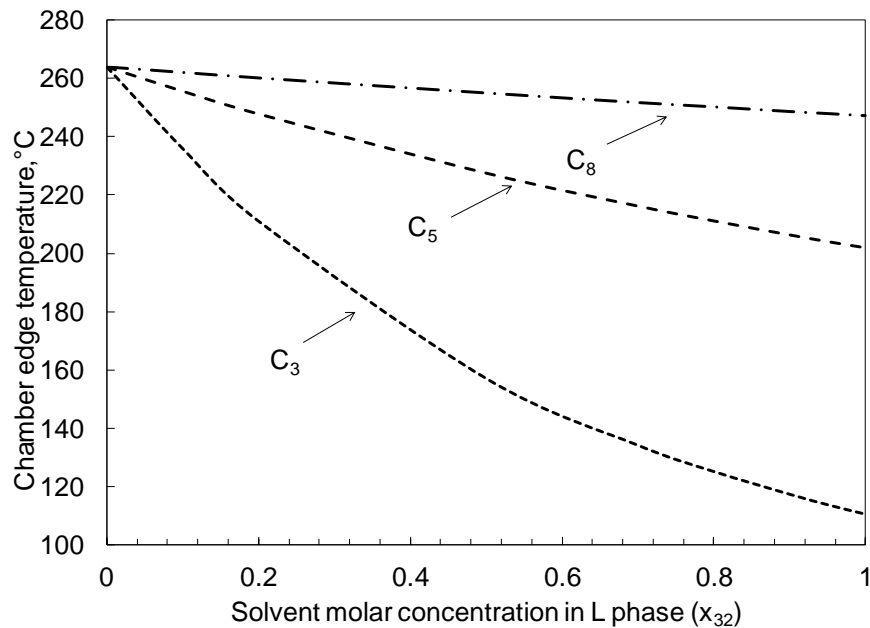


**Figure 4-2. Tie triangle for a system of water, single component solvent and reservoir oil at a sample pressure and temperature.**

The overall composition lays on the tie line connecting the W phase and L phase, i.e. conditions at the chamber edge.



(a)



(b)

**Figure 4-3. Variations of chamber edge temperature vs. solvent mole fraction in the L phase ( $x_{32}=z_3/(z_3+z_2)$ )**

(a) 2000 kPa and, (b) 5000 kPa. Reservoir oil is an Athabasca type of bitumen with the properties listed in Table 4-1. Note that due to zero mutual solubility assumption between water and hydrocarbon components, chamber edge temperature will be dependent on the overall composition ratio of solvent and oil,  $z_3/z_2$ , rather than the overall composition of all components. According to the results of calculations, a lower chamber edge temperature is expected for the same solvent concentration in the L phase as the solvent becomes more volatile.

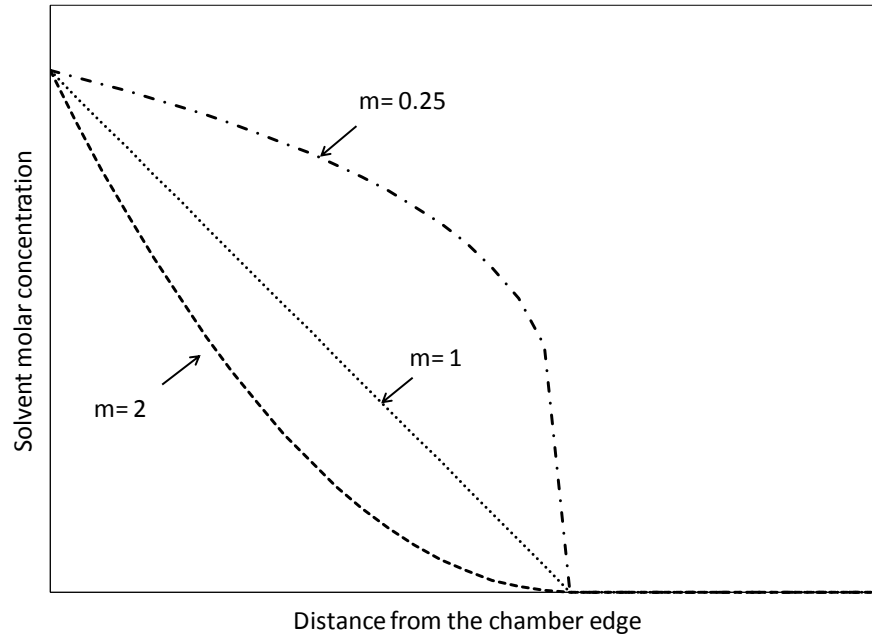
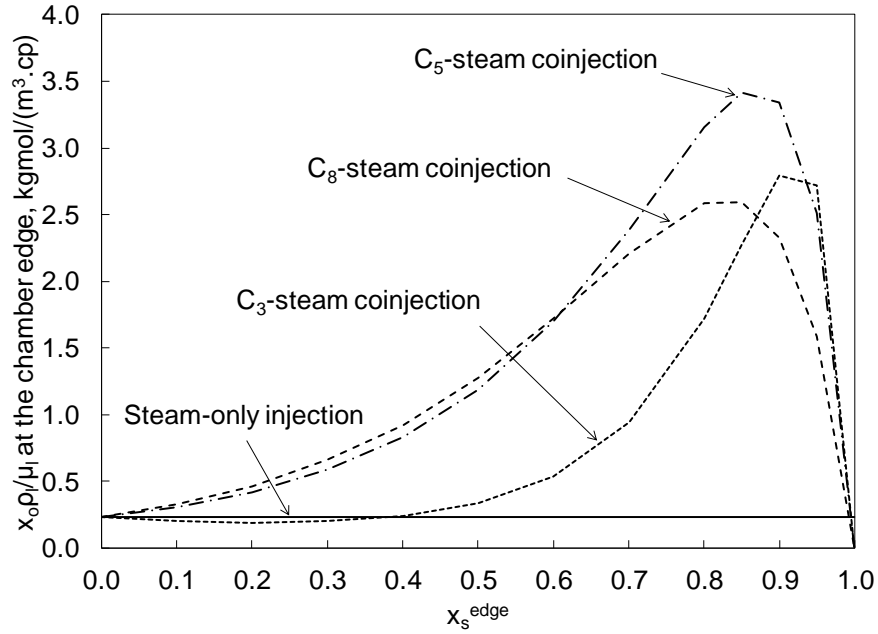


**Figure 4-4. Different forms of solvent distribution profile in the L phase beyond the chamber edge as predicted by Equation 4-16.**

Similar values of  $x_s^{edge}$  and  $\xi_t$  but different values of  $m$  have been used. If  $m < 1$  the profile would be convex upward with an abrupt advancing front at  $\xi_t$ . Such profile resembles the results from experimental measurements by Oballa and Butler (1989).



**4-5. Variations of the oil component molar flux integrand in Equation 4-14 vs. the molar concentration of solvent in the L phase right at the chamber interface.**

Operation pressure is 2000 kPa and the reservoir oil is a typical Athabasca bitumen. The horizontal line shows this ratio for steam-only injection process. Properties of all components are listed in Tables 4-1 and 4-2. The break-over point in each curve is a result of the balance between oil component content of the L phase and its mobility at the chamber edge.

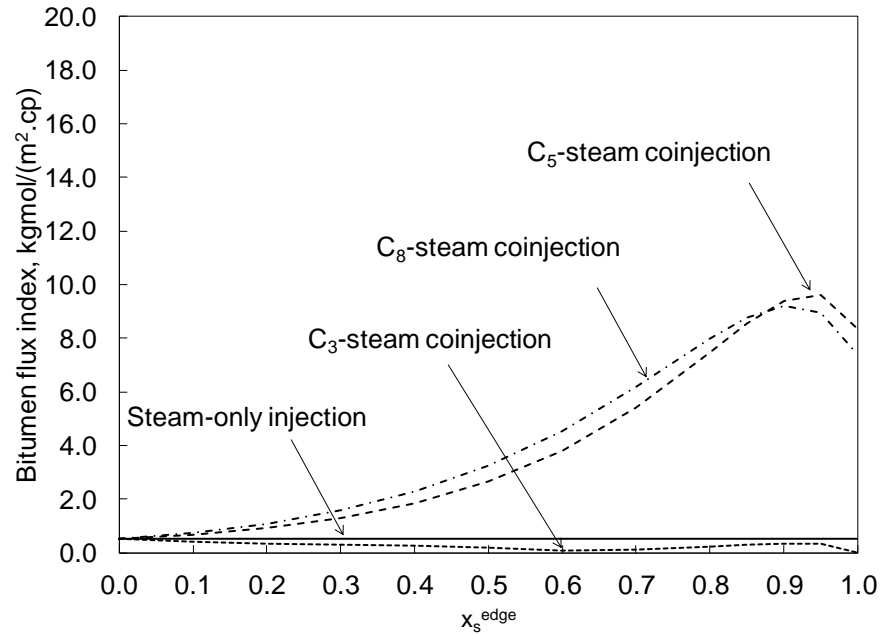


**Figure 4-6. Profiles of the oil component drainage flux index in Equation 4-14 vs. the molar concentration of solvent in the L phase right at the chamber interface.**

Operation pressure is 2000 kPa and the reservoir oil is a typical Athabasca bitumen. The horizontal line represents the steam-only injection process. Properties of all components are listed in Tables 4-1 and 4-2. Values of the integral in Equation 4-14 are evaluated numerically and are expected to exhibit negligible deviation from the analytical evaluation.

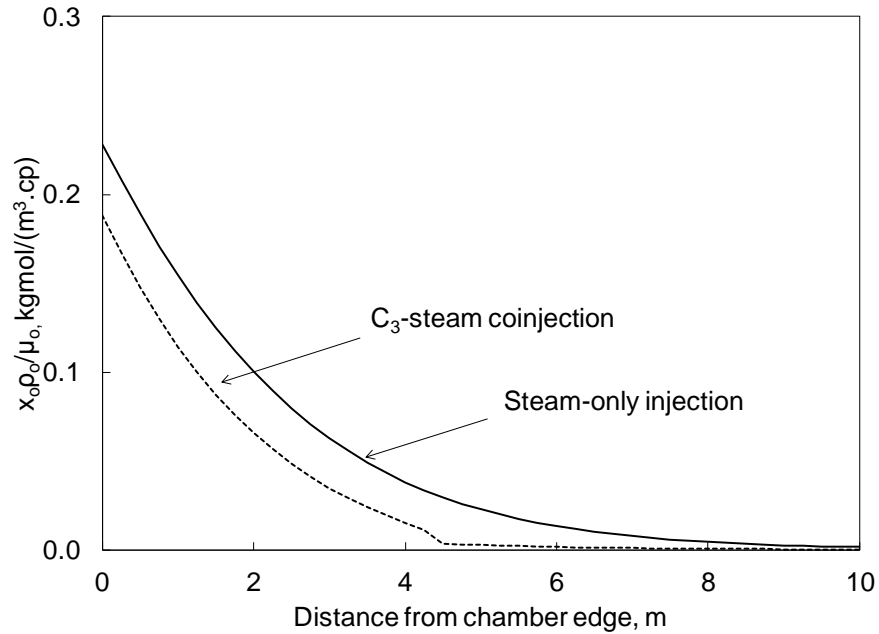


**Figure 4-7. Profiles of the oil component molar flux integrand in Equation 4-14 vs. the perpendicular distance from the chamber interface for an assumed value of  $x_s^{edge} = 0.25$ .**

Operation pressure is 2000 kPa and the reservoir oil is a typical Athabasca bitumen. Properties of all components are listed in Tables 4-1 and 4-2. The profile of C<sub>3</sub>-steam coinjection remains below that of steam-only injection. This is due to insufficient dilution effects to compensate the negative effects of unfavorable temperature distribution on the L phase viscosity beyond the chamber interface.

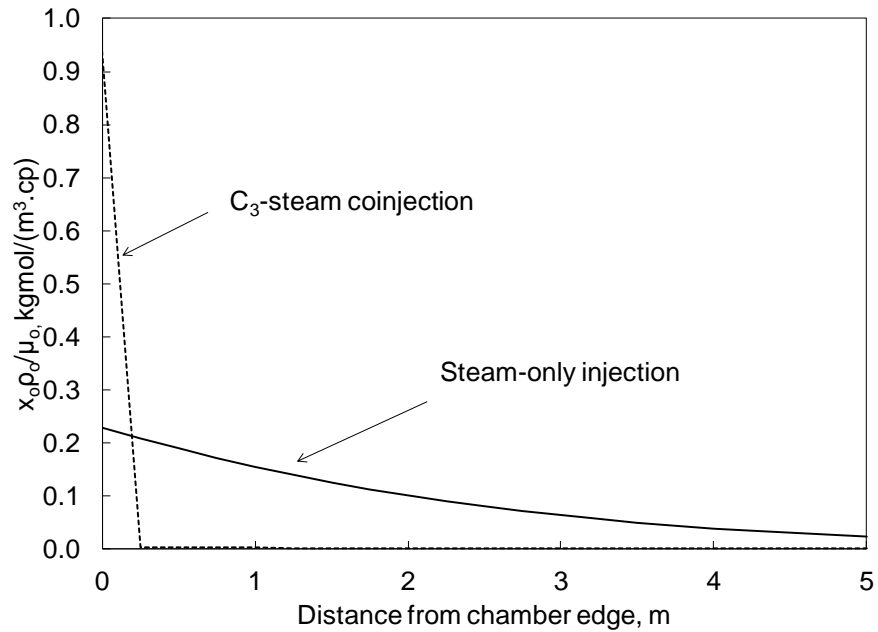
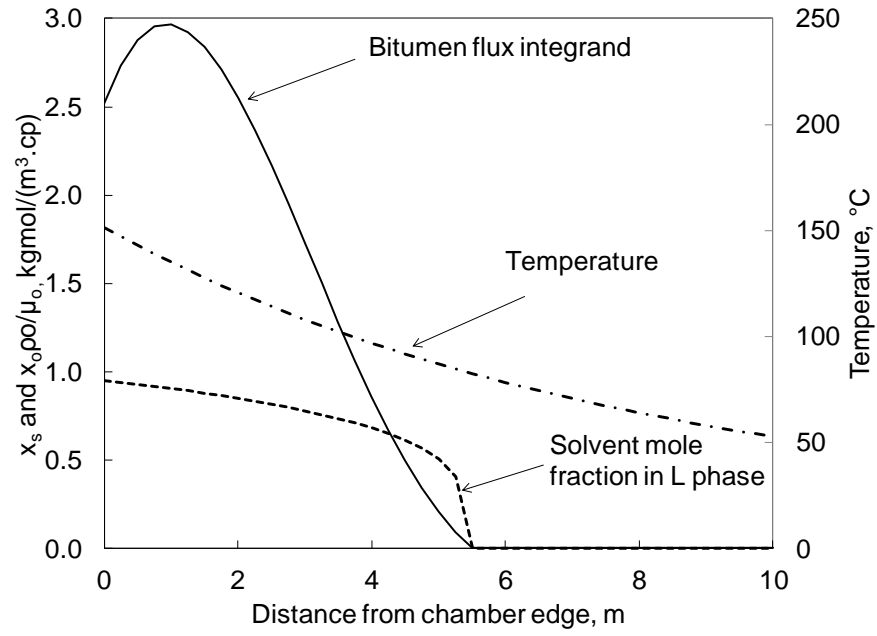
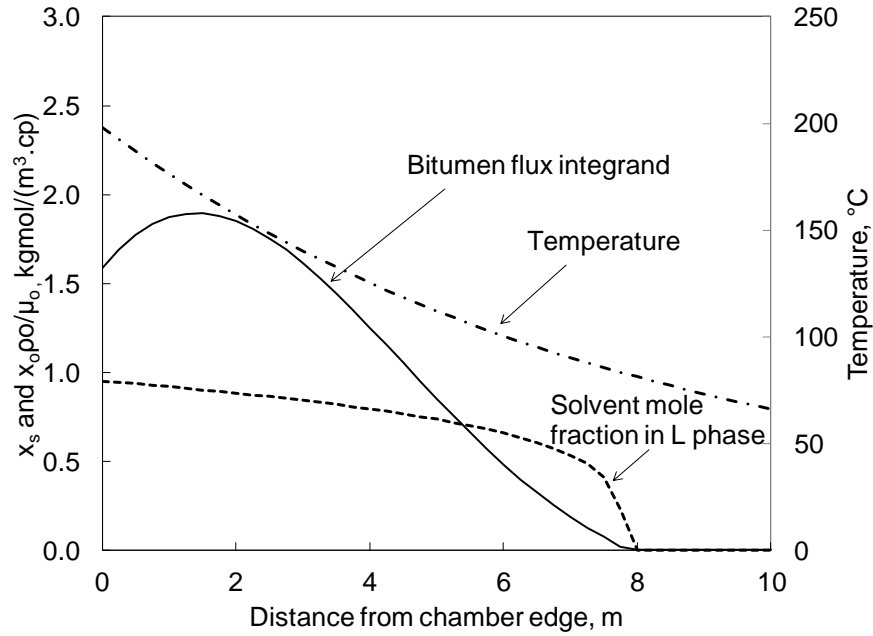


**Figure 4-8. Profiles of the oil component molar flux integrand in Equation 4-14 vs. the perpendicular distance from the chamber interface for an assumed value of  $x_s^{edge} = 0.7$ .**

Operation pressure is 2000 kPa and the reservoir oil is a typical Athabasca bitumen. Properties of all components are listed in Tables 4-1 and 4-2. The profile of C<sub>3</sub>-steam coinjection remains above that in steam-only injection only for a fraction of meter beyond the chamber edge. Considerably lowered temperature due to significant accumulation of C<sub>3</sub> at the chamber edge has resulted in a very viscous L phase and a thin solvent mixing zone beyond the vapor-liquid interface.



(a)



(b)

**Figure 4-9. Profiles of the oil component molar flux integrand, temperature and solvent molar concentration in L phase vs. the perpendicular distance from the chamber interface for an assumed value of  $x_s^{edge} = 0.95$ .**

(a) C<sub>5</sub>-steam coinjection; (b) C<sub>8</sub>-steam coinjection. A more favorable temperature profile has resulted in a thicker C<sub>8</sub> mixing zone beyond the chamber edge compared to C<sub>5</sub>; however, dilution is less effective with C<sub>8</sub> due to its more viscous nature. The overall effect has resulted in profile of bitumen flux integrand in C<sub>5</sub> coinjection to lie above that in C<sub>8</sub> coinjection in the first 4 meters from the chamber interface.

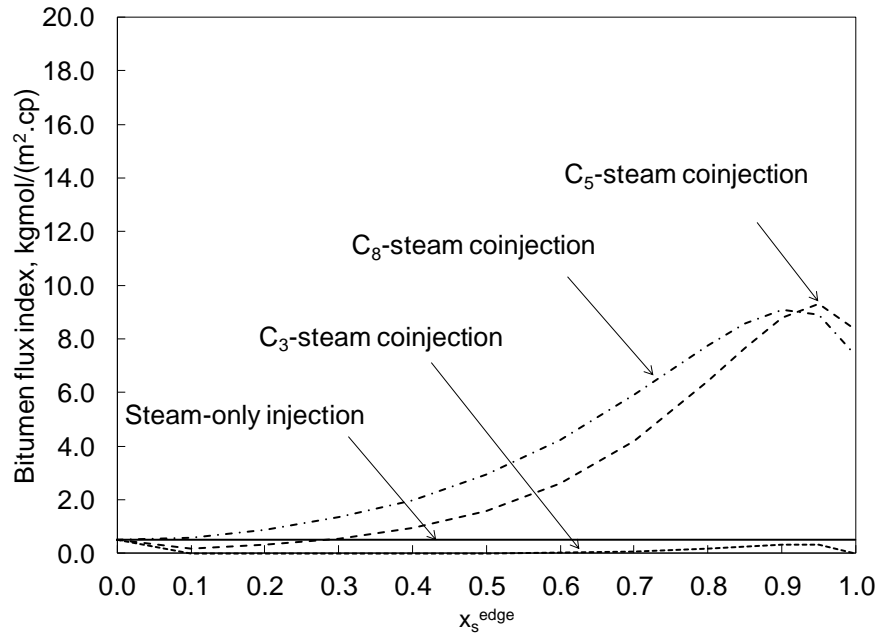


**Figure 4-10. Profiles of the oil component drainage flux index in Equation 4-14 vs. the molar concentration of solvent in the L phase right at the chamber interface.**

Operation pressure is 2000 kPa and the reservoir oil is a typical Athabasca bitumen. The horizontal line represents the steam-only injection process. Chamber edge temperature is estimated using a simplified representation of binary mixture of water and solvent. This will underestimate the performance of  $C_3$ - and  $C_5$ -steam coinjection cases relative to  $C_8$ -steam coinjection. One may erroneously pick  $C_8$  as the optimum solvent based on this figure; however  $C_5$  is more likely to be the optimum in practice (compare with Figure 4-6).

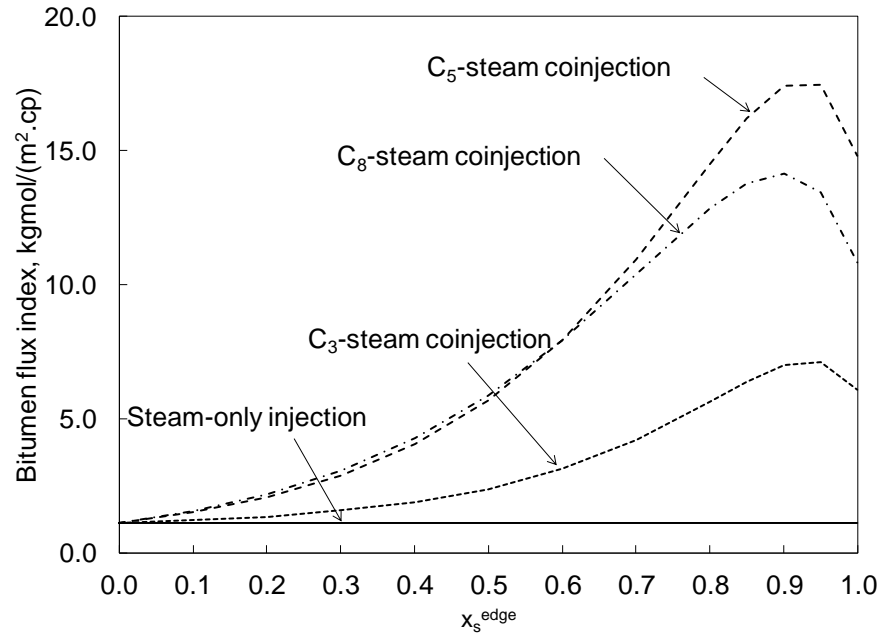


**Figure 4-11. Profiles of the numerically evaluated oil component drainage flux index in Equation 4-14 vs. the molar concentration of solvent in the L phase right at the chamber interface.**

Operation pressure is increased to 5000 kPa and the reservoir oil is a typical Athabasca bitumen. The horizontal line represents the steam-only injection process. Performance of volatile solvents such as C<sub>3</sub> in this study is expected to be improved in terms of oil production rates, under a higher operating pressure.

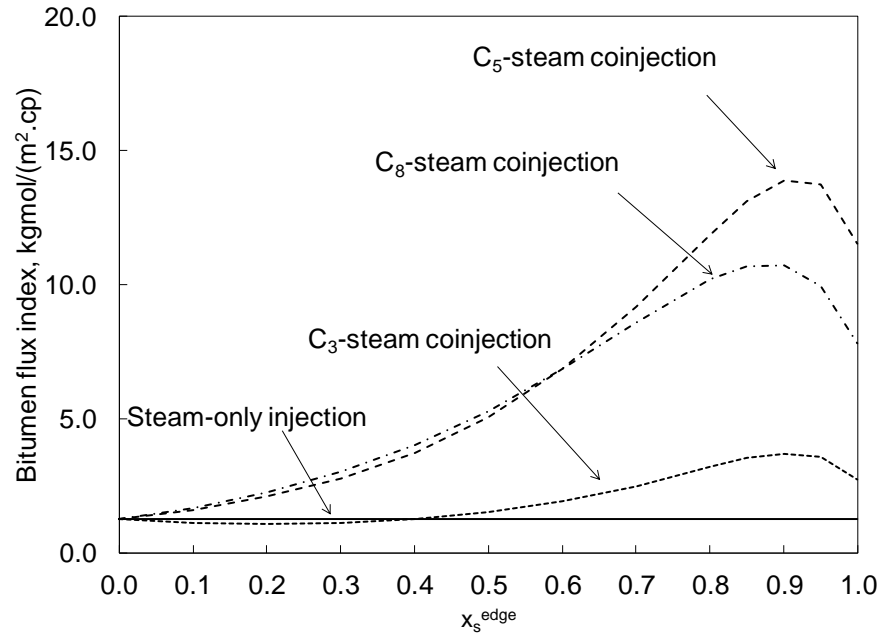
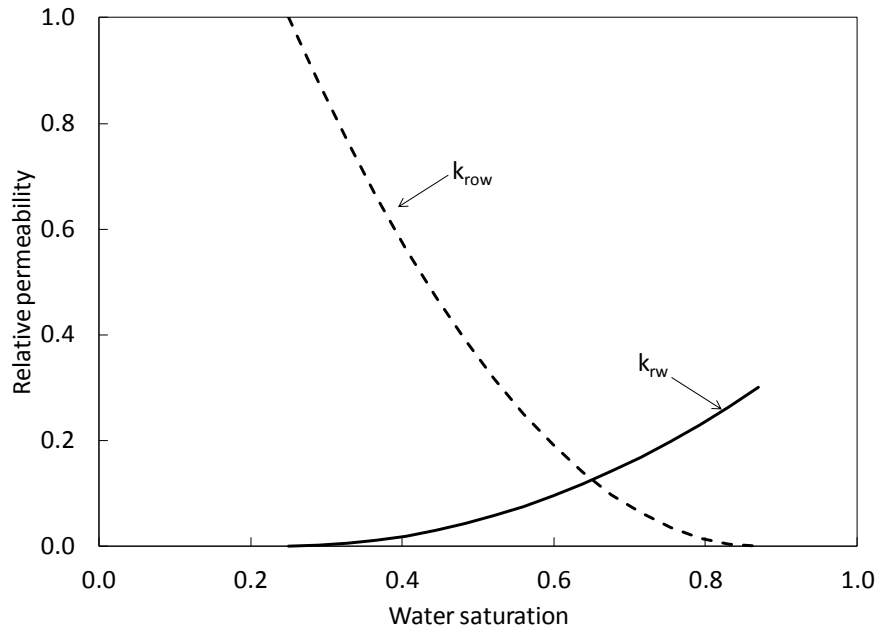
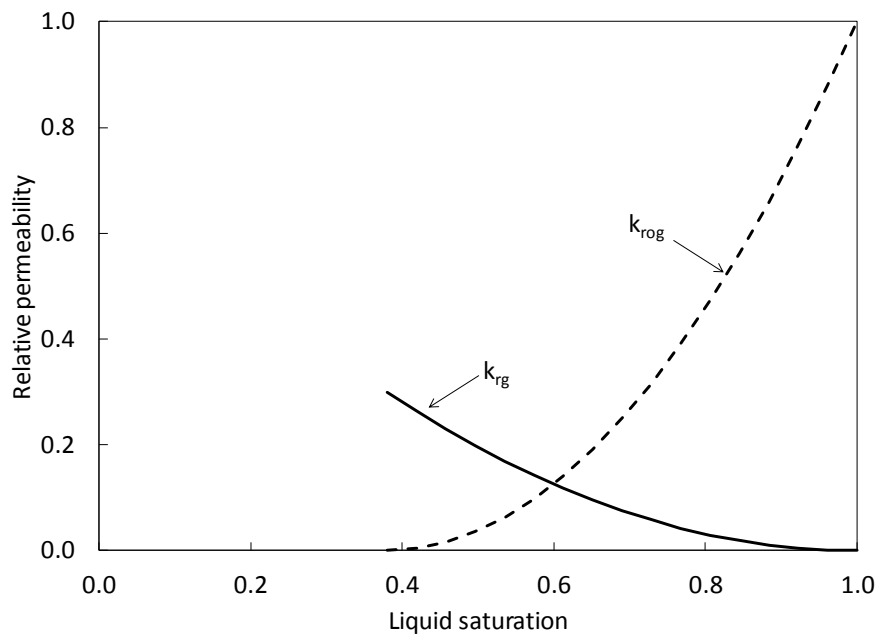


**Figure 4-12. Profiles of the numerically evaluated oil component drainage flux index in Equation 4-14 vs. the molar concentration of solvent in the L phase right at the chamber interface.**

Operation pressure is 2000 kPa. Reservoir oil less viscous than Athabasca bitumen with viscosity-temperature profile as presented in Table 4-3. The horizontal line represents the steam-only injection process. Performance of volatile solvents such as C<sub>3</sub> in this study is expected to be improved in terms of oil production rates when the reservoir oil is less viscous.



(a)



(b)

**Figure 4-13. Relative permeability curves used in the simulation cases**

(a) The water-oil system and (b) the oil-gas system.

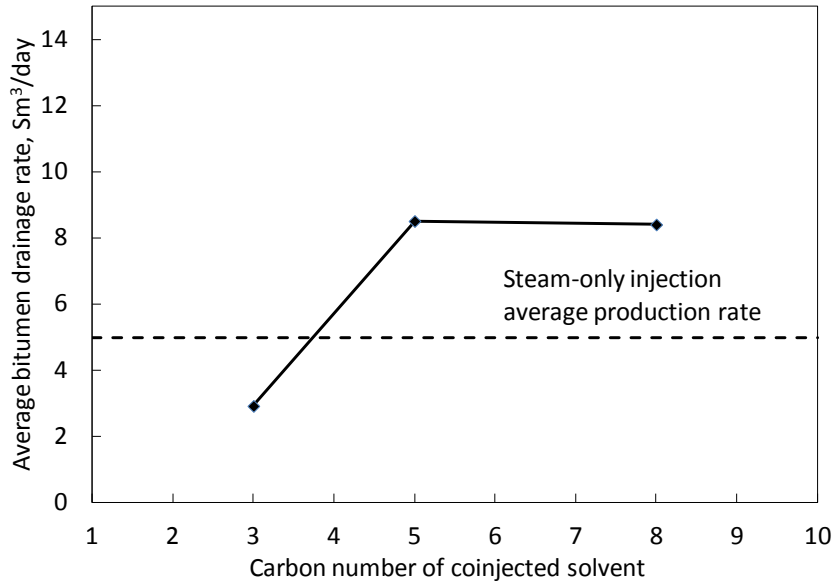


**Figure 4-14. Results of numerical simulations of the base case for the average bitumen production rate after the 9th month of coinjection until the 20th month for 3 solvent-steam coinjection processes.**

The time interval is chosen within the lateral expansion period of chamber before it arrives to the other boundary of the reservoir. The average rate for SAGD during this time period is shown with a horizontal line. Both C<sub>5</sub> and C<sub>8</sub> coinjections with steam have resulted in improved production rates while C<sub>3</sub>-steam coinjection has deteriorated the production rate compared to steam-only injection. C<sub>5</sub> is most likely to be selected as the optimum solvent for this case.

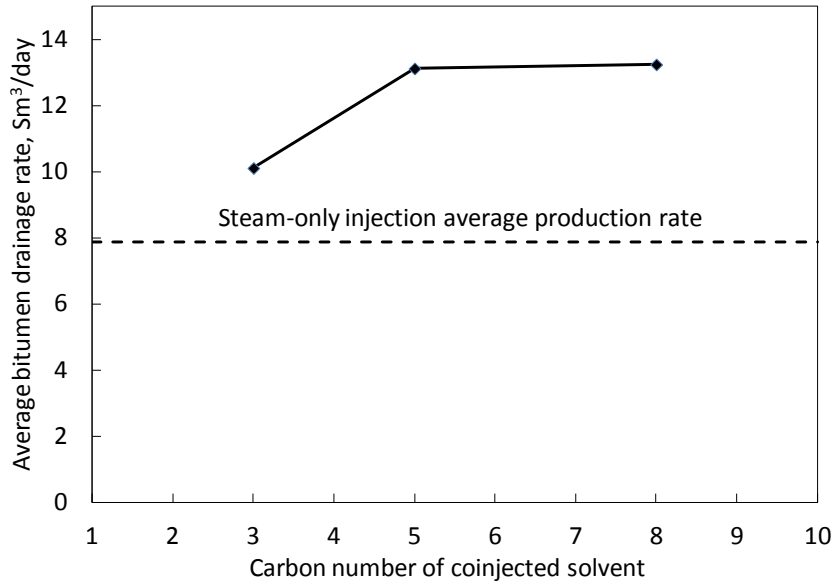


**Figure 4-15. Results of numerical simulations of case 2 for the average bitumen production rate after the 5<sup>th</sup> month of coinjection until the 15<sup>th</sup> month for 3 solvent-steam coinjection processes.**

The average production rate for SAGD during this time period is shown with a horizontal line. Unlike the base case, all solvent-steam coinjection cases including C<sub>3</sub>-steam coinjection have improved oil production rate compared to steam-only injection.

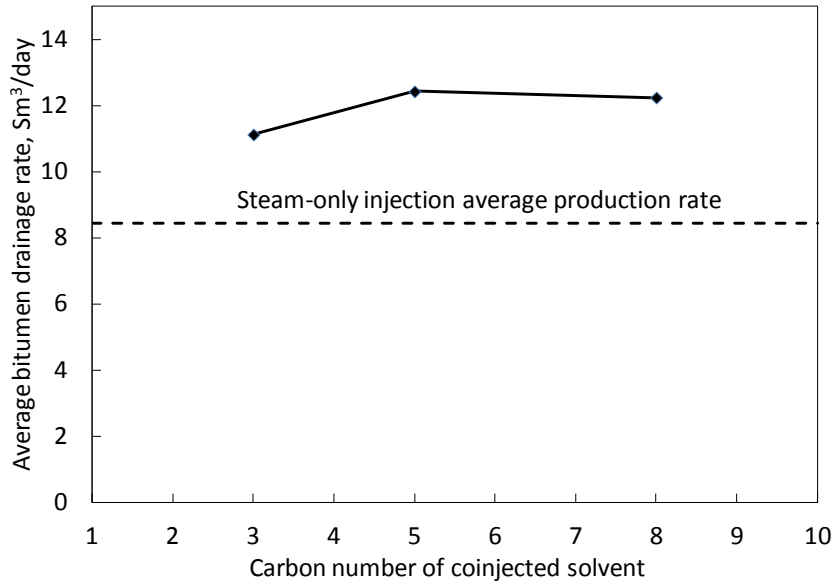


**Figure 4-16. Results of numerical simulations of case 3 for the average bitumen production rate after the 4<sup>th</sup> month of coinjection until the 15<sup>th</sup> month for 3 solvent-steam coinjection processes.**

The average rate for SAGD during this time period is shown with a horizontal line. As expected by the analytical solution, all coinjection processes have exhibited improved performance compared to steam-only injection. C<sub>5</sub> is most likely to be selected as the optimum solvent for this case.

## References

- Ardali, M., Barrufet, M., and Mamora, D.D. 2012a. Laboratory Testing of Addition of Solvents to Steam to Improve SAGD Process. Paper SPE 146993 presented at SPE Heavy Oil Conference Canada, Calgary, Alberta, Canada, 12-14 June.
- Butler, R.M. 1997. *Thermal Recovery of Oil and Bitumen*. Prentice Hall.
- Butler, R.M. 1985. A New Approach to Modelling Steam Assisted Gravity Drainage. *Journal of Canadian Petroleum Technology* **24** (3): 42-51.
- Canbolat, S., Akin, S., and Kovscek A.R. 2002. A Study of Steam-Assisted Gravity Drainage Performance in the Presence of Noncondensable Gases. Paper SPE 75130 presented at Improved Oil Recovery Symposium, Tulsa, Oklahoma, USA, April 13-17.
- Dong, L. 2012. Effect of Vapor-Liquid Phase Behavior of Steam-Light Hydrocarbon Systems on Steam Assisted Gravity Drainage Process for bitumen recovery. *Fuel* **95**: 159-168.
- Dunn, S.G., Nenninger, E.H., and Rajan, V.S.V. 1989. A Study of Bitumen Recovery by Gravity Drainage Using Low Temperature Soluble Gas Injection. *Canadian Journal of Chemical Engineering* **67** (6): 978-99.1
- Farouq Ali, S.M. 1997. Is There Life After SAGD? *Journal of Canadian Petroleum Technology* **36** (6): 97-06-DAS.
- Gotawala, D., and Gates, I.D. 2008. Steam Fingering at the Edge of a Steam Chamber in a Heavy Oil Reservoir. *Canadian Journal of Chemical Engineering* **86** (6): 1011-1022.
- Gupta, S., and Gittins, S.D. 2012. An Investigation Into Optimal Solvent Use and the Nature of Vapor/Liquid Interface in Solvent-Aided SAGD Process With a Semianalytical Approach. *SPE Journal* **17** (4): 1255-1264.
- Gupta, S. And, Gittins, S.D. 2006. Christina Lake Solvent Aided Process Pilot. *Journal of Canadian Petroleum Technology* **45** (9): 15-18.
- Gupta, S., Gittins, S., and Picherack, P. 2005. Field Implementation of Solvent Aided Process. *Journal of Canadian Petroleum Technology* **44** (11): 8-13.
- Hosseininejad Mohebbati, M., Maini, B.B., and Harding, T.G. 2010. Optimization of Hydrocarbon Additives with Steam in SAGD for Three Major Canadian Oil Sand Deposits. Paper CSUG/SPE 138151 presented at the Canadian Unconventional Resources and International Petroleum Conference, Calgary, Alberta, Canada, October 19-21.
- Ivory, J., Zheng, R., Nasr, T., Deng, X., Beauulieu, G., and Heck, G. 2008. Investigation of Low Pressure ES-SAGD. Paper SPE 117759 presented at 2008 SPE International Thermal Operations and Heavy Oil Symposium, Calgary, Alberta, Canada, October 20-23.
- Jiang, Q., Butler, R., and Yee, C.T. 1998. The Steam and Gas Push (SAGP)-2: Mechanism Analysis And Physical Model Testing. Petroleum Society's 49th Annual Technical Meeting, Calgary, Alberta, Canada, June 8-10.

- Keshavarz, M., Okuno, R., and Babadagli, T. 2013. Optimal application conditions for steam-solvent coinjection. Submitted for publication to *SPE Reservoir Evaluation & Engineering* on May 9, 2013.
- Keshavarz, M., Okuno, R., and Babadagli, T. 2012. Efficient Oil Displacement Near the Chamber Edge in ES-SAGD. Submitted for publication to *Journal of Petroleum Science and Engineering* on July 27, 2012.
- Leaute, R.P. 2002. Liquid Addition to Steam for Enhancing Recovery of Bitumen with CSS: Evolution of Technology from Research Concept to a Field Pilot at Cold Lake. SPE/Petroleum Society of CIM/CHOA Paper Number 79011, Calgary, Alberta, Canada, November 4-7.
- Leaute, R.P., and Carey, B.S. 2005. Liquid Addition to Steam for Enhancing Recovery (LASER) of Bitumen with CSS: Results from the First Pilot Cycle. Paper Number 2005-161 presented at the 56<sup>th</sup> Canadian International Petroleum Conference, Calgary, Alberta, Canada, June 7-9.
- Li, W., Mamora, D.D., and Li, Y. 2011b. Solvent-Type and -Ratio Impacts on Solvent-Aided SAGD Process. *SPE Reservoir Evaluation and Engineering*. **14** (3): 320-331
- Li, W. and Mamora, D.D. 2010. Phase Behavior of Steam with Solvent Coinjection under Steam Assisted Gravity Drainage (SAGD) Process. Paper SPE 130807 presented at the SPE EUROPEC/EAGE Annual Conference and Exhibition, Barcelona, Spain, June 14-17.
- Mohammadzadeh, O., Rezaei, N., and Chatzis, I. 2012. More Insight into the Pore-Level Physics of the Solvent-Aided SAGD (SA-SAGD) Process for Heavy Oil and Bitumen Recovery. Paper SPE 157776 presented at SPE Heavy Oil Conference Canada, Calgary, Alberta, Canada, June 12-14.
- Nasr, T.N., Beaulieu, G., Golbeck, H., and Heck, G. 2003. Novel Expanding Solvent-SAGD Process "ES-SAGD". *Journal of Canadian Petroleum Technology*. **42** (1): 13-16.
- Oballa, V., and Butler, R.M. 1989. An Experimental Study of Diffusion in the Bitumen-Toluene System. *Journal of Canadian Petroleum Technology*. **28** (2): 63-69.
- Okazawa, T. Impact of Concentration-Dependence of Diffusion Coefficient on VAPEX Drainage Rates. *Journal of Canadian Petroleum Technology*. **48** (2): 47-54.
- Redford, D.A., and McKay, A.S. 1980. Hydrocarbon-Steam Processes for Recovery of Bitumen from Oil Sands. Paper SPE 8823 presented at SPE/DOE Enhanced Oil Recovery Symposium, Tulsa, Oklahoma, USA, April 20-23.
- Sharma, J., and Gates, I.D. 2011. Interfacial Stability of In-Situ Bitumen Thermal Solvent Recovery Processes. *SPE Journal* **16** (1): 55-64.
- Sharma, J., and Gates, I.D. 2010b. Multiphase Flow at the Edge of a Steam Chamber. *The Canadian Journal of Chemical Engineering* **88** (3): 312-321.

- Sharma, J., and Gates, I.D. 2010a. Steam-Solvent Coupling at the Chamber Edge in an In Situ Bitumen Recovery Process. Paper SPE 128045 presented at the SPE Oil and Gas India Conference and Exhibition, Mumbai, India, January 20-22.
- Sharma, J., Moor, R.G., and Mehta, S.A. 2011. Effect of Methane Co-injection in SAGD- Analytical and Simulation Study. Paper SPE 148917 presented at the Canadian Unconventional Resources Conference, Calgary, Alberta, Canada, November 15-17.

**CHAPTER 5 : CONTRIBUTIONS AND  
RECOMMENDATIONS**

## **Overview, Contributions and Conclusions**

In this chapter a general overview of the research is provided and the key findings and contributions are highlighted.

Coinjection of solvent with steam has been proposed as an alternative to steam-only injection processes to achieve a number of economical and environmental advantages. Improved oil production rate and ultimate recovery factor, as well as reduced steam-oil ratio (SOR) are the key advantages of coinjection over steam-only injection. Generally, in steam-based recovery process, the lower the SOR, the more economic and environmental friendly the process will be. Nevertheless, all the potential advantages of coinjection are subject to proper design of the process. This includes the appropriate choice of solvent as well as coinjection scenario which are specific to each reservoir and operating conditions. The key to an optimum design of a coinjection process is a sound knowledge of the key mechanisms involved.

In this work, we identified the key mechanisms and fundamental physics of the coinjection process. Based on this improved knowledge, we demonstrated how different solvents, reservoir fluids or operating conditions can affect these mechanisms and the performance of the process.

In Chapter one, a mechanistic simulation study of a specific type of coinjection process, ES-SAGD, was conducted. The key findings, however, can be extended to any other coinjection process with similar nature. We demonstrated that the determining factors for improved oil production rates are relative positions to the temperature and solvent fronts, the steam and solvent contents of the chamber at its interface with reservoir bitumen, and solvent diluting effects on the mobilized bitumen just ahead of the chamber edge. Then, the key mechanisms for improved oil displacement are solvent propagation, solvent accumulation at the chamber edge, and phase transition.

In Chapter 2, a simplistic representation of phase behavior inside the coinjection chamber was presented by a binary system of water and solvent. We then compared the accuracy of estimations of chamber edge temperature from this simplistic model with the results from numerical simulation of flow in

reservoir in which some of the simplistic assumptions were relaxed. Results show that an optimum volatility of solvent can be typically observed in terms of the oil production rate for given operation conditions. This optimum volatility occurs as a result of the balance between two factors affecting the oil mobility along the chamber edge; i.e., reduction of the chamber-edge temperature and superior dilution of oil in coinjection of more volatile solvent with steam.

We demonstrated that it is possible to maximize oil recovery while minimizing solvent retention in situ by controlling the concentration of a given coinjection solvent. Coinjection starts with high solvent concentrations in the injectant. This promotes the advantages of coinjection at early stages of process. Then, solvent concentration is gradually decreased to prevent the formation of a very thick solvent rich bank at the chamber edge. Subsequently, coinjection is stopped in the final period of project to allow for the drainage of the solvent already accumulated. Simulation case studies show the validity of the oil recovery mechanisms described.

Eventually, in Chapter 3, a simple algorithm was proposed to estimate the chamber edge temperature in a system of three components; i.e, water, solvent and oil. Then a semi-analytical approach was taken to predict the temperature and solvent distribution profiles beyond the edge of chamber. The semi-analytical method was applied to several solvent-steam coinjection processes to qualitatively evaluate their performances in terms of oil production rates. Validation of the predictions with the results from numerical simulations showed that the proposed semi-analytical method can be reliable for a preliminary screening of solvents for coinjection with steam.

The key findings and contributions of this research are as follows:

1. Solvent-steam coinjection can achieve oil saturation lower than the residual saturation in the chamber. The oil saturation reduction results mainly from two processes: (1) Solvent accumulation in the oleic phase outside the chamber edge, and (2) phase transition near the chamber edge (i.e., vapor-liquid-aqueous inside and liquid- aqueous outside the chamber edge). The solvent accumulation lowers the oil-component

concentrations. The diluted oil is then redistributed in the gaseous and oleic phases in the presence of the water phase during the phase transition. The amount of the oleic phase after this phase transition can be significantly small, resulting in low oil saturations in the coinjection chamber.

2. The difference between the oil production rate in coinjection and that in steam-only injection depends mainly on three factors: i.e., Solvent accumulation, temperature distribution, and bitumen dilution with solvent near the chamber edge. Our simulation and theoretical case studies show that an optimum combination of these factors can result in oil production rates significantly greater than that in steam-only injection.
3. Chamber edge temperature in a solvent-steam coinjection can vary from steam saturation temperature at the operating pressure to the dew point of binary mixture of water and solvent. Thus a temperature gradient will form inside the coinjection chamber while it does not exist in a steam-only injection process. Steam will gradually condense along this temperature gradient inside the chamber. Temperature and steam availability at the edge is a function of solvent type and its accumulation at the chamber edge.
4. Solvent volatility and accumulation both act to reduce the temperature and steam availability at the chamber edge. The lighter the solvent and the more the accumulation of it, the lower the temperature and steam availability would be at the chamber edge. A higher production rate compared to steam-only injection is achieved only when solvent diluting effects can compensate the negative effects of unfavorable temperature distribution on the viscosity of the draining oleic phase.
5. During a specific solvent coinjection with steam, solvent accumulation up to an optimum amount improves the dilution efficiency. Further accumulation, however, is not beneficial as it further reduces the temperature, thickness of the solvent mixing zone, and the oil content of the draining L phase beyond the chamber edge. The best performance of

a specific coinjection process in terms of oil production rate is expected to occur when the average solvent accumulation at the chamber edge is maintained at this optimum.

6. Among the solvents of different volatility, a less volatile solvent results in a more favorable temperature and a thicker solvent mixing zone ahead of the chamber edge. However, the diluting effects are expected to be less effective. Thus an optimum solvent volatility is theoretically expected in terms of oil production rates when the above mentioned factors take a balance. Based on this balance, a systematic workflow was proposed for optimum selection of solvent.
7. Results showed that the bitumen viscosity-temperature behavior as well as the operating pressure are the two important factors than can affect the performance of coinjection and the optimum choice of solvent. According to our results, the coinjection of a very volatile solvent such as  $C_3$  at low operating pressures will not be economical for an Athabasca type of bitumen. A higher operating pressure or less viscous reservoir oil increases the practicality of coinjecting more volatile solvents with steam.
8. We also proposed an optimum strategy for the coinjection of solvent. It is possible to maximize oil recovery while minimizing solvent retention in situ by controlling the concentration of a given coinjection solvent. Initiation of coinjection right after achieving the inter-well communication enables to enhance oil recovery early in the process. Subsequently, the solvent concentration should be gradually decreased until it becomes zero for the final period of the coinjection. This coinjection procedure can minimize solvent retention in the oleic phase in situ while keeping oil recovery.
9. We proposed a semi-analytical method for preliminary screening of the coinjection solvent when there is a meaningful contrast between the production rates. This can be much faster and more convenient than

running full numerical simulations of flow and can eliminate the need to run unnecessary simulations.

### **Suggested Future Work**

1. Due to the complexity of phase behavior, the reservoir oil and the solvent in this study are considered to be single-component. A single-component representation of the reservoir oil, however, is not an accurate assumption. Furthermore, the available solvent for coinjection may be multi-component. Extension of the current work to a system of multi-component oil and solvent can improve the practical significance of the research.
2. In this study, the mutual solubility between water and hydrocarbon components is considered to be negligible. This may not be true in certain circumstances in practice. Extension of this study with a phase behavior model that can properly handle the mutual solubility of water and hydrocarbon components can improve the reliability of the results.
3. To capture the key mechanisms of the coinjection process, a simplistic reservoir model was used in numerical simulations. For example, the reservoir was assumed to be homogeneous. Also, asphaltene precipitation and physical dispersion/diffusion were not incorporated in the numerical models. While these simplifying assumptions are not expected to alter the key mechanisms identified, an extension of the current work in which some or all of these assumptions are relaxed can add to the accuracy of predictions.
4. The current work does not cover the pore-scale physics of the solvent-steam coinjection. There are a very limited number of studies focused on the pore-scale mechanics of coinjection. Yet, a more comprehensive study is needed to cover the followings and to show their effects on large-scale mechanisms:
  - local mass and heat transfer mechanisms at pore-scale
  - mixing of oil and solvent in presence of water and/or gas bubbles
  - potential alterations of interfacial tension as a result of solvent-oil mixing.

5. This work concentrates on coinjection as an alternative to SAGD. A study of the mechanisms of coinjection in reservoirs that are not good candidates for SAGD is worthy. For this purpose, the improved knowledge can be extended to coinjection in other types of steam-based recovery processes such as cyclic steam stimulation (CSS) or steam flooding.
6. Coinjection processes are typically expensive. Solvent retention inside the reservoir (also called solvent loss) has been a principal challenge in these applications. A detailed economical analysis of these processes is recommended to be incorporated in optimization studies.

**APPENDIXES**

## Appendix A: Generating of K-values for STARS input files

Phase equilibrium in STARS is specified via phase equilibrium ratios (K-values). K-values are used to determine the number of equilibrium phases and the composition of each phase. The more accurate the K-values, the more reliable the phase behavior estimations is going to be in simulation models.

Consider  $i$  as the index for components ( $i=1,2,\dots,N_c$ ) and  $j$  as the index for phases ( $j=1,2,\dots,N_p$ ), where  $N_c$  and  $N_p$  are the number of components and equilibrium phases, respectively. The equilibrium ratio,  $K_{ij}$ , is defined as:

$$K_{ij} = \frac{x_{ij}}{x_{iN_p}}, \quad (\text{A-1})$$

where  $x_{ij}$  is the mole fraction of component  $i$  in phase  $j$  and  $N_p$  is chosen to be the reference phase.

Based on this definition, the K-value for a component can be interpreted as a measure for the tendency of that component to exist in phase  $j$  compared to the reference phase. The higher the K-value, the greater this tendency.

This section provides brief instructions on how K-values were generated for SATRS input files in this study. Instructions are mainly extracted from STARS and WinProp user manuals (2012).

### K-values for water component

Gas-liquid K-values for the water component are defined as the mole fraction of the water component in the gaseous (V) phase divided by the mole of water component in the aqueous (W) phase. Use of STARS' default internal K-value table is recommended for the water component; however, the water component can also be considered in the feed to an equation of state to generate K-values by a series of flash calculations.

A portion of STARS' default K-value table for the water component is provided in **Table A-1**. The reference phase is the W phase here. No mutual solubility is considered between the W and L phases throughout this study and the W phase consists of only water component. With this assumption, STARS' default K-values for water shows a close agreement with K-values obtained from Raoult's law as below:

$$K_w(P, T) = \frac{P_w^{vap}(T)}{P}, \quad (A-2)$$

where  $P_w^{vap}(T)$  is the water vapor pressure at the temperature T. A K-value greater than 1 corresponds to a superheated state for steam.

#### **K-values for oil-like components**

Due to zero mutual solubility assumption between W and L phase, liquid-liquid (L-W) K-value set is not defined in this study. Only gas-liquid (V-L) K-values are defined with the L phase being the reference phase. The V-L K-value for oil-like components is defined as the mole fraction of that component in the V phase divided by the mole fraction of the same component in the L phase.

There are two ways to feed the necessary K-values into STARS:

- STARS internal correlations: which can be used for well-defined components to provide K-values as a function of pressure and temperature through the following correlation:

$$K(P, T) = \frac{KV1}{P} \cdot e^{\frac{KV4}{T-KV5}}, \quad (A-3)$$

where KV1, KV4 and KV5 are component specific constants and can be found in STARS user manual.

This correlation is based on Raoult's law. Vapor pressure of components is estimated by the Clausius-Clapeyron equation. For a detailed derivation procedure refer to Appendix D.3 of the STARS user manual (2012). This correlation is derived under a number of simplifying assumptions which may not always be accurate. Thus, the phase behavior prediction based on these K-values can be questionable.

- K-value tables based on an equation of state: An equation of state is used to conduct a series of flash calculations on a hydrocarbon mixture containing the reservoir oil and solvent components. Flash calculations are conducted at different pressures and temperatures within the pressure and temperature range of the simulation.

The dependence of component K-values on the concentration of a single key component can be determined by WinProp and output in the form of composition-dependent K-value tables. A key component,

its minimum and maximum global mole fraction as well as the mole fraction steps have to be specified for this purpose. A K-value table will be generated for each component for each of the specified mole fraction steps. If K-values are assumed to be composition-independent, a fixed feed composition has to be specified by the user.

#### **Some notes about K-value tables**

A K-value table for an arbitrary component is shown in **Table A-2**.  $T_{\text{low}}$ ,  $T_{\text{high}}$ ,  $P_{\text{low}}$  and  $P_{\text{high}}$  determine the temperature and pressure limits of the K-value table, respectively. The maximum allowed number of table entries assigned to a component, is 1500. The maximum allowed number of rows (temperature values) is 50. The maximum allowed number of columns (pressure values) is 30. There must be at least two columns and two rows.

All gas-liquid tables must have the same number of columns and the same number of rows. All liquid-liquid tables must have the same number of columns and the same number of rows. Also, all pressure steps have to be equal. All temperature steps have to be equal.

Between two K-value table entries for two adjacent pressures, K-value is interpolated linearly with respect to  $1/p$ . Between two non-zero K-value table entries for two adjacent temperatures,  $\ln(K\text{-value})$  is linearly interpolated with respect to  $1/T$ . To achieve the highest accuracy, we recommend using the maximum number of columns and rows allowed for the K-value table. When one of the K-value entries is zero, K-value varies linearly with  $1/T$ .

The gas-liquid K-values of all water-like components must be specified the same way, that is, either table or correlation. Similarly, the gas-liquid K-values of all oleic components must be specified the same way, that is, either table or correlation. The only combination not allowed is table for aqueous and correlation for oleic components.

K-values are calculated using a two-phase negative flash which allows generation of K-values outside of the two-phase region. There are limits in pressure and temperature beyond which the negative flash will be unable to converge. K-values which lie outside the range of convergence of the negative

flash are estimated by linear extrapolation. Values which have been extrapolated are marked in the tables with the notation “<extrap.>”.

<b>Table A- 1. STARS default K-value table for water component</b>						
<b>Temperature (°C)</b>	<b>Pressure (kPa)</b>					
	200	400	600	800	2000	4000
25	0.0058	0.0029	0.0019	0.0014	0.0006	0.0003
50	0.0447	0.0223	0.0149	0.0112	0.0045	0.0022
100	0.5210	0.2600	0.1740	0.1300	0.0521	0.0260
150	2.5100	1.2500	0.8360	0.6270	0.2510	0.1250
200	8.0000	4.0000	2.6700	2.0000	0.8000	0.4000

<b>Table A- 2. A sample K-value table for STARS input file</b>		
$K(T_{low}, P_{low})$	...	$K(T_{low}, P_{high})$
⋮	⋮	⋮
$K(T_{high}, P_{low})$	...	$K(T_{high}, P_{high})$

## **References**

Computer Modelling Group (CMG) Ltd. STARS User Manual. Version 2011. Calgary, Alberta, Canada, 2011.

Computer Modelling Group (CMG) Ltd. WinProp User Manual. Version 2011. Calgary, Alberta, Canada, 2011.

## Appendix B: A sample STARS' data file for simulation of the coinjection process

In this section a sample STARS' data (.dat) file is presented for a simulation of a simple coinjection process. This data file corresponds to C<sub>5</sub>-steam coinjection model in chapter 3. This model was used to verify the results from simplistic representation of phase behavior by a binary mixture of solvent and water only. K-value tables are excluded from the code presented here due to space restriction. They can easily be reproduced by following the procedure described in Appendix A.

```
*INUNIT *SI
** ===== INPUT/OUTPUT CONTROL =====
DIM MDICLU 200000
*OUTUNIT *SI
WRST TIME
**RESTART 185
**REWIND XXXX
OUTPRN GRID OBHLOSS PRES SG SO SW TEMP VISO
OUTPRN WELL ALL
OUTSRF GRID FLUXRC FLUXSC KRO KRW KVALYW MASDENG MASDENO
MASDENW MOLDENG MOLDENO MOLDENW
      OILMOB PRES SG SO STEAMQUAL SW TEMP VISO X Y Z

OUTSRF GRID ELCURDEN KRO KRW KVALYX MASDENO MOLDENO PRES SG SO
SW TEMP
      VISO W X Y Z
OUTSRF WELL COMPONENT 'WATER' 'Heavy' 'NC5' 'CH4'
OUTSRF GRID KVALYX MASDENO PRES SG SO SW TEMP X Y Z
WPRN GRID TIME
*PRNTORIEN 2 0
WPRN ITER 1
WSRF SECTOR TIME
OUTPRN ITER NEWTON
**$ Distance units: m
RESULTS XOFFSET 0.0000
RESULTS YOFFSET 0.0000
```

RESULTS ROTATION 0.0000 \*\*\$ (DEGREES)

RESULTS AXES-DIRECTIONS 1.0 -1.0 1.0

\*\*\$

\*\*\*\*\*

\*\*\$ Definition of fundamental cartesian grid

\*\*\$

\*\*\*\*\*

GRID VARI 70 1 20

KDIR DOWN

DI IVAR

70\*1

DJ JVAR

37.5

DK ALL

1400\*1.

DTOP

70\*500

\*\*\$ Property: NULL Blocks Max: 1 Min: 1

\*\*\$ 0 = null block, 1 = active block

NULL CON 1

\*\*\$ Property: Porosity Max: 0.33 Min: 0.33

POR CON 0.33

\*\*\$ Property: Permeability I (md) Max: 4000 Min: 4000

PERMI CON 4000

\*\*\$ Property: Permeability J (md) Max: 4000 Min: 4000

PERMJ CON 4000

\*\*\$ Property: Permeability K (md) Max: 3000 Min: 3000

PERMK CON 3000

\*\*\$ Property: Pinchout Array Max: 1 Min: 1

\*\*\$ 0 = pinched block, 1 = active block

PINCHOUTARRAY CON 1

\*\*NINEPOINT \*IJ

\*END-GRID

\*PRPOR 7600

```

*ROCKTYPE      1
*CPOR      1.8E-5
ROCKCP 2.6E6 0
THCONR 660E3
*THCONW      1.5E5
THCONO 11.5E3
THCONG 2892
***THCONW      5E4 *THCONO  2.0E4 *THCONG      1.4E2
HLOSSPROP OVERBUR 2600E3 660E3
      UNDERBUR 2600E3 660E3
*****
**
** THE FOLLOWING KEYWORDS CAN BE USED IN THE INITIALIZATION SECTION
IN STARS
*****
**
** MFRAC_OIL 'Heavy' 'CON 9.4583E-01
** MFRAC_OIL 'NC5' 'CON 5.0249E-02
** MFRAC_OIL 'CH4' 'CON 3.9250E-03
*****
**
** THE FOLLOWING SECTION CAN BE USED FOR THE COMPONENT PROPERTY
INPUT INTO STARS
*****
**
** PVT UNITS CONSISTENT WITH *INUNIT *SI
**$ Model and number of components
MODEL 4 4 4 1
COMPNAME 'WATER' 'Heavy' 'NC5' 'CH4'
**      -----
CMM
0 0.5946 0.0722 0.016
PCRIT
0 785.98 3374.12 4600.15
TCRIT
0.00 817.75 196.45 -82.55

```

\*\* low/high pressure; low/high temperature

KVTABLIM 100 3000 10 255

\*\*\$ Gas-liquid K Value tables

KVTABLE 'Heavy'

\*\*\$

\*\* Table excluded due to space restrictions

\*\*\$ Gas-liquid K Value tables

KVTABLE 'NC5'

\*\*\$

\*\* Table excluded due to space restrictions

\*\* Comparison of WinProp (W) and STARS K-value (S) phase split calculations

\*\* Table excluded due to space restrictions

\*\*\$ Gas-liquid K Value tables

KVTABLE 'CH4'

\*\*\$

\*\* Table excluded due to space restrictions

\*\* reference pressure, corresponding to the density

PRSR 101.32

\*\* reference temperature, corresponding to the density

TEMR 15

\*\* pressure at surface, for reporting well rates, etc.

PSURF 101.325

\*\* temperature at surface, for reporting well rates, etc.

TSURF 15.556

\*\*\$ Surface conditions

SURFLASH KVALUE

K\_SURF 'Heavy' 1.5819e-022

K\_SURF 'NC5' 0.87858

K\_SURF 'CH4' 244.56

MASSDEN

0 1073.85 630.739 332.64

CP

0 3.238e-007 1.685e-006 4.285e-006

CT1  
 0 2.258e-005 0.000232 0.001682  
 CT2  
 0 6.309e-007 2.821e-006 3.141e-006  
 CPT  
 0 2.637e-009 4.558e-009 5.529e-008

VISCTABLE

```
**$  temp
      10    0 1362543.805 0.244838909 0.02639449
      50    0 6653.880476 0.17855046 0.023529647
     100    0 192.6374951 0.132343138 0.021100204
     150    0 28.63243322 0.105287768 0.01941524
     200    0 9.481936735 0.08791164 0.018181841
     250    0 4.807492815 0.075978008 0.017241763
```

\*\* The following is the complete WinProp fluid model description.

```
WINPROP *TITLE1  ''
WINPROP *TITLE2  ''
WINPROP *TITLE3  ''
WINPROP *INUNIT *SI
WINPROP *MODEL  *PR  *1978
WINPROP *NC    3  3
WINPROP *PVC3  1.2000000E+00
WINPROP *COMPNAME
WINPROP 'Heavy ' 'NC5  ' 'CH4  '
WINPROP *HCFLAG
WINPROP 1 1 1
WINPROP *SG
WINPROP 1.0770000E+00 6.3100000E-01 3.0000000E-01
WINPROP *TB
WINPROP 6.6395000E+02 3.6050000E+01 -1.6145000E+02
WINPROP *PCRIT
WINPROP 7.7570000E+00 3.3300000E+01 4.5400000E+01
WINPROP *VCRIT
WINPROP 1.6048646E+00 3.0400000E-01 9.9000000E-02
WINPROP *TCRIT
```

WINPROP 1.0909000E+03 4.6960000E+02 1.9060000E+02  
 WINPROP \*AC  
 WINPROP 1.3611000E+00 2.5100000E-01 8.0000000E-03  
 WINPROP \*MW  
 WINPROP 5.9460000E+02 7.2151000E+01 1.6043000E+01  
 WINPROP \*VSHIFT  
 WINPROP 4.0600199E-01 -4.2858134E-02 0.0000000E+00  
 WINPROP \*ZRA  
 WINPROP 2.0471108E-01 2.6850000E-01 2.8760000E-01  
 WINPROP \*VISVC  
 WINPROP 1.6048646E+00 3.0400000E-01 9.9000000E-02  
 WINPROP \*VISCOR \*MODPEDERSEN  
 WINPROP \*VISCOEFF  
 WINPROP 1.3040000E-04 2.3030000E+00 5.9024000E-03 1.0000000E+00 6.1405339E-01  
 WINPROP \*OMEGA  
 WINPROP 4.5723553E-01 4.5723553E-01 4.5723553E-01  
 WINPROP \*OMEGB  
 WINPROP 7.7796074E-02 7.7796074E-02 7.7796074E-02  
 WINPROP \*PCHOR  
 WINPROP 1.1313498E+03 2.3150000E+02 7.7000000E+01  
 WINPROP \*ENTHALPY  
 WINPROP 0.0000000E+00 -2.5347407E-02 3.6071068E-04 -5.3428590E-08 0.0000000E+00  
 0.0000000E+00  
 WINPROP -1.0205230E+01 2.0805470E-01 -2.8154380E-06 3.3566500E-07 -1.7637810E-10  
 3.0188050E-14  
 WINPROP -5.5811400E+00 5.6483400E-01 -2.8297300E-04 4.1739900E-07 -1.5255760E-10  
 1.9588570E-14  
 WINPROP \*COMPOSITION \*PRIMARY  
 WINPROP 9.6000000E-01 0.0000000E+00 4.0000000E-02  
 WINPROP \*COMPOSITION \*SECOND  
 WINPROP 0.0000000E+00 1.0000000E+00 0.0000000E+00

\*\* ===== ROCK-FLUID PROPERTIES =====

\*ROCKFLUID  
 RPT 1 LININTERP WATWET

\*\* Sw Krw Krow

SWT

**\$	Sw	krw	krow
0.25	0	1	
0.28875	0.00117188	0.878906	
0.3275	0.0046875	0.765625	
0.36625	0.0105469	0.660156	
0.405	0.01875	0.5625	
0.44375	0.0292969	0.472656	
0.4825	0.0421875	0.390625	
0.52125	0.0574219	0.316406	
0.56	0.075	0.25	
0.59875	0.0949219	0.191406	
0.6375	0.117187	0.140625	
0.67625	0.141797	0.0976563	
0.715	0.16875	0.0625	
0.75375	0.198047	0.0351562	
0.7925	0.229687	0.015625	
0.83125	0.263672	0.00390625	
0.87	0.3	0	

\*\*1.00 0.14000 0.00000

\*\* Sl Krg Krog

SLT

**\$	Sl	krg	krog
0.38	0.3	0	
0.41875	0.263672	0.00390625	
0.4575	0.229687	0.015625	
0.49625	0.198047	0.0351562	
0.535	0.16875	0.0625	
0.57375	0.141797	0.0976563	
0.6125	0.117188	0.140625	
0.65125	0.0949219	0.191406	
0.69	0.075	0.25	
0.72875	0.0574219	0.316406	
0.7675	0.0421875	0.390625	
0.80625	0.0292969	0.472656	
0.845	0.01875	0.5625	

0.88375 0.0105469 0.660156  
0.9225 0.0046875 0.765625  
0.96125 0.00117188 0.878906  
1 0 1

\*\* ===== INITIAL CONDITIONS =====

\*INITIAL

\*VERTICAL \*DEPTH\_AVE

REFPRES 1500

REFDEPTH 500

\*\*\$ Property: Temperature (C) Max: 13 Min: 13

TEMP CON 13

\*\*\$ Property: Oil Saturation Max: 0.75 Min: 0.75

SO CON 0.75

\*\*\$ Property: Oil Mole Fraction(CH4) Max: 0 Min: 0

MFRAC\_OIL 'CH4' CON 0

\*\*\$ Property: Oil Mole Fraction(Heavy) Max: 1 Min: 1

MFRAC\_OIL 'Heavy' CON 1

\*\* ===== NUMERICAL CONTROL =====

\*NUMERICAL

\*\*\*AIM \*OFF

DTMAX 15.0

\*\*12

ITERMAX 60

SDEGREE 2

\*\*\*REDBLACK

SORDER RCMRB

NORM PRESS 400 SATUR 0.3 TEMP 50 Y 0.3 X 0.2

NEWTONCYC 17

\*\*RANGECHECK \*OFF

\*\*PVTOSCMAX 4

UPSTREAM KLEVEL

\*\*converge totres normal

\*\* ===== RECURRENT DATA =====

\*RUN

\*DATE 1996 01 01

DTWELL 0.1

\*\*\$

WELL 'Injector'

INJECTOR MOBWEIGHT EXPLICIT 'Injector'

INCOMP WATER 1. 0. 0. 0.

TINJW 227.5

QUAL 0.9

OPERATE MAX BHP 2730. CONT

\*\*\$ rad geofac wfrac skin

GEOMETRY J 0.086 0.249 1. 0.

PERF GEOA 'Injector'

\*\*\$ UBA ff Status Connection

1 1 14 1. OPEN FLOW-FROM 'SURFACE'

\*\*\$

WELL 'Producer'

PRODUCER 'Producer'

OPERATE MIN BHP 1500. CONT

OPERATE MAX STL 200. CONT

OPERATE MAX STEAM 1. CONT

\*\*\$ rad geofac wfrac skin

GEOMETRY J 0.086 0.249 1. 0.

PERF GEOA 'Producer'

\*\*\$ UBA ff Status Connection

1 1 18 1. OPEN FLOW-TO 'SURFACE'

SHUTIN 'Producer'

\*DATE 1996 02 01

\*DATE 1996 03 01

\*DATE 1996 04 01

DTWELL 0.0001

DATE 1996 5 1.00000

\*DATE 1996 05 25

DTWELL 0.01

DATE 1996 6 1.00000

DATE 1996 7 1.00000

PRODUCER 'Producer'

OPERATE MIN BHP 1500. CONT

OPERATE MAX STL 200. CONT

OPERATE MAX STEAM 1. CONT

OPEN 'Producer'

INJECTOR MOBWEIGHT EXPLICIT 'Injector'

INCOMP WATER-OIL 0.885 0. 0.115 0.

TINJW 227.5

QUAL 0.9

OPERATE MAX BHP 2730. CONT

\*DATE 1996 07 15

DTWELL 0.001

DATE 1996 8 1.00000

DATE 1996 9 1.00000

\*DATE 1996 09 30

DATE 1996 10 1.00000

DATE 1996 11 1.00000

DATE 1996 12 1.00000

\*DATE 1996 12 31

DATE 1997 1 1.00000

DATE 1997 2 1.00000

DATE 1997 3 1.00000

DATE 1997 4 1.00000

DATE 1997 5 1.00000

DATE 1997 6 1.00000

DATE 1997 7 1.00000

DATE 1997 8 1.00000

DATE 1997 9 1.00000  
\*DATE 1997 09 30  
DATE 1997 10 1.00000  
DATE 1997 11 1.00000  
DATE 1997 12 1.00000  
\*DATE 1997 12 31  
DATE 1998 1 1.00000  
DATE 1998 2 1.00000  
DATE 1998 3 1.00000  
DATE 1998 4 1.00000  
DATE 1998 5 1.00000  
DATE 1998 6 1.00000  
DATE 1998 7 1.00000  
DATE 1998 8 1.00000  
DATE 1998 9 1.00000  
DATE 1998 10 1.00000  
DATE 1998 11 1.00000  
DATE 1998 12 1.00000  
\*DATE 1998 12 31  
DATE 1999 1 1.00000  
DATE 1999 2 1.00000  
DATE 1999 3 1.00000  
DATE 1999 4 1.00000  
DATE 1999 5 1.00000  
DATE 1999 6 1.00000  
DATE 1999 7 1.00000  
DATE 1999 8 1.00000  
DATE 1999 9 1.00000  
DATE 1999 10 1.00000  
DATE 1999 11 1.00000  
DATE 1999 12 1.00000  
  
\*DATE 1999 12 31  
DATE 2000 1 1.00000  
DATE 2000 2 1.00000  
DATE 2000 3 1.00000  
DATE 2000 4 1.00000

DATE 2000 5 1.00000  
DATE 2000 6 1.00000  
DATE 2000 7 1.00000  
DATE 2000 8 1.00000  
DATE 2000 9 1.00000  
DATE 2000 10 1.00000  
DATE 2000 11 1.00000  
DATE 2000 12 1.00000  
\*DATE 2000 12 31  
DATE 2001 1 1.00000  
DATE 2001 2 1.00000  
DATE 2001 3 1.00000  
DATE 2001 4 1.00000  
DATE 2001 5 1.00000  
DATE 2001 6 1.00000  
DATE 2001 7 1.00000  
DATE 2001 8 1.00000  
DATE 2001 9 1.00000  
DATE 2001 10 1.00000  
DATE 2001 11 1.00000  
DATE 2001 12 1.00000  
\*DATE 2001 12 31  
DATE 2002 1 1.00000  
DATE 2002 2 1.00000  
DATE 2002 3 1.00000  
DATE 2002 4 1.00000  
DATE 2002 5 1.00000  
DATE 2002 6 1.00000  
DATE 2002 7 1.00000  
DATE 2002 8 1.00000  
DATE 2002 9 1.00000  
DATE 2002 10 1.00000  
DATE 2002 11 1.00000  
DATE 2002 12 1.00000  
\*DATE 2002 12 31  
DATE 2003 1 1.00000  
DATE 2003 2 1.00000

DATE 2003 3 1.00000  
DATE 2003 4 1.00000  
DATE 2003 5 1.00000  
DATE 2003 6 1.00000  
DATE 2003 7 1.00000  
DATE 2003 8 1.00000  
DATE 2003 9 1.00000  
DATE 2003 10 1.00000  
DATE 2003 11 1.00000  
DATE 2003 12 1.00000  
\*DATE 2003 12 31  
DATE 2004 1 1.00000  
DATE 2004 2 1.00000  
DATE 2004 3 1.00000  
DATE 2004 4 1.00000  
DATE 2004 5 1.00000  
DATE 2004 6 1.00000  
DATE 2004 7 1.00000  
DATE 2004 8 1.00000  
DATE 2004 9 1.00000  
DATE 2004 10 1.00000  
DATE 2004 11 1.00000  
DATE 2004 12 1.00000  
\*DATE 2004 12 31